Towards a contact formulation for efficient numerical simulation of marine ice-sheet instabilities

Auteur : Bosten, Armin
Promoteur(s) : Arnst, Maarten
Faculté : Faculté des Sciences appliquées
Diplôme : Master en ingénieur civil physicien, à finalité approfondie
Année académique : 2018-2019
URI/URL : http://hdl.handle.net/2268.2/6728

Université de Liège
Faculté des Sciences Appliquées

Towards a contact formulation for efficient numerical simulation of marine ice-sheet instabilities

Thesis submitted in partial fulfillment of the requirements for the degree of master in engineering physics

Author
Armin **Bosten**

Supervisors
Pr. Maarten **Arnst**
Kevin **Bulthuis**

Jury
Pr. Benjamin **Dewals**
Kim **Liegeois**

Academic year: **2018-2019**

Remerciements

Je souhaite remercier le professeur Maarten Arnst de m'avoir proposé un sujet aussi intéressant. De plus je le remercie pour sa patience et sa bienveillance.

Je remercie aussi le professeur Benjamin Dewals d'avoir accepté de faire partie du jury.

Ensuite je tiens à remercier Kevin Bulthuis pour l'aide précieuse qu'il m'a apporté tout au long de ce projet.

Je souhaite remercier Kim Liégeois d'avoir accepté de faire partie du jury.

Je remercie aussi toute la team COSTMO. La bonne humeur qui y règnait a constitué un cadre de travail adéquat pour pouvoir avancer de façon sereine.

Je souhaite aussi remercier ma famille pour leur soutien durant mes études.

Finalement, je tiens particulièrement à remercier la Faculté des Sciences Appliquées. Entamer des études d'ingénieur fut la meilleure décision de ma vie. J'aime la FSA. Cela vient du fond du coeur.

Contents

Introduction

Marine ice sheets play an important role in the Earth's climate system. A thorough understanding and efficient ways of modeling them numerically is therefore essential for predicting future consequences of climate change. Marine ice sheets are difficult problems governed by coupled partial differential equations translating the laws of continuum mechanics. These are often referred to as the Stokes model. Moreover, glaciologists have to deal with uncertain data and modeling parameters. The trend is therefore to move towards uncertainty quantified prediction of the response of marine ice sheets to changes in climate. There are two possible resolution approaches. The first approach consists in solving the full Stokes model directly on large computers using elaborate numerical methods. Such an approach is difficult to with uncertainty quantification as they it uses up too much time and resources. Therefore, the use of "essential" ice sheet models is more appropriate. Based on a physical understanding of ice sheets some hypotheses can be made to simplify the equations without loosing the most important aspects governing the dynamics of marine ice sheets. Especially the transition zone between the grounded ice sheet and the floating ice sheet has to be modeled correctly. It determines the dynamics of the grounding line, which is the location where the ice sheet becomes afloat. Mathematically, such models are derived by studying the behaviour of the equations when the aspect ratio of the ice sheet tends to zero in certain scaling regimes. The most famous ones are the Shallow Ice Approximation (SIA) and the Shallow Shelf Approximation (SSA). Such models are better suited for long term parametric studies and the use of uncertainty quantification. In this work we will consider a fast sliding regime, where shear stress is negligible with respect to normal stress and the ice movement is dominated by sliding over the bedrock.

Similar to other large scale climatic subsystems, ice sheets are characterized by a high degree of complexity. Some underlying physical processes can feedback on each other and cause the system to exhibit irreversible bifurcations. Additionally, one has to deal with non-linearities stemming from the complicated rheological behaviour of ice, which leads to a p-Laplace equation [1] for the momentum balance. Moreover, the contact between the ice sheet and the bedrock is challenging. Local processes can have a significant impact on the response of marine ice sheets. In particular, the West Antarctic Ice Sheet (WAIS) has the potential to undergo Marine Ice Sheet Instabilities (MISI) [2]. Their occurrence and dynamics are strongly impacted by the shape of the bedrock in the transition zone [3]. The ladder is characterized by small scale surface roughness. Moreover, the coupling of a large grounded ice sheet and a thin ice shelf leads to strong velocity and ice thickness gradients near their interface.

A currently widespread approach for solving the equations uses a finite difference method. These are done on coarse meshes to save computation time. The presence of large gradients

in the transition zone between the grounded and the floating parts of the ice sheet leads to a bad approximation of velocities near the grounding line. This has a large impact on the velocity field inside the ice shelf. Moreover, coarse meshes are not capable of capturing the shape of the bedrock correctly. Subgrid sized rugosity plays an important role in the mechanism of MISI. A straightforward solution would be to refine the spatial discretization close to the grounding line. This is not always possible due to limited computational resources. In that case an often used approach consists in replacing the numerical ice flux by an analytic expression deduced from simplified one dimensional models [4]. It has been shown to work for coarse meshes on simple models [4], but the implications of a direct transposition to a full scale three dimensional model are not yet well understood [5]. Furthermore, often employed friction laws predict a friction force solely depending on the sliding velocity of the ice sheet and not on the effective contact pressure. Not only does it lead to a discontinuous friction distribution across the grounding line, it also predicts a strong and unphysical increase of the friction force in the transition zone before suddenly dropping to zero when the ice sheet becomes afloat. It also raises the more fundamental and unanswered question of mathematical well posedness of the model.

Weak formulations have less restrictive regularity requirements of the solution. Therefore, they constitute the appropriate framework for facing the mathematical challenges mentioned earlier. They are also better suited for exploiting available computational resources in a systematic way. Efficient implementation methods have been studied extensively in Applied Mathematics and Computational Mechanics [6]. This would allow fast but reliable calculations to be performed for a large number of parameters and thus be an adequate framework for the application of methods from uncertainty quantification.

In this work we study numerical methods based on variational formulations for the solution of essential ice sheet models. We carry out our study by applying these numerical methods to a simple marine ice sheet model. It describes the evolution of a fast sliding marine ice sheet coupled with a floating ice shelf by means of a non-linear transport equation for the ice thickness, very similar to the shallow flow equations in oceanography. It is coupled to a non-linear p-Laplace equation corresponding to the horizontal momentum balance and it requires a procedure for identifying the position of the grounding line. For the reduced-order model vertical equilibrium simplifies to a flotation condition that can be used for that purpose. We take the more general approach of solving a weak unilateral contact formulation inspired by the Signorini problem from elastic contact mechanics [6]. It allows to draw from efficient numerical methods originating from frictional contact mechanics. In this work a Mortar Finite Element discretization is adopted [7]. Such a segment to segment approach allows taking into account subgrid bedrock rugosity on a coarse grid to a certain extend.

This work is divided into two parts. The first part establishes the geophysical and mathematical context of marine ice sheets. The system of equations describing the mechanical behaviour of marine ice sheets is presented. Some key physical processes are presented and current trends in their numerical modeling are explained.
The second part is dedicated to the application of variational approaches to the problem of marine ice sheets. The complete problem is broken down into solving a p-Laplace equation for the horizontal momentum balance, a unilateral contact problem for the vertical equilibrium and a transport equation for the ice thickness. Each subproblem has a dedicated chapter. A final chapter presents the coupling of the equations.

More specifically, this work has the following structure:

Chapter 1 is a short introduction to marine ice sheets. Some vocabulary from glaciology is explained and a motivation for studying marine ice sheets is given.

Chapter 2 establishes a mechanical model for marine ice sheets. The classical approach from continuum mechanics is taken. Starting from the general conservation laws and particularising them to the case of marine ice sheets by taking into account their specificities. These are mainly their small aspect ratio, their non-linear rheological behaviour and the presence of friction on some part of their boundary. The full Stokes model is thereby obtained.

In chapter 3 we derive in detail the reduced-order model for a fast sliding ice regime. Starting from the previously established full Stokes model we will see how the equations behave as the aspect ratio tends to zero. A closed system of two equations will emerge, where the form of certain terms depend on whether the grounded or the floating subdomain is considered. The distinction between the two domains is done by a simple criterion.

Chapter 4 explains the mechanism of Marine Ice Sheet Instabilities. An irreversible rapid movement of the grounding line that marine ice sheets resting below sea-level can undergo. They can have a significant impact on the global response of large continental ice sheets. An analytic expression for the flux at the grounding line is found to be a monotonically increasing function of the ice thickness. Steady-state profiles for the ice-sheet geometry are deduced both in the case a power friction law and a Coulomb friction law.

Chapter 5 takes on the p-Laplace equation that describes the horizontal equilibrium of the marine ice sheet. First, the problem is expressed in its weak form. An equivalent minimization problem is derived and the mathematical difficulties originating from the discontinuous friction term are illustrated. Then a finite element discretization is combined with a Newton algorithm to solve the horizontal momentum equation numerically. It is found that a coarse discretization leads to a bad approximation of steep gradients in the transition zone between the grounded and the floating parts of the marine ice sheet. As a consequence velocity is systematically overestimated in the ice shelf. The attempt for explaining the implications of a flux condition is made.

In chapter 6 the contact problem stemming from the vertical equilibrium of the ice sheet is studied. Starting from the complementarity problem an equivalent variational inequality is derived. This inequality is reformulated as a constrained optimization problem. An equivalent saddle point problem is constructed. It is discretized using Mortar Finite Elements and solved by a semi-smooth Newton algorithm. Then test cases are illustrated.

Chapter 7 is dedicated to the hyperbolic ice thickness equation. The issue of time integration and its combination with Finite Elements is briefly discussed. It is found that implicit are more appropriate for long term simulations of complex systems. The chapter concludes with numerical illustrations.

In chapter 8 all the methods derived in the previous chapter are assembled together to solve the coupled problem. Numerical experiments are presented to illustrate the marine ice sheet instability.

The final chapter discusses potential future developments that could built on this work.

Part I

Geophysical context

Chapter 1

Marine ice sheets

This first chapter is dedicated to a short presentation of marine ice sheets. As they are an important part of the terrestrial climate system their study is of particular interest. It starts by a brief explanation of the specific vocabulary used in glaciology in section 1.1, followed by a more detailed description of marine ice sheets and their importance in the Earth's climate system in 1.2. Finally, in section 1.3, the role played by marine ice sheets in the context of climate change is addressed. Indeed, the study of ice sheets and glaciers is mostly motivated by the fact that they are well suited for studying the Earth's climate, but are also strongly impacted by global warming.

1.1 The Cryosphere

Scientists refer to the cryosphere when speaking about the frozen part of the earth's climate system. It covers approximately 10% of the earth's surface. It includes all terrestrial subsystems containing frozen water such as: ice sheets, glaciers, sea ice, frozen lakes, snowy regions or permafrost. Ice sheets denominate large ice formations with a surface larger than 50000 km^2, resting on solid ground. They make up about 70% of the global fresh water reserves. On Earth, only the Antarctic ice sheet and the Greenland ice sheet are considered to be ice sheets. Glaciers are ice masses constrained by their surrounding geography. They are usually significantly smaller than ice sheets. Figure 1.1 shows the Greenland ice sheet and the Skoltbre glacier. Interestingly, the Greenland ice sheet, also called Greenland inlandsis, carries 10% of the total amount of terrestrial fresh water. Sea ice forms by freezing water on the surface of the ocean and then floats on it. In the same manner, ice on frozen lakes originates directly from the freezing of water. They differ from ice shelves, as will be explained in the next section. Permafrost refers to frozen regions, where the temperature is sufficiently low during the entire year to maintain the ground in a frozen state. Finally, snowy regions appear when crystallized water amasses on the ground to form a layer of material less dense than ice. The main focus of this work are ice sheets and ice shelves. The next section describes in more detail the kind of physical system that will be studied.

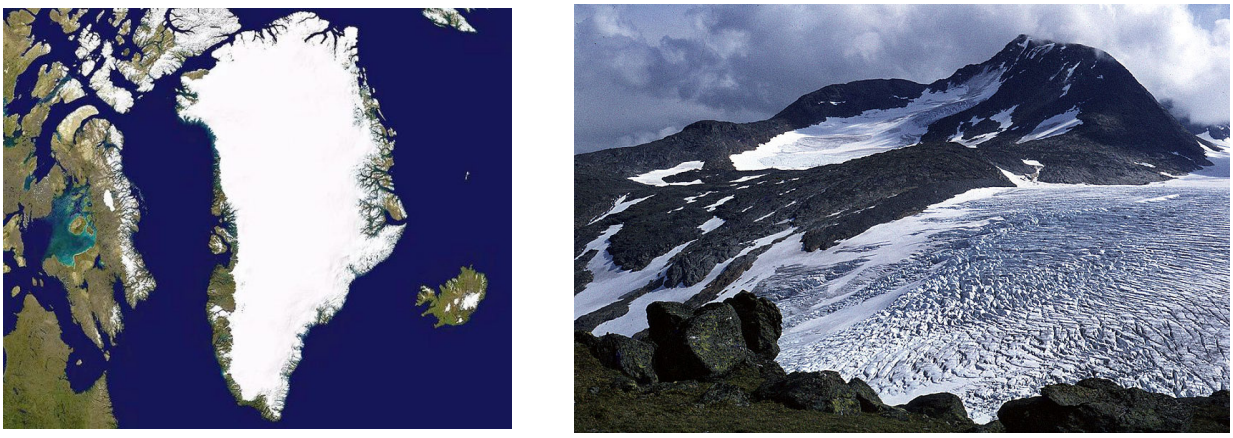

Figure 1.1: Left: Image of Greenland, as seen from space. Picture taken from [8]. Right: Image of the Skoltbre glacier in Norway. Picture taken from [9].

1.2 Ice sheets and ice shelves

Marine ice sheets rest on bedrock below sea level, as shown schematically in figure 1.2. It is the case for the West Antarctic Ice Sheet, whose bedrock is more than 2500 m deep at some locations. The ice can reach a maximum thickness of several thousands of meters. The flow inside the ice sheet is driven by gravity. The ice spreads horizontally over the bed, becoming thinner by the process, similar to what happens when honey is deposited on top of a large ball. Moreover, ice sheets have the possibility to slide over the bedrock. The total movement of the ice is the superposition of both effects. At the edges, ice is sufficiently thin for buoyancy to counteract gravity, thereby leading to a part of the ice being afloat, called the ice shelf, which is attached to the ice sheet. These ice shelves can be several hundreds of kilometers long. The sudden release of large chunks of ice into the ocean, as a result of ice stretching, is referred to as calving. Together with melting and snow fall in the interior regions it dictates the dynamic equilibrium of the ice sheet.

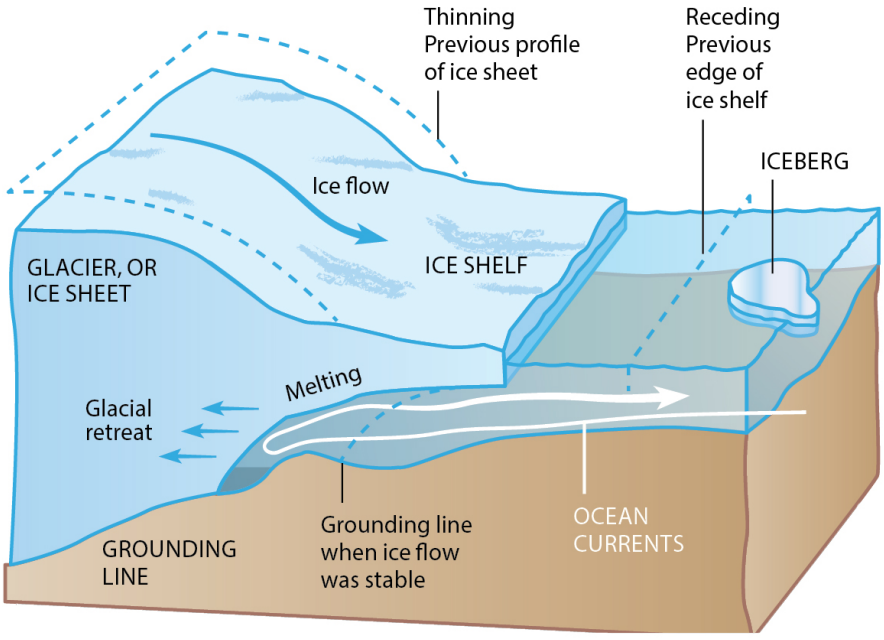

Figure 1.2: Schematic representation of a marine ice sheet. Image taken from [10].

Ice-ocean interactions give rise to complicated physical mechanisms, making the study of marine ice sheets particularly interesting.

1.3 Impact of climate change

In recent years ice sheets and glaciers have increasingly gained attention due to their sensitivity to global warming. Especially the smaller inland glaciers respond strongly to perturbations in climate conditions. Some of them have experienced a spectacular retreat during the last century as for example the Muir glacier in Alaska depicted in figure 1.3. Between 1892 and 2005 this glacier receded more than 50 km. Still, their potential for sea level rise remains rater limited compared to the potential contribution of continental ice sheets, such as the Antarctica. Indeed for glaciers it is around 0.5 m, whereas for ice sheets it is close to 70 m. However, due their large size, ice sheets respond much slower to a change in climate. Surprisingly, for the some parts of the Antarctic ice sheet the trend over the short and medium term even seems to be an advancing one. This can be explained by increased snow fall as a consequence of higher atmospheric temperatures that is not compensated by other physical mechanisms.

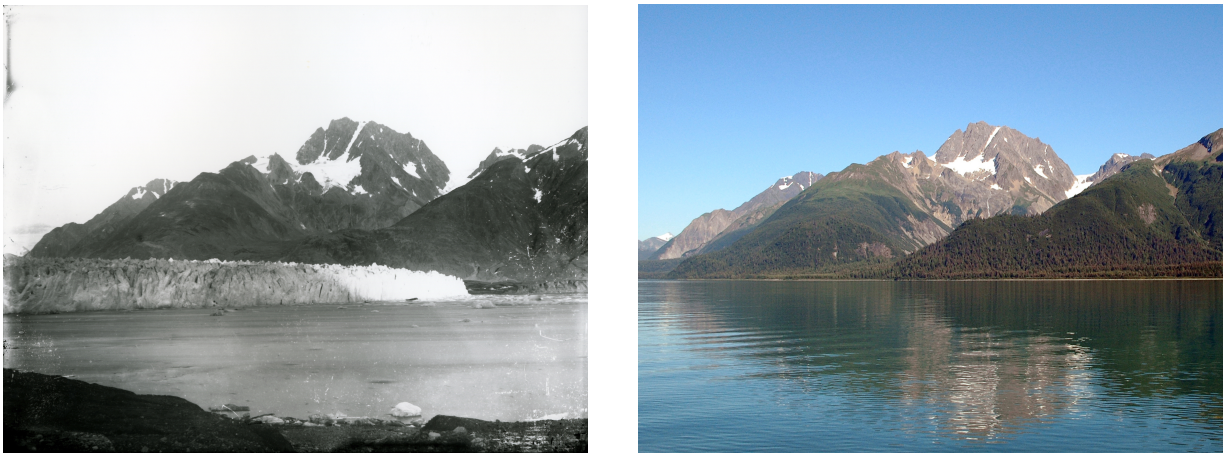

Figure 1.3: Left: Image of the Muir glacier in Alaska: year 1892. Picture taken from [11]. Right: Image of the Muir glacier in Alaska: year 2005. Picture taken from [11].

Still, in the future ice sheets will continue to shrink and melting will overcome increased precipitation at in these regions of the Antarctic ice sheet, thereby adding another strong contributor to sea level rise. Predicting the response of ice sheets over long time scales proves difficult, due to model uncertainties and the possibility of various scenarios of human activity, to be added to a lack of understanding of non-linear ice sheet dynamics. One example of such dynamics are thermally induced oscillations [12], where ice streams exhibit variability over extremely long time scales through a thermal feedback between the ice and the bedrock. It is responsible for Heinrich events in the North Atlantic, where large amounts of cold and fresh water are discharged into the ocean, potentially modifying the salinity and temperature of the ocean. This has for effect to alter the density-driven thermohaline ocean currents. This particular example shows clearly that the cryosphere is intricately linked to other climate subsystems and changes in the first necessarily induce modifications in the latter. A second example is the potential partial disintegration of the West Antarctic Ice Sheet due to Marine Ice Sheet Instabilities (MISI). A phenomenon that will be discussed in later chapters 4.

Chapter 2

Mechanical model for marine ice sheets

Before deriving the reduced order model for marine ice sheets, let us first set the complete problem mathematically. In this chapter the equations for an isothermal ice sheet are introduced. They describe the mechanical behaviour of the ice sheet. It is referred to as the full Stokes model in the literature. "Full model", as opposed to "Essential model" means apart from some basic hypothesis on the aspect ratio of the ice sheet no simplification to the equations have been made. These equations are difficult to solve numerically and this will not be attempted in this work. But since simplified models are based on the Stokes model, it is useful to recall the derivation of the governing equations as it can give the physical insight needed for improving numerical methods for ice sheets.

In section 2.1 the usual approach for deriving balance equations from the laws of continuum mechanics is applied in the case of ice sheet dynamics. Starting with the conservation of mass and followed by the momentum balance equation, the field equations for a typical grounded ice sheet with an ice shelf attached to it are derived. The system of equations is then closed by a constitutive equation for polycrystalline ice in section 2.2. Finally, boundary conditions for the studied problem are detailed in section 2.3. This chapter is based on the works of Greve and Blatter [13], Maze [14] and Bulthuis [16].

2.1 Balance equations

In figure 2.1 the cross section of a marine ice sheet is represented schematically. The ice volume is denoted Ω and its boundary is defined by $\Gamma = \Gamma_b \cup \Gamma_s \cup \Gamma_c \cup \Gamma_w$, where the interfaces between the ice sheet and the bedrock, the ice sheet and the ocean, the ice sheet and the atmosphere and the calving front are denoted Γ_b, Γ_s, Γ_c, Γ_w respectively. A coordinate system is introduced, implicitly assuming a flat Earth, where $\mathbf{e_x}\mathbf{e_y}$ corresponds to the horizontal plane and $\mathbf{e_z}$ is oriented vertically upward. The usual approach is to describe the evolution of the ice interface elevations as a function of (x, y, t). This will be done in the next chapter for the derivation of the reduced order model. The ice sheet is assumed isothermal. Thus thermo-mechanical coupling will not be considered. Nevertheless, snowfall and accumulation at the superior ice surface, melting and freezing at the bedrock-interface, as well as melting and calving at the ice-ocean interface are taken into account. The velocity field is denoted $\mathbf{v} = [u, v, w]^T$. The common interface between the ice, the bedrock and the ocean is called the grounding line. It is denoted GL on the figure. It is the location, where the ice turns from grounded to floating.

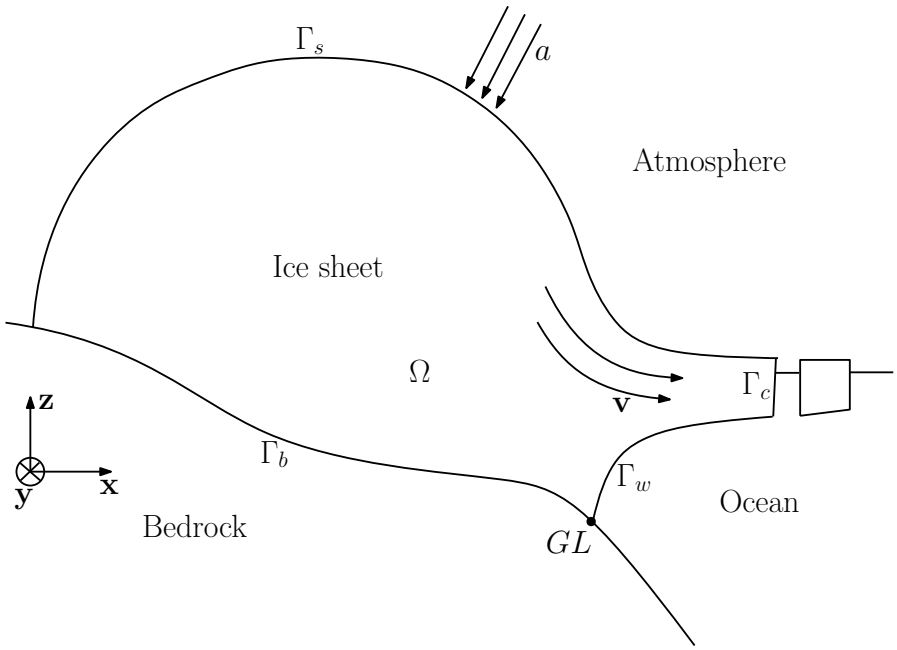

Figure 2.1: Schematic illustration of a marine ice sheet. The ice domain is denoted Ω, the ice-air interface Γ_s, the ice-ocean interface Γ_w, the ice-bedrock interface Γ_b and the calving front Γ_c. The grounding line is denoted GL. The parameter a is the accumulation function. It is the net result of snowfall and melting at the surface.

2.1.1 Conservation of mass

The ice sheet is a homogeneous continuum made of polycrystalline ice. The presence or absence of matter is described by the density field $\rho(\mathbf{x}, t)$. The local form of the conservation of mass is then given by the evolution equation

$$\frac{\partial \rho}{\partial t} + \operatorname{div}_{\mathbf{x}}(\rho \mathbf{v}) = 0, \tag{2.1}$$

Assuming an incompressible flow for the ice sheet, meaning constant density within a fluid particle, simplifies equation 2.1 to

$$\operatorname{div}_{\mathbf{x}} \mathbf{v} = 0. \tag{2.2}$$

Equation 2.2 indicates that the velocity field $\mathbf{v}$ has to be divergence free.

2.1.2 Momentum balance

The momentum conservation for a continuous and homogeneous medium is given by Cauchy's first law of motion. It writes

$$\rho \frac{\mathrm{d}\mathbf{v}}{\mathrm{dt}} = \operatorname{div}_{\mathbf{x}} \boldsymbol{\sigma} + \mathbf{f}, \tag{2.3}$$

where $\boldsymbol{\sigma}$ denotes the Cauchy stress tensor. The operator $\dfrac{\mathrm{d}\,\cdot}{\mathrm{dt}}$ denotes the material derivative. In the case of marine ice sheets the force per unit volume $\mathbf{f}$ has three contributions. The Coriolis force and the centrifugal force acting on the ice sheet due to the earth's rotation as well as the force of gravity. The latter two are combined into one effective force of gravity $\mathbf{g}$. The external force $\mathbf{f}$ is thus given by

$$\mathbf{f} = \rho \mathbf{g} - 2\rho \boldsymbol{\Omega} \times \mathbf{v}, \tag{2.4}$$

where $\mathbf{\Omega}$ is the earth rotation vector. In fluid mechanics it is the usual practice to split the stress tensor into its hydrostatic and deviatoric part.

$$\boldsymbol{\sigma} = -\pi\mathbb{I} + \boldsymbol{\sigma}^{\nu}, \tag{2.5}$$

where $\pi = \sigma_{kk}$ is the pressure and $\boldsymbol{\sigma}^{\nu}$ denotes the deviatoric stress tensor of $\boldsymbol{\sigma}$. The rate of deformation tensor $\mathbf{D}$ is linked to the velocity field by

$$\mathbf{D} = \frac{1}{2}(\nabla\mathbf{v} + \nabla\mathbf{v}^{T}). \tag{2.6}$$

A constitutive equation for polycrystalline relates the deviatoric stress tensor to the rate of deformation tensor by

$$\boldsymbol{\sigma}^{\nu} = 2\eta\mathbf{D}. \tag{2.7}$$

The viscosity η of ice is in general not constant. A more detailed analysis of equation 2.7 is provided in section 2.2. Inserting 2.4 and 2.5 in 2.3 yields

$$\rho\frac{\mathrm{d}\mathbf{v}}{\mathrm{dt}} = -\nabla\pi + \mathrm{div}_{\mathbf{x}}(2\eta\mathbf{D}) + \rho\mathbf{g} - 2\rho\mathbf{\Omega}\times\mathbf{v}. \tag{2.8}$$

It is the general equation governing the behaviour of ice sheets and glaciers. A series of simplifications can be done. Indeed earth rotation speed $|\mathbf{\Omega}| \approx 10^{-4}\mathrm{s}^{-1}$. Moreover, velocities inside the ice sheet are relatively small. Therefore, the Coriolis term can be neglected with respect to gravity in equation 2.4. Additionaly, an analysis of orders of magnitude shows that the acceleration term is much smaller than the pressure gradient in equation 2.8. Therefore, it is dropped as well. This leads to the Stokes equation 2.9.

$$-\nabla_{\mathbf{x}}\pi + \mathrm{div}_{\mathbf{x}}(2\eta\mathbf{D}) + \rho\mathbf{g} = \mathbf{0} \tag{2.9}$$

Together with equation 2.2 it describes the mechanical behaviour of ice sheets and glaciers. This type of equation typically arises when studying creeping flows in lubrication problems. Completed with appropriate boundary conditions it is often referred to as the *full Stokes model*. A presentation of the boundary conditions is given in section 2.3. Often glaciologists work on simplified versions of the full Stokes model, such as the Shallow Ice Approximation (SIA) [13] and the Shallow Shelf Approximation (SSA) [13]. These models are derived by assuming a small aspect ratio for the ice sheet and noting that certain components of the stress tensor are negligible compared to others as a consequence. A similar approach is taken in chapter3 to derive the equations governing the behaviour of a fast sliding marine ice sheet on which this work will focus. The full Stokes model can be coupled with a model for the evolution of temperature inside the ice sheet [13] and [16] to determine the value of $\eta(T)$ and models for the melting of the ice sheet, giving rise to the classic thermo-mechanical model for ice sheets and glaciers. This type of multiphysical aspect of the problem will not be taken into account.

2.2 Rheology of polycrystalline ice

Water molecules inside ice crystals arrange themselves as layers of hexagons as shown in figure 2.2 on the left. These layers are called basal planes. Under shear stress these basal planes have the possibility to slide relatively to each other. As long as stress is applied the deformation continues, similar to the creeping of a fluid. The respond of the crystal depends on the direction of the applied stress. This anisotropy is true for single ice crystals. In nature, ice comes as an aggregate of a large number of randomly oriented ice crystals, called polycrystalline ice. This

type of situation is illustrated in figure 2.2 on the right. The locally directional dependence of ice crystal properties averages out in polycrystalline ice. Thus one can assume it to be an isotropic material.

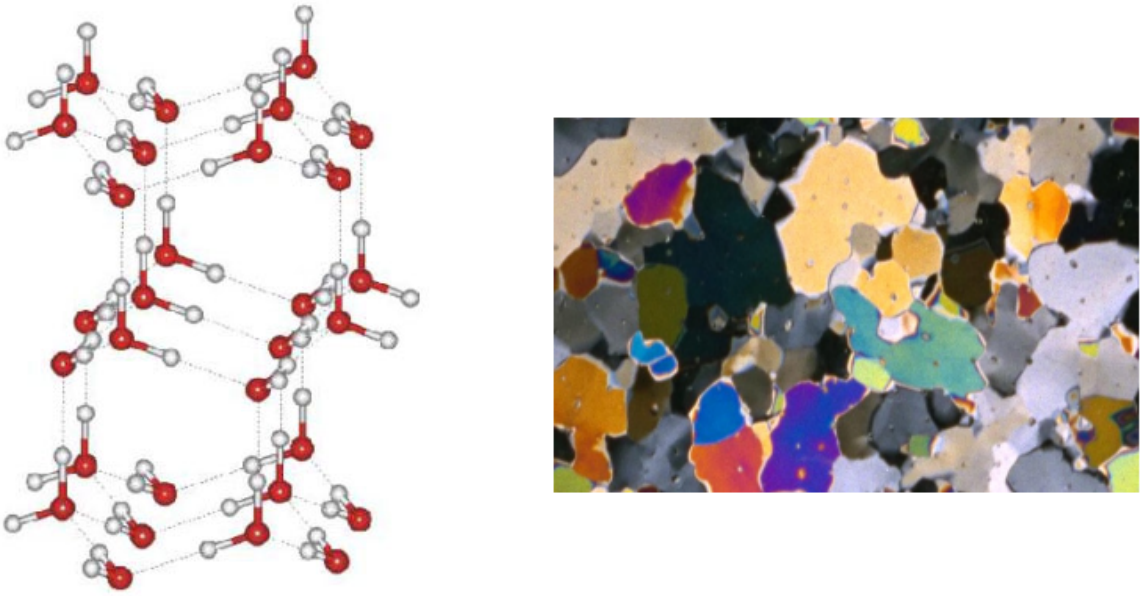

Figure 2.2: Left: Schematic representation of an ice crystal lattice. Picture taken from [17]. Right: Polycrystalline ice seen under polarized light. Due to the birefringence of ice it is possible to observe individual ice crystals. Picture taken from [18].

As mentioned earlier, polycrystalline ice deforms by creep. This was confirmed by several experiments. Indeed, data indicate that under simple shearing conditions as shown in figure 2.3 ice behaves as a non-linear viscous fluid. The shear rate $\dot{\gamma}$ can be expressed as a function of shear stress τ, pressure p and temperature T in the following way

$$\dot{\gamma} = \frac{1}{\eta(|\tau|, p, T)}\tau, \tag{2.10}$$

where η is the fluid viscosity from equation 2.7. It is common practise to factor out the dependencies on p and T such that the relation takes the form of

$$\dot{\gamma} = 2A(p, T)f(|\tau|)\tau. \tag{2.11}$$

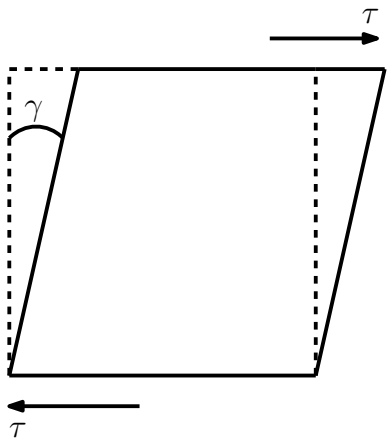

Figure 2.3: Schematic representation of a simple shearing experiment. The applied shear stress and the shear angle are denoted τ and γ respectively. Image inspired from [13].

Since we assumed an incompressible flow the pressure p is simply a free quantity that adapts in order to ensure that the continuity equation is enforced. It is not considered as a real thermodynamic quantity. Indeed, the Stokes problem can be reformulated as a quasi unconstrained optimisation problem were the pressure plays the role of a Langrange multiplier. The reader is referred to [16], [6] and [19] for more information. Moreover, we do not couple the Stokes problem with an equation for temperature in our model. Temperature is seen as a known parameter translating the effects of for example a climate perturbation through the value of A. By analogy with equation 2.11 one can extend the flow law to any deformation as opposed to simple shear. Thus one has the following relation linking the strain rate tensor $\mathbf{D}$ to the deviatoric stress tensor $\boldsymbol{\sigma}^{\nu}$:

$$\mathbf{D} = 2A(p,T)f(\sigma_e)\boldsymbol{\sigma}^{\nu}. \tag{2.12}$$

To have equation 2.12 independent of any coordinate system the just defined scalar quantity σ_e is chosen to be the second invariant of deviatoric stress tensor, that is

$$\sigma_e = \sqrt{\frac{1}{2}\mathrm{tr}\,(\boldsymbol{\sigma}^{v})^2}. \tag{2.13}$$

The quantity σ_e is called the effective stress. It is always positive. It translates the state of stress inside the ice. The function f takes the form of a power law

$$f(\sigma_e) = \sigma_e^{n-1}, \tag{2.14}$$

where n is the stress exponent. The correct value for n is still a matter of debate, but it usually taken equal to 3 [13]. Equation 2.12 together with 2.13 and 2.14 form *Glen's flow law*. If the effective strain rate d_e is defined as

$$d_e = \sqrt{\frac{1}{2}\mathrm{tr}\,(\mathbf{D})^2}, \tag{2.15}$$

one can invert Glen's flow law to obtain

$$\boldsymbol{\sigma} = 2\eta_0 \left(\sqrt{2}||\mathbf{D}||_{\mathrm{F}}\right)^{1/n-1}\mathbf{D}, \tag{2.16}$$

where the ν for denoting the deviatoric stress tensor has been dropped to simplify notations. The symbol $||\cdot||_{\mathrm{F}}$ denotes the Frobenius norm. It is defined by

$$||\cdot||_{\mathrm{F}} = \sqrt{\mathrm{tr}\,(\cdot)^2}. \tag{2.17}$$

The nominal viscosity η_0 can be identified as $A^{-1/n}$. Equation 2.16 is indeed the constitutive equation we were searching for. By analogy with equation 2.7 one has for the fluid viscosity

$$\eta(\mathbf{D}) = \eta_0 \left(\sqrt{2}||\mathbf{D}||_{\mathrm{F}}\right)^{1/n-1}. \tag{2.18}$$

It is this power law that models the rheological behaviour of ice that leads to the presence of the p-Laplacian operator in the momentum balance equation.

2.3 Boundary conditions

The Stokes model formed by equations 2.9 and 2.2 has to be completed with appropriate boundary conditions. As mentioned earlier, the boundary of the domain Ω is denoted Γ. It

is separated into four parts, that do not overlap. These are: the ice-air interface Γ_s, the ice-bedrock interface Γ_b, the ice-water interface Γ_w and the calving front Γ_c. On each boundary a different boundary condition has to be imposed. These are presented and discussed in this section.

Even though the Stokes model does not explicitly contain a derivative with respect to time the problem is still a dynamic one. Indeed ice moves inside the ice sheet, snow precipitates on of top it, ice melts at the interfaces and ice masses break off at the calving front. Thus the ice sheet interfaces are functions of time. Using kinematic arguments it is possible to write evolution equations for these boundaries and to deduce a transport equation for the ice thickness, similar to what is done in geophysical fluid dynamics [13] and [20]. This kind of approach is used in the next chapter to derive the reduced order model for fast sliding ice sheets. To have a complete problem, the evolution of the ice boundaries has to be prescribed in terms of ice velocity, accumulation and ablation. Next to dynamic boundary conditions, the model is also in need of kinematic boundary conditions.

At the ice-air interface Γ_s the ice is in contact with the atmosphere. The applied surface force is zero.

$$(-\pi\mathbb{I} + \boldsymbol{\sigma}) \cdot \mathbf{n} = \mathbf{0} \tag{2.19}$$

where $\mathbf{n}$ is the unit outward normal at the ice surface. The deviatoric stress tensor $\boldsymbol{\sigma}$ is related to the derivatives of $\mathbf{v}$ through the strain rate tensor $\mathbf{D}$. Thus condition 2.19 is a homogeneous Neuman boundary condition. The kinematic boundary condition imposed at Γ_s is a surface mass balance.

$$(\mathbf{w} - \mathbf{v}) \cdot \mathbf{n} = a_s \tag{2.20}$$

The vector $\mathbf{w}$ is the velocity of the interface and a_s is the ice volume flux across the ice-air interface. It is called the accumulation-ablation function. It represents the net result of snowfall, ablation and ice melting at the top of the ice sheet.

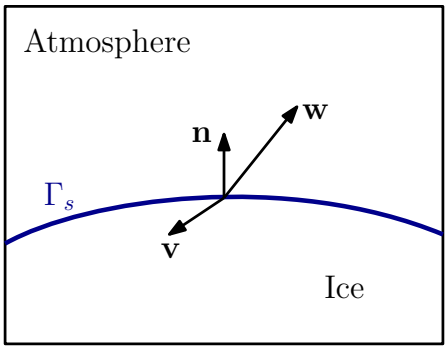

Figure 2.4: Schematic representation of the ice-air interface. Vector $\mathbf{n}$ denotes the unit outward normal, $\mathbf{v}$ is the ice velocity whereas $\mathbf{w}$ is the velocity of the interface. Image inspired from [13].

Writing a dynamic boundary condition for the ice-bedrock interface is less straightforward. Continuity of the stress tensor requires the knowledge of the stress state inside the bedrock, which is not available. Therefore empirical sliding laws are used. They express tangential basal stress $\mathbf{t}_\tau$ in terms of the tangential basal sliding velocity $\mathbf{v}_\tau$. There are several possible friction laws that can be considered.

- Classical Coulomb law:

$$||\mathbf{t}_\tau|| \leq \nu_b|\sigma_n|, \qquad \mathbf{t}_\tau = \begin{cases} -\nu_b|\sigma_n|\dfrac{\mathbf{v}_\tau}{||\mathbf{v}_\tau||} & \text{if } \mathbf{v}_\tau \neq \mathbf{0} \\ \mathbf{0} & \text{if } \mathbf{v}_\tau = \mathbf{0}, \end{cases} \tag{2.21}$$

- Slip-rate dependent sliding law:

$$||\mathbf{t}_\tau|| \leq \nu_b\left(||\mathbf{v}_\tau||\right)|\sigma_n|, \qquad \mathbf{t}_\tau = \begin{cases} -\nu_b\left(||\mathbf{v}_\tau||\right)|\sigma_n|\dfrac{\mathbf{v}_\tau}{||\mathbf{v}_\tau||} & \text{if } \mathbf{v}_\tau \neq \mathbf{0} \\ \mathbf{0} & \text{if } \mathbf{v}_\tau = \mathbf{0}. \end{cases} \tag{2.22}$$

where ν_b is the friction coefficient. It is a property of the bedrock. The amplitude of the normal stress is denoted $|\sigma_n|$. Physically the Coulomb law means that as long as the tangential basal does not exceed a certain threshold the glacier does not move. And the friction force is exactly the force needed to prevent the ice from moving. As soon as the the ice starts to move the friction force reaches a plateau. It is important to note that the friction force always opposes the movement.

- Weertman type friction law:

$$\mathbf{t}_\tau = \begin{cases} -C||\mathbf{v}_\tau||^{m-1}\mathbf{v}_\tau & \text{if } \mathbf{v}_\tau \neq \mathbf{0} \\ \mathbf{0} & \text{if } \mathbf{v}_\tau = \mathbf{0}. \end{cases} \tag{2.23}$$

The Weertman friction law is the most commonly used friction law in glaciology. For sliding on hard rock the friction exponent m is usually set to $1/3$. The friction coefficient is found by solving an inverse problem. That means it is not constant across the ice sheet. However, the friction force is not explicitly written as a function of the normal force as it is the case for the Coulomb friction law. Which is surprising, given the fact that ice thickness is absolutely not homogeneous throughout the ice sheet. Intuitively, the friction force in a certain point should be related to the weight of the ice column above it. Moreover, it gives rise to a potentially problematic discontinuity of the basal stress across the grounding line. This point will be discussed in chapter 4.

These were all local friction laws. The friction force at one certain point only depends on what happens at that point. It is also possible to write non-local friction laws. Their study exceeds the scope of this work.

Similar to condition 2.20 one can impose a kinematic boundary condition at the ice-bedrock interface.

$$(\mathbf{w} - \mathbf{v}) \cdot \mathbf{n} = -a_b, \tag{2.24}$$

where a_b is positive. It takes the melting at Γ_b into account.

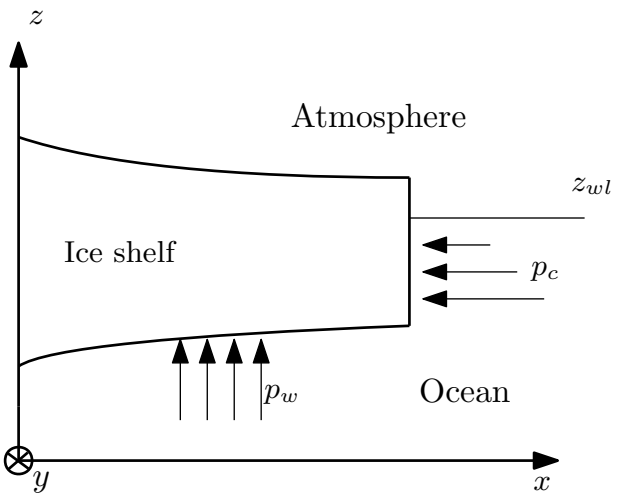

Figure 2.5: Zoom on the ice shelf with focus on the boundary conditions: p_c is the water pressure at the calving front, p_w is the water pressure at the ice-water interface.

At the ice-water interface Γ_w stress tensor continuity with water pressure serves as dynamic boundary condition and a mass balance is imposed as well.

$$\begin{cases} (-\pi \mathbb{I} + \boldsymbol{\sigma}) \cdot \mathbf{n} = -p_w \mathbf{n} \\ (\mathbf{w} - \mathbf{v}) \cdot \mathbf{n} = -a_w, \end{cases} \tag{2.25}$$

where p_w is the water pressure and $a_w \geq 0$ translates the sub-shelf melting at the ice-water interface.

At the calving front Γ_c a dynamic boundary condition is provided by the hydrostatic pressure distribution and a kinematic condition is given by imposing a calving rate. An evolution equation for the calving front position can be derived from the latter.

$$\begin{cases} (-\pi \mathbb{I} + \boldsymbol{\sigma}_c) \cdot \mathbf{n} = -\pi_c \mathbf{n} \\ c = (\mathbf{w} - \mathbf{v}) \cdot \mathbf{n}, \end{cases} \tag{2.26}$$

where $\boldsymbol{\sigma}^c$ denotes the stress tensor evaluated at the calving front and the pressure at the calving front p^c is given by

$$\pi_c = \begin{cases} 0 \text{ if } z > z_{wl} \\ \rho_w g (z_{sl} - z) \text{ if } z \leq z_{wl}, \end{cases} \tag{2.27}$$

where $\rho_w > \rho$ denotes the density of sea-water and z_{wl} is the sea level. It is often used as a reference for the vertical coordinate, such that the equations degenerate to simpler expressions.

One of the major challenges in glaciology is the identification of the grounding line position. One possibility is to solve a contact problem as proposed by Durand et al. [21]. The contact conditions express that the ice base cannot enter the bedrock. If the ice touches the bedrock it is grounded and the overburden pressure is larger than zero. If the ice is floating the overburden pressure vanishes and the ice base is above the bedrock. The overburden pressure is the difference between the basal normal stress, positive in compression, and sea water pressure. For the reduced order model, finding the position of the grounding line reduces to a simple flotation condition. Both possibilities will be discussed in later chapters.

Chapter 3

Reduced model: The fast sliding ice regime

Reduced order models can be deduced from the Stokes equations, describing the mechanical behaviour of the ice sheet, through studying the behaviour of the equations when the aspect ratio tends to zero in certain scaling regimes. This chapter is dedicated to the derivation of a simplified model in a fast sliding regime, where membrane stresses dominate over shear stresses and the fluid's motion is due to sliding rather than shearing. We restrict our study to a two dimensional ice sheet. Ultimately, the reduced model is expressed under form of an ice thickness equation and a vertically integrated horizontal momentum balance equation, that can be solved for the ice thickness and horizontal velocity. The latter can be integrated to obtain the ice discharge rate. The grounded part and the floating part of the ice are still treated separately. The position of the grounding line can be directly be obtained from the flotation condition. In later chapters the same problem will be rewritten as an obstacle problem over the entire domain, where the contact conditions determine the location of the grounding line.

Section 3.1 summarizes the equations to be solved for the full mechanical model. In section 3.2 the problem is formulated in cartesian coordinates and particularized to the two dimensional case. In section 3.3 the equations are written in dimensionless form. It is followed by the presentation of the vertically integrated equations in section 3.4. In section 3.5 the equations are particularized to the case of fast sliding. In section 3.6 we come back to the original variables and complete the reduced model with suitable boundary conditions.

Such reduced models are commonly employed in glaciology [13]. Maarten Arnst and Kevin Bulthuis rederived the reduced model by employing methods from applied mathematics for shallow non-Newtonian flows [22]. This chapter is strongly inspired by their work. A large part of the calculation steps were kept since the derivation is done differently than in [13]. For more information on perturbation methods see [23]. The reader only interested in the final version of the reduced model can directly jump to section 3.6.

3.1 Summary of the mechanical problem

The mechanical behaviour of ice sheets is governed by the Stokes equations of an incompressible non-Newtonian fluid with moving boundaries flowing under the effect of gravity, as described in previous chapters. If the problem is assumed isothermal it can be summarized as solving the following equations:

- Stokes equations in $\Omega(t)$:

$$-\nabla_{\mathbf{x}}\pi + \mathrm{div}_{\mathbf{x}}\boldsymbol{\sigma} + \rho\mathbf{g} = \mathbf{0}, \tag{3.1a}$$
$$\mathrm{div}_{\mathbf{x}}\mathbf{v} = 0, \tag{3.1b}$$

- Non-Newtonian fluid in $\Omega(t)$:

$$\boldsymbol{\sigma} = 2\eta_0(\sqrt{2}||\mathbf{D}||_{\mathrm{F}})^{1/n-1}\mathbf{D}, \tag{3.2a}$$
$$\mathbf{D} = \frac{1}{2}(\nabla_{\mathbf{x}}\mathbf{v} + \nabla_{\mathbf{x}}\mathbf{v}^T), \tag{3.2b}$$

- Upper free surface at $\Gamma_s(t)$:

$$(-\pi\mathbb{I} + \boldsymbol{\sigma})(\mathbf{n}) = \mathbf{0}, \tag{3.3}$$

- Non-linear friction at $\Gamma_b(t)$:

$$\mathbf{v}_\tau = -c_b||\mathbf{t}_\tau||^{m-1}||\mathbf{t}_\tau||, \tag{3.4a}$$
$$-\mathbf{v}\cdot\mathbf{n} = -a_b, \tag{3.4b}$$

- Water pressure at $\Gamma_w(t)$:

$$(-\pi\mathbb{I} + \boldsymbol{\sigma})(\mathbf{n}) = -\pi_w\mathbf{n}, \tag{3.5}$$

- Boundary evolution

$$(\mathbf{w} - \mathbf{v})\cdot\mathbf{n} = a_s \quad \text{at } \Gamma_s(t), \tag{3.6a}$$
$$\mathbf{w}\cdot\mathbf{n} = 0 \quad \text{at } \Gamma_b(t), \tag{3.6b}$$
$$(\mathbf{w} - \mathbf{v})\cdot\mathbf{n} = -a_w \quad \text{at } \Gamma_w(t). \tag{3.6c}$$

Note that the bedrock is assumed to be fixed and without melting as is expressed by equation 3.6b. Moreover, the calving front is not considered.

3.2 In cartesian coordinates

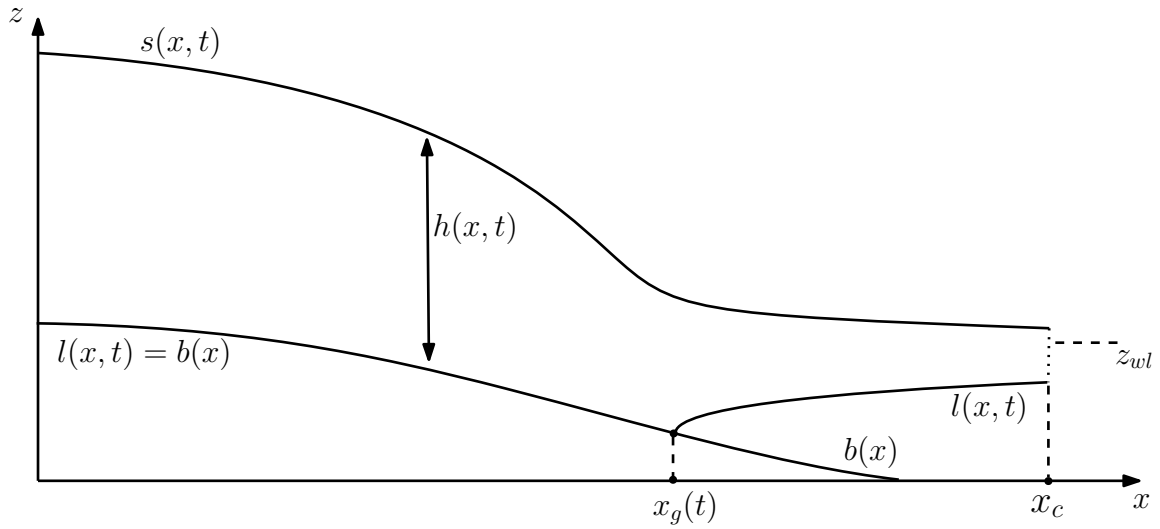

Figure 3.1: Schematic representation of the 1D problem.

A 2D coordinate system is defined, where the x-axis and the z-axis are placed as shown in figure 3.1. The functions $s(x,t)$, $h(x,t)$, $l(x,t)$, $b(x)$ and $x_c(t)$ are the functions describing the evolution of the upper ice surface, the ice thickness, the lower ice surface, the bedrock elevation and the grounding line position. Rigorously, the boundaries of $\Omega(t)$ are defined as:

$$\Gamma_s(t) \equiv \{(x,z) : z = s(x,t)\}, \tag{3.7}$$
$$\Gamma_b(t) \equiv \{(x,z) : z = l(x,t) = b(x),\ x < x_g(t)\}, \tag{3.8}$$
$$\Gamma_w(t) \equiv \{(x,z) : z = l(x,t),\ x > x_g(t)\}. \tag{3.9}$$

In cartesian coordinates the system writes:

- Stokes equations in $\Omega(t)$:

$$-\frac{\partial \pi}{\partial x} + \frac{\partial \sigma_{xx}}{\partial x} + \frac{\partial \sigma_{xz}}{\partial z} = 0, \tag{3.10a}$$
$$-\frac{\partial \pi}{\partial z} + \frac{\partial \sigma_{xz}}{\partial x} + \frac{\partial \sigma_{zz}}{\partial z} = 0, \tag{3.10b}$$
$$\frac{\partial u}{\partial x} + \frac{\partial w}{\partial z} = 0, \tag{3.10c}$$

- Non-Newtonian fluid in $\Omega(t)$:

$$\begin{pmatrix} \sigma_{xx} & \sigma_{xz} \\ \sigma_{xz} & \sigma_{zz} \end{pmatrix} = 2\eta_0 \left(\sqrt{4\left|\frac{\partial u}{\partial x}\right|^2 + \left|\frac{\partial u}{\partial z} + \frac{\partial w}{\partial x}\right|^2} \right)^{1/n-1} \begin{pmatrix} \frac{\partial u}{\partial x} & \frac{1}{2}\left(\frac{\partial u}{\partial z} + \frac{\partial w}{\partial z}\right) \\ \frac{1}{2}\left(\frac{\partial u}{\partial z} + \frac{\partial w}{\partial z}\right) & \frac{\partial w}{\partial z} \end{pmatrix}, \tag{3.11}$$

- Ice-air interface at $\Gamma_s(t)$:

$$\pi(s)\left(\frac{\partial s}{\partial x}\right) - \sigma_{xx}(s)\left(\frac{\partial s}{\partial x}\right) + \sigma_{xz}(s) = 0, \tag{3.12a}$$
$$-\sigma_{xz}(s)\left(\frac{\partial s}{\partial x}\right) - \pi(s) + \sigma_{zz}(s) = 0, \tag{3.12b}$$
$$\frac{\partial s}{\partial t} + u(s)\frac{\partial s}{\partial x} - w(s) = \sqrt{1 + \left|\frac{\partial s}{\partial x}\right|^2}\, a_s, \tag{3.12c}$$

- Ice-bedrock interface at $\Gamma_b(t)$:

$$u(l) + w(l)\frac{\partial l}{\partial x} = c_b \frac{\left|\sigma_{xz}\left(1 - \left|\frac{\partial l}{\partial x}\right|^2\right) - 2\sigma_{xx}\frac{\partial l}{\partial x}\right|^{m-1}}{\left(1 + \left|\frac{\partial l}{\partial x}\right|^2\right)^{m-1/2}} \left(\sigma_{xz}\left(1 - \left|\frac{\partial l}{\partial x}\right|^2\right) - 2\sigma_{xx}\frac{\partial l}{\partial x}\right), \tag{3.13a}$$

$$\frac{\partial l}{\partial t} + u(l)\frac{\partial l}{\partial x} - w(l) = \sqrt{1 + \left|\frac{\partial l}{\partial x}\right|^2}\, a_b, \tag{3.13b}$$

- Ice-water interface at $\Gamma_w(t)$:

$$-\pi(s)\left(\frac{\partial l}{\partial x}\right)+\sigma_{xx}(l)\left(\frac{\partial l}{\partial x}\right)-\sigma_{xz}(l)=-\rho_w g(z_{wl}-l)\frac{\partial l}{\partial x}, \tag{3.14a}$$

$$\sigma_{xz}(l)\left(\frac{\partial l}{\partial x}\right)+\pi(l)-\sigma_{zz}(l)=\rho_w g(z_{wl}-l), \tag{3.14b}$$

$$\frac{\partial l}{\partial t}+u(l)\frac{\partial l}{\partial x}-w(l)=\sqrt{1+\left|\frac{\partial l}{\partial x}\right|^2}a_w. \tag{3.14c}$$

3.3 Adimensionalization

Let L be a typical horizontal length scale of the problem and H a typical vertical scale. Furthermore, let U be a reference horizontal velocity. An aspect ratio is defined as $\epsilon = H/L$, assumed small in the present case. Coordinates x, z and t, as well as unknowns u, w, π, s, l and parameters a_s, a_b, a_w are nondimensionalized:

$$\begin{aligned}
&\tilde{x}=\frac{x}{L}, \qquad \tilde{z}=\frac{z}{\epsilon L}, \qquad \tilde{t}=\frac{t}{\frac{L}{U}},\\
&\tilde{u}=\frac{u}{U}, \qquad \tilde{w}=\frac{w}{\epsilon U}, \qquad \tilde{p}=\frac{\pi}{\rho g H},\\
&\tilde{s}=\frac{s}{H}, \qquad \tilde{l}=\frac{b}{H}, \qquad \tilde{a_s}=\frac{a_s}{\epsilon U}\\
&\tilde{a_b}=\frac{a_b}{\epsilon U}, \qquad \tilde{a_w}=\frac{a_w}{\epsilon U}.
\end{aligned}$$

Inserting these into the governing equations and adapting the differential operators one obtains the adimensional version of the problem. First, note that the strain rate expressed in adimensional variables writes

$$\tilde{\gamma}=\sqrt{4\epsilon^2\left|\frac{\partial \tilde{u}}{\partial \tilde{x}}\right|^2+\left|\frac{\partial \tilde{u}}{\partial \tilde{z}}+\epsilon^2\frac{\partial \tilde{w}}{\partial \tilde{x}}\right|^2}. \tag{3.15}$$

Then the problem can be summarized as:

- Stokes equation in $\Omega(\tilde{t})$:

$$\frac{\partial}{\partial \tilde{z}}\left(\tilde{\gamma}^{1/n-1}\frac{\partial \tilde{u}}{\partial \tilde{z}}\right)=\epsilon\frac{Re}{Fr^2}\frac{\partial \tilde{p}}{\partial \tilde{x}}-\epsilon^2\left(\frac{\partial}{\partial \tilde{x}}\left(2\tilde{\gamma}^{1/n-1}\frac{\partial \tilde{u}}{\partial \tilde{x}}\right)+\frac{\partial}{\partial \tilde{z}}\left(\tilde{\gamma}^{1/n-1}\frac{\partial \tilde{w}}{\partial \tilde{x}}\right)\right), \tag{3.16a}$$

$$\epsilon\frac{\partial}{\partial \tilde{z}}\left(2\tilde{\gamma}^{1/n-1}\frac{\partial \tilde{w}}{\partial \tilde{z}}\right)-\frac{Re}{Fr^2}\frac{\partial \tilde{p}}{\partial \tilde{z}}+\frac{Re}{Fr^2}=-\epsilon\left(\tilde{\gamma}^{1/n-1}\left(\frac{\partial \tilde{u}}{\partial \tilde{z}}+\epsilon^2\frac{\partial \tilde{w}}{\partial \tilde{x}}\right)\right), \tag{3.16b}$$

$$\frac{\partial \tilde{u}}{\partial \tilde{x}}+\frac{\partial \tilde{w}}{\partial \tilde{z}}=0, \tag{3.16c}$$

- Non-Newtonian fluid in $\Omega(\tilde{t})$:

$$\begin{pmatrix}\sigma_{xx} & \sigma_{xz}\\ \sigma_{xz} & \sigma_{zz}\end{pmatrix}=2\eta_0\frac{U^{1/n}}{H^{1/n}}\tilde{\gamma}^{1/n-1}\begin{pmatrix}\epsilon\frac{\partial \tilde{u}}{\partial \tilde{x}} & \frac{1}{2}\left(\frac{\partial \tilde{u}}{\partial \tilde{z}}+\frac{\partial \tilde{w}}{\partial \tilde{z}}\right)\\ \frac{1}{2}\left(\frac{\partial \tilde{u}}{\partial \tilde{z}}+\frac{\partial \tilde{w}}{\partial \tilde{z}}\right) & \epsilon\frac{\partial \tilde{w}}{\partial \tilde{z}}\end{pmatrix}, \tag{3.17}$$

- Ice-air interface at $\Gamma_{\tilde{s}}(\tilde{t})$:

$$\epsilon\frac{Re}{Fr^2}\tilde{p}(\tilde{s})\frac{\partial\tilde{s}}{\partial\tilde{x}} - \epsilon^2 2\tilde{\gamma}^{1/n-1}(\tilde{s})\frac{\partial\tilde{u}}{\partial\tilde{x}}(\tilde{s}) + \tilde{\gamma}^{1/n-1}(\tilde{s})\left(\frac{\partial\tilde{u}}{\partial\tilde{z}} + \epsilon^2\frac{\partial\tilde{w}}{\partial\tilde{x}}\right) = 0, \tag{3.18a}$$

$$-\epsilon\tilde{\gamma}^{1/n-1}(\tilde{s})\left(\frac{\partial\tilde{u}}{\partial\tilde{z}} + \epsilon^2\frac{\partial\tilde{w}}{\partial\tilde{x}}\right)\frac{\partial\tilde{s}}{\partial\tilde{x}} - \frac{Re}{Fr^2}\tilde{p}(\tilde{s}) + \epsilon 2\tilde{\gamma}^{1/n-1}(\tilde{s})\frac{\partial\tilde{w}}{\partial\tilde{z}}(\tilde{s}) = 0, \tag{3.18b}$$

$$\frac{\partial\tilde{s}}{\partial t} + \tilde{u}(\tilde{s})\frac{\partial\tilde{s}}{\partial x} - \tilde{w}(\tilde{s}) = \sqrt{1+\epsilon^2\left|\frac{\partial\tilde{s}}{\partial x}\right|^2}\,\tilde{a}_S, \tag{3.18c}$$

- Ice-bedrock interface at $\Gamma_{\tilde{b}}(\tilde{t})$:

$$\begin{aligned}\tilde{\gamma}^{1/n-1}(\tilde{l})\left(\frac{\partial\tilde{u}}{\partial\tilde{z}}(\tilde{l}) + \epsilon^2\frac{\partial\tilde{w}}{\partial\tilde{x}}(\tilde{l})\right)\left(1-\epsilon^2\left|\frac{\partial\tilde{l}}{\partial\tilde{x}}\right|^2\right) + 2\tilde{\gamma}^{1/n-1}(\tilde{l})\epsilon\frac{\partial\tilde{u}}{\partial\tilde{x}}(\tilde{l})\,(-2\epsilon)\,\frac{\partial\tilde{l}}{\partial\tilde{x}} \\ = C^{-1/m}\left(\tilde{u}(\tilde{l}) + \epsilon^2\tilde{w}(\tilde{l})\frac{\partial\tilde{l}}{\partial\tilde{x}}\right)^{1/m-1}\left(1+\epsilon^2\left|\frac{\partial\tilde{l}}{\partial\tilde{x}}\right|^2\right)^{1-1/2m},\end{aligned} \tag{3.19a}$$

$$\frac{\partial\tilde{l}}{\partial\tilde{t}} + \tilde{u}(\tilde{l})\frac{\partial\tilde{l}}{\partial\tilde{x}} - \tilde{w}(\tilde{l}) = \sqrt{1+\epsilon^2\left|\frac{\partial\tilde{l}}{\partial\tilde{x}}\right|^2}\,\tilde{a}_b, \tag{3.19b}$$

- Ice-water interface at $\Gamma_{\tilde{l}}(\tilde{t})$:

$$\epsilon\frac{Re}{Fr^2}\tilde{p}(\tilde{l}) - \epsilon^2 2\tilde{\gamma}^{1/n-1}(\tilde{l})\frac{\partial\tilde{u}}{\partial\tilde{x}}(\tilde{l})\frac{\partial\tilde{l}}{\partial\tilde{x}} + \tilde{\gamma}^{1/n-1}\left(\frac{\partial\tilde{u}}{\partial\tilde{z}}(\tilde{l}) + \epsilon^2\frac{\partial\tilde{w}}{\partial\tilde{x}}(\tilde{l})\right) = \epsilon\frac{Re}{Fr^2}\frac{\rho_w}{\rho}(\tilde{z}_{wl} - \tilde{l})\frac{\partial\tilde{l}}{\partial\tilde{x}} \tag{3.20a}$$

$$-\epsilon\tilde{\gamma}^{1/n-1}\left(\frac{\partial\tilde{u}}{\partial\tilde{z}}(\tilde{l}) + \epsilon^2\frac{\partial\tilde{w}}{\partial\tilde{x}}(\tilde{l})\right)\frac{\partial\tilde{l}}{\partial\tilde{x}} - \epsilon\frac{Re}{Fr^2}\tilde{p}(\tilde{l}) + \epsilon 2\tilde{\gamma}^{1/n-1}(\tilde{l})\frac{\partial\tilde{w}}{\partial\tilde{z}}(\tilde{l}) = -\frac{Re}{Fr^2}\alpha(\tilde{z}_{sl} - \tilde{l}) \tag{3.20b}$$

$$\frac{\partial\tilde{l}}{\partial\tilde{t}} + \tilde{u}(\tilde{l})\frac{\partial\tilde{l}}{\partial\tilde{x}} - \tilde{w}(\tilde{l}) = \sqrt{1+\epsilon^2\left|\frac{\partial\tilde{l}}{\partial\tilde{x}}\right|^2}\,\tilde{a}_w. \tag{3.20c}$$

Two non-dimensional numbers appear naturally. The Reynolds number and the square of the Froude number. They are defined as

$$Re = \frac{\rho U^{2-1/n}H^{1/n}}{\eta_0}, \qquad Fr = \frac{U}{\sqrt{gH}}.$$

The first compares the relative importance of inertial and viscous effects in the studied flow. The second compares the relative importance of inertia and gravity. In equation 3.19a a non-dimensional friction coefficient is introduced

$$C = c_b\frac{\eta_0 U^{m/n-1}}{H^{m/n}}.$$

3.4 Exact thickness integrated equations

The continuity equation 3.16c and the horizontal momentum equation 3.16a can be integrated vertically along the ice thickness. Using Leibniz' formula, and introducing the upper kinematic 3.18c and horizontal dynamic boundary conditions 3.18a as well as the lower kinematic

boundary condition 3.19b one obtains.

$$\frac{\partial(\tilde{s}-\tilde{l})}{\partial\tilde{t}}+\frac{\partial}{\partial\tilde{x}}\int_{\tilde{l}}^{\tilde{s}}\tilde{u}(\tilde{z})\mathrm{d}\tilde{z}=\sqrt{1+\epsilon^2\left|\frac{\partial\tilde{s}}{\partial\tilde{x}}\right|^2}\tilde{a}_s-\sqrt{1+\epsilon^2\left|\frac{\partial\tilde{l}}{\partial\tilde{x}}\right|^2}\tilde{a}, \tag{3.21a}$$

$$\begin{aligned}\epsilon\frac{Re}{Fr^2}\frac{\partial}{\partial\tilde{x}}\int_{\tilde{l}}^{\tilde{s}}\tilde{p}\mathrm{d}\tilde{z}+\epsilon\frac{Re}{Fr^2}\tilde{p}(\tilde{l})\frac{\partial\tilde{l}}{\partial\tilde{x}}-\gamma^{1/n-1}(\tilde{l})\left(\frac{\partial\tilde{u}}{\partial\tilde{z}}(\tilde{l})+\epsilon^2\frac{\partial\tilde{w}}{\partial\tilde{x}}(\tilde{l})\right)\\ =\epsilon^2 2\tilde{\gamma}^{1/n-1}(\tilde{l})\frac{\partial\tilde{u}}{\partial\tilde{x}}(\tilde{l})\frac{\partial\tilde{l}}{\partial\tilde{x}}+\epsilon^2\frac{\partial}{\partial\tilde{x}}\int_{\tilde{l}}^{\tilde{s}}2\tilde{\gamma}^{1/n-1}\frac{\partial\tilde{u}}{\partial\tilde{x}}\mathrm{d}\tilde{z},\end{aligned} \tag{3.21b}$$

where $\tilde{a}=\tilde{a}_b$ if the ice grounded and $\tilde{a}=\tilde{a}_l$ if it is floating. Since the boundary conditions differ from one case to the other, the governing equations for both parts are different as well. Indeed, inserting the lower dynamic boundary condition 3.20b into the vertically integrated momentum equation 3.21b leads to the following system valid when the ice is floating:

$$\frac{\partial(\tilde{s}-\tilde{l})}{\partial\tilde{t}}+\frac{\partial}{\partial\tilde{x}}\int_{\tilde{l}}^{\tilde{s}}\tilde{u}(\tilde{z})\mathrm{d}\tilde{z}=\sqrt{1+\epsilon^2\left|\frac{\partial\tilde{s}}{\partial\tilde{x}}\right|^2}\tilde{a}_s-\sqrt{1+\epsilon^2\left|\frac{\partial\tilde{l}}{\partial\tilde{x}}\right|^2}\tilde{a}_w, \tag{3.22a}$$

$$\epsilon\frac{Re}{Fr^2}\frac{\partial}{\partial\tilde{x}}\int_{\tilde{l}}^{\tilde{s}}\tilde{p}\mathrm{d}\tilde{z}=-\epsilon\frac{Re}{Fr^2}\alpha(\tilde{z}_{wl}-\tilde{l})\frac{\partial\tilde{l}}{\partial\tilde{x}}+\epsilon^2\frac{\partial}{\partial\tilde{x}}\int_{\tilde{l}}^{\tilde{s}}2\tilde{\gamma}^{m-1}\frac{\partial\tilde{u}}{\partial\tilde{x}}\mathrm{d}\tilde{z}. \tag{3.22b}$$

A similar system can be obtained for the ice resting on solid ground by inserting equation 3.19a into equation 3.21b one obtains the following system valid for grounded ice.

$$\frac{\partial(\tilde{s}-\tilde{l})}{\partial\tilde{t}}+\frac{\partial}{\partial\tilde{x}}\int_{\tilde{l}}^{\tilde{s}}\tilde{u}(\tilde{z})\mathrm{d}\tilde{z}=\sqrt{1+\epsilon^2\left|\frac{\partial\tilde{s}}{\partial\tilde{x}}\right|^2}\tilde{a}_s-\sqrt{1+\epsilon^2\left|\frac{\partial\tilde{l}}{\partial\tilde{x}}\right|^2}\tilde{a}_b, \tag{3.23a}$$

$$\begin{aligned}&\epsilon\frac{Re}{Fr^2}\frac{\partial}{\partial\tilde{x}}\int_{\tilde{l}}^{\tilde{s}}\tilde{p}\mathrm{d}\tilde{z}=-\epsilon\frac{Re}{Fr^2}\tilde{p}(\tilde{l})\frac{\partial\tilde{l}}{\partial\tilde{x}}\\ &+C^{-1/m}\left(\tilde{u}(\tilde{l})+\epsilon^2\tilde{w}(\tilde{l})\frac{\partial\tilde{l}}{\partial\tilde{x}}\right)^{1/m-1}\left(1+\epsilon^2\left|\frac{\partial\tilde{l}}{\partial\tilde{x}}\right|^2\right)^{1-1/2m}\\ &+\gamma^{1/n-1}(\tilde{l})\epsilon^2\frac{\partial\tilde{w}}{\partial\tilde{x}}(\tilde{l})+\epsilon^2\frac{\partial}{\partial\tilde{x}}\int_{\tilde{l}}^{\tilde{s}}2\tilde{\gamma}^{1/n-1}\frac{\partial\tilde{u}}{\partial\tilde{x}}\mathrm{d}\tilde{z}\\ &+2\epsilon^2\tilde{\gamma}^{m-1}(\tilde{l})\frac{\partial\tilde{u}}{\partial\tilde{x}}(\tilde{l})\frac{\partial\tilde{l}}{\partial\tilde{x}}.\end{aligned} \tag{3.23b}$$

3.5 Scaled problem

Different scaling regimes can be identified. Under the hypothesis of fast sliding ice sheets one has that

$$\frac{Re}{Fr^2}\approx\epsilon, \tag{3.24}$$

where one should keep in mind that ϵ is the aspect ratio, which compares vertical and horizontal length scales. For marine ice sheets it is approximately 10^{-3}. Indeed we have that

$$\frac{Re}{Fr^2}=\frac{\rho g H^{1/n+1}}{\eta_0 U^{1/n}}. \tag{3.25}$$

Thus for 3.24 to hold the velocity at the denominator must be sufficiently large. Hence we speak of a rapid scaling regime. Note that in this scaling regime the horizontal momentum equation indicates that $\frac{\partial \tilde{u}}{\partial \tilde{x}} = O(\epsilon^2)$ and the deviatoric stress tensor writes

$$\begin{pmatrix} \sigma_{xx} & \sigma_{xz} \\ \sigma_{xz} & \sigma_{zz} \end{pmatrix} = 2\rho g H \frac{\epsilon}{\frac{Re}{Fr^2}} \tilde{\gamma}^{1/n-1} \begin{pmatrix} \frac{\partial \tilde{u}}{\partial \tilde{x}} & \frac{\epsilon}{2}\left(\frac{1}{\epsilon^2}\frac{\partial \tilde{u}}{\partial \tilde{z}} + \frac{\partial \tilde{w}}{\partial \tilde{z}}\right) \\ \frac{\epsilon}{2}\left(\frac{1}{\epsilon^2}\frac{\partial \tilde{u}}{\partial \tilde{z}} + \frac{\partial \tilde{w}}{\partial \tilde{z}}\right) & \frac{\partial \tilde{w}}{\partial \tilde{z}} \end{pmatrix}, \tag{3.26}$$

therefore shear stress is much smaller than the normal stress components of the deviatoric stress tensor. Assuming a solution for $\tilde{u}$, $\tilde{w}$ and $\tilde{p}$ in the form of a power series of ϵ and keeping only the leading order terms leads to

- Stokes equations in $\Omega(\tilde{t})$:

$$\frac{\partial}{\partial \tilde{z}}\left(\left|\frac{\partial \tilde{u}}{\partial \tilde{x}}\right|^{1/n-1}\frac{\partial \tilde{u}}{\partial \tilde{z}}\right) = 0, \tag{3.27a}$$

$$\epsilon\frac{Re}{Fr^2}\frac{\partial}{\partial \tilde{z}}\left(2(2\epsilon)^{1/n-1}\left|\frac{\partial \tilde{u}}{\partial \tilde{x}}\right|^{1/n-1}\frac{\partial \tilde{w}}{\partial \tilde{z}}\right) - \frac{\partial \tilde{p}}{\partial \tilde{z}} - 1 = 0, \tag{3.27b}$$

$$\frac{\partial \tilde{u}}{\partial \tilde{x}} + \frac{\partial \tilde{w}}{\partial \tilde{z}} = 0 \tag{3.27c}$$

- Ice-air interface at $\Gamma_{\tilde{s}}(\tilde{t})$:

$$\left|\frac{\partial \tilde{u}}{\partial \tilde{x}}(\tilde{s})\right|^{1/n-1}\frac{\partial \tilde{u}}{\partial \tilde{z}}(\tilde{s}) = 0, \tag{3.28a}$$

$$\epsilon\frac{Re}{Fr^2}2(2\epsilon)^{1/n-1}\left|\frac{\partial \tilde{u}}{\partial \tilde{x}}(\tilde{s})\right|^{1/n-1}\frac{\partial \tilde{w}}{\partial \tilde{z}}(\tilde{s}) - \tilde{p}(\tilde{s}) = 0, \tag{3.28b}$$

$$\frac{\partial \tilde{s}}{\partial t} + \tilde{u}(\tilde{s})\frac{\partial \tilde{s}}{\partial \tilde{x}} - \tilde{w}(\tilde{s}) = \tilde{a}_s \tag{3.28c}$$

Only the leading order terms were kept. Depending if the ice sheet is grounded or floats, the lower boundary condition differs. Let us first derive the common features of a fast sliding ice regime. Both the grounded and floating ice are characterized by a velocity independent of the vertical coordinate. In other words: there is no shearing deformation, since horizontal equilibrium and the horizontal dynamic boundary condition at the surface yield

$$\frac{\partial \tilde{u}}{\partial \tilde{z}} = 0. \tag{3.29}$$

Vertical momentum and the vertical dynamic boundary condition indicate that the vertical normal stress field is hydrostatic. Indeed one has by combining the two equations

$$-\epsilon\frac{Re}{Fr^2}2(2\epsilon)^{m-1}\left|\frac{\partial \tilde{u}}{\partial \tilde{x}}(\tilde{z})\right|^{1/n-1}\frac{\partial \tilde{w}}{\partial \tilde{z}}(\tilde{z}) + \tilde{p}(\tilde{z}) = \tilde{s} - \tilde{z}. \tag{3.30}$$

For floating ice the lower boundary condition at first order writes

- Ice-water interface at $\Gamma_{\tilde{l}}(\tilde{t})$:

$$\epsilon\frac{Re}{Fr^2}\tilde{p}(\tilde{l})\frac{\partial\tilde{l}}{\partial\tilde{x}}+\epsilon^2(2\epsilon)^{1/n-1}\left|\frac{\partial\tilde{u}}{\partial\tilde{x}}(\tilde{l})\right|\left(-2\frac{\partial\tilde{u}}{\partial\tilde{x}}(\tilde{l})\frac{\partial\tilde{l}}{\tilde{x}}+\frac{\partial\tilde{w}}{\partial\tilde{x}}(\tilde{l})\right)=\epsilon\frac{Re}{Fr^2}\alpha(\tilde{z}_{sl}-\tilde{l})\frac{\partial\tilde{l}}{\partial\tilde{x}}, \tag{3.31a}$$

$$\epsilon\frac{Re}{Fr^2}2(2\epsilon)^{1/n-1}\left|\frac{\partial\tilde{u}}{\partial\tilde{x}}(\tilde{l})\right|^{1/n-1}\frac{\partial\tilde{w}}{\partial\tilde{z}}(\tilde{l})-\tilde{p}(\tilde{l})=-\alpha(\tilde{z}_{sl}-\tilde{l}), \tag{3.31b}$$

$$\frac{\partial\tilde{l}}{\partial t}+\tilde{u}(\tilde{l})\frac{\partial\tilde{s}}{\partial\tilde{x}}-\tilde{w}(\tilde{l})=\tilde{a}_w. \tag{3.31c}$$

Knowing the hydrostatic stress distribution of the vertical normal stress one can rewrite the vertical dynamic boundary condition at the ice-water interface as the flotation condition

$$\tilde{l}=\tilde{z}_{sl}-\frac{1}{\alpha}(\tilde{s}-\tilde{l}), \tag{3.32}$$

which simply translates Archimedes' principle. Introducing 3.29, 3.30 and 3.32 into 3.22a and 3.22b vertically integrated continuity and horizontal momentum balance reduce at leading order to

$$\frac{\partial(\tilde{s}-\tilde{l})}{\partial\tilde{t}}+\frac{\partial}{\partial\tilde{x}}(\tilde{u}(\tilde{s}-\tilde{l}))=\tilde{a}_s-\tilde{a}_w, \tag{3.33a}$$

$$-\epsilon^2\frac{\partial}{\partial\tilde{x}}\left(4(2\epsilon)^{m-1}(\tilde{s}-\tilde{l})\left|\frac{\partial\tilde{u}}{\partial\tilde{x}}\right|^{1/n-1}\frac{\partial\tilde{u}}{\partial\tilde{x}}\right)=-\epsilon\frac{Re}{Fr^2}(\tilde{s}-\tilde{l})\frac{\partial\tilde{s}}{\partial\tilde{x}}. \tag{3.33b}$$

It can be shown that the fast sliding ice approximation satisfies the zero-th order vertically integrated continuity equation up to an error or the order ϵ^2 and the thickness-averaged horizontal momentum equation up to an error or order ϵ^{m+3}. For grounded ice the lower boundary condition writes at leading order

- Ice-bedrock interface at $\Gamma_{\tilde{b}}(\tilde{t})$

$$\tilde{u}(\tilde{l})=C\left|\left|\frac{\partial\tilde{u}}{\partial\tilde{z}}(\tilde{l})\right|^{1/n-1}\frac{\partial\tilde{u}}{\partial\tilde{z}}(\tilde{l})\right|^{m-1}\left|\frac{\partial\tilde{u}}{\partial\tilde{z}}(\tilde{l})\right|^{n-1}\frac{\partial\tilde{u}}{\partial\tilde{z}}(\tilde{l}), \tag{3.34a}$$

$$\frac{\partial\tilde{l}}{\partial t}+\tilde{u}(\tilde{l})\frac{\partial\tilde{l}}{\partial\tilde{x}}-\tilde{w}(\tilde{l})=\tilde{a}_b. \tag{3.34b}$$

In a similar way as before the reduced form for the vertically integrated equations can be obtained by introducing 3.29, 3.30, 3.34b and 3.34a into 3.23a and 3.23b. They are given by

$$\frac{\partial(\tilde{s}-\tilde{l})}{\partial\tilde{t}}+\frac{\partial}{\partial\tilde{x}}(\tilde{u}(\tilde{s}-\tilde{l}))=\tilde{a}_s-\tilde{a}_B \tag{3.35a}$$

$$\begin{aligned}-\epsilon^2\frac{\partial}{\partial\tilde{x}}\left(4(2\epsilon)^{1/n-1}(\tilde{s}-\tilde{l})\left|\frac{\partial\tilde{u}}{\partial\tilde{x}}\right|^{1/n-1}\frac{\partial\tilde{u}}{\partial\tilde{x}}\right)+C^{-1/m}\left|\tilde{u}(\tilde{l})\right|^{1/m-1}\tilde{u}(\tilde{l})\\ =-\epsilon\frac{Re}{Fr^2}(\tilde{s}-\tilde{l})\frac{\partial\tilde{s}}{\partial\tilde{x}}-\epsilon^2 2(2\epsilon)^{1/n-1}\left|\frac{\partial\tilde{u}}{\partial\tilde{x}}\right|^{1/n-1}\frac{\partial\tilde{u}}{\partial\tilde{x}}\frac{\partial\tilde{l}}{\tilde{x}},\end{aligned} \tag{3.35b}$$

where the last term can be neglected if the variations of the bedrock profile are assumed to occur only over large horizontal length scales. This assumption is not necessary since this term is cancelled out in later stages of the development.

3.6 Complete reduced model

In this section we present the complete reduced model for a marine ice sheet that has the geometry of figure 3.1. It constitutes the setting in which will continue to work for the remainder of this document.

3.6.1 Governing equations

The equations derived in the previous section were written in dimensionless form. Coming back to the original variables and writing the problem in terms of the ice thickness $h = s - l$ and the net accumulation rate a yields

$$\left.\begin{aligned} &\frac{\partial h}{\partial t} + \frac{\partial}{\partial x}(hu) = a \\ &\frac{\partial}{\partial x}\left(2A^{-1/n} h \left|\frac{\partial u}{\partial x}\right|^{1/n-1} \frac{\partial u}{\partial x}\right) = \rho g h \frac{\partial (h+l)}{\partial x} + \underbrace{C^{-1/m}|u|^{1/m-1}u}_{\tau_B} \end{aligned}\right\} \quad \text{if } 0 \leq x \leq x_g(t) \tag{3.36}$$

$$\left.\begin{aligned} &\frac{\partial h}{\partial t} + \frac{\partial}{\partial x}(hu) = a \\ &\frac{\partial}{\partial x}\left(2A^{-1/n} h \left|\frac{\partial u}{\partial x}\right|^{1/n-1} \frac{\partial u}{\partial x}\right) = \rho g h \frac{\partial (h+l)}{\partial x} \end{aligned}\right\} \quad \text{if } x_g(t) < x \leq x_c(t) \tag{3.37}$$

The first equation in 3.37 and 3.36 is a non linear transport equation representing conservation of the ice mass. It is written in conservative form. The ice flux is $q = hu$. Ice moves under the effect of gravity and is accumulated or lost at the surfaces. As a consequence the ice thickness varies. The second equation in 3.37 and 3.36 translates horizontal force balance. The first term corresponds to the divergence of the stresses inside the ice, the second to the force of gravity. In the model for the grounded part an additional friction term appears.

3.6.2 Distinction between grounded and floating subdomains

Grounded and floating parts are distinguished using the flotation condition. The position of the grounding line is precisely the location where the mass of the ice column is exactly balanced out by buoyancy. Thus the ice thickness at the grounding line is imposed by the geometry of the bedrock. This can serve as a boundary condition if only the grounded part is considered. The condition writes:

$$\begin{cases} \rho h > -\rho_w l & \text{if } x < x_g \\ \rho h = -\rho_w l & \text{at } x = x_g \\ \rho h < -\rho_w l & \text{if } x > x_g \end{cases} \tag{3.38}$$

3.6.3 Boundary conditions

The reduced order model has to be completed by boundary conditions on the horizontal extremities of the ice sheet. As we restrict ourselves to the study of "half" an ice sheet that is symmetric at $x = 0$ we can assume that there no horizontal ice flux at the left boundary. Therefore we impose the following boundary condition:

$$u = 0 \qquad \text{at } x = 0. \tag{3.39}$$

It is both imposed on the transport equation and on the horizontal momentum equation.

Let us recall the boundary condition at the calving front that expresses the continuity of the stress tensor. It writes

$$(-\pi \mathbb{I} + \boldsymbol{\sigma}_{\mathbf{c}}) \cdot \mathbf{n} = -\pi_c \mathbf{n}, \qquad \text{at } x_c(t) \tag{3.40}$$

where π_c is the hydrostatic pressure acting on the calving front. If z_{wl} is chosen to be 0 it is

$$\pi_c = \begin{cases} 0 \text{ when } z \geq 0 \\ -\rho_w g z \text{ when } z < 0 \end{cases} \tag{3.41}$$

In the one dimensional case we simply have by introducing Glen's law 2.18:

$$2A^{-1/n} \left| \frac{\partial u}{\partial x} \right|^{1/n-1} \frac{\partial u}{\partial x} = \pi_h + \pi_c, \tag{3.42}$$

where π_h is the hydrostatic pressure inside the ice. Since for the shallow shelf approximation u is independent of z one can integrate this boundary condition vertically to obtain

$$2A^{-1/n} h \left| \frac{\partial u}{\partial x} \right|^{1/n-1} \frac{\partial u}{\partial x} = \frac{1}{2}(1 - \rho/\rho_w)\rho g h^2, \qquad \text{at } x_c(t). \tag{3.43}$$

3.6.4 Additional boundary condition at the grounding line

An additional boundary condition at the grounding line can be obtained by integrating the horizontal momentum equation for floating ice 3.37 from the grounding line to the calving front, thereby excluding the ice shelf from the study [24]. Only the grounded ice sheet needs to be considered. For that h, u and u_x have to be continuous at x_g. A boundary layer analysis in the transition zone between the grounded and the floating part indicates that it is indeed the case [3]. The boundary condition writes

$$2A^{-1/n} h_g \left| \frac{\partial u}{\partial x} \right|^{1/n-1} \frac{\partial u}{\partial x} = \frac{1}{2}\rho \left(1 - \frac{\rho}{\rho_w}\right) g h_g^2 \qquad \text{at } x = x_g. \tag{3.44}$$

Chapter 4

The marine ice sheet instability and steady states

It is expected that the contribution of the Antarctic ice sheet to sea level rise is going to increase substantially in the next centuries due to a potential collapse of the West Antarctic Ice Sheet (WAIS) [2] and [25]. This is due to the occurrence of Marine Ice Sheet Instabilities in these regions. They can destabilize ice sheets grounded below sea-level on an upward slope [3]. Such a situation appears to be the case in the West Antarctic Ice Sheet as can be seen in figure 4.1.

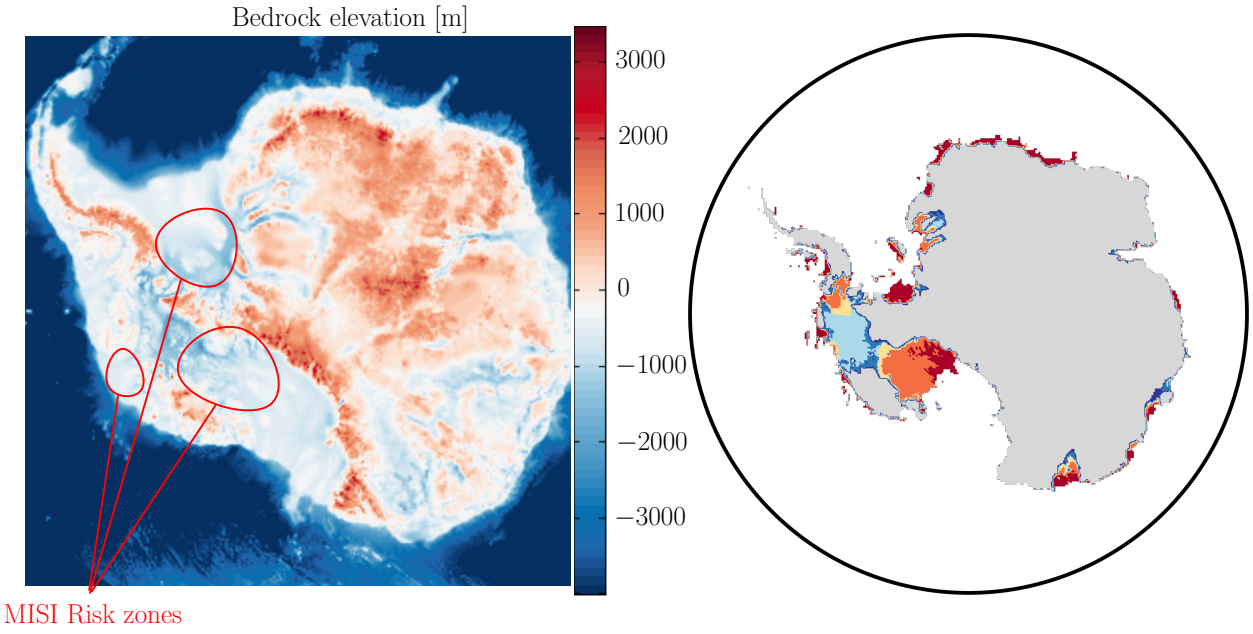

Figure 4.1: Left: Bedrock profile of the Antarctic ice sheet. Data adapted from [26]. Right: MISI risk map. Darker red tones indicate a higher probability of ice sheet collapse under certain conditions. For more details see [2]. Image taken from [2].

Often the existence of instability mechanisms is first discovered on paper by studying a mathematical model after being confirmed by observational data. This is also the case for the marine ice sheet instability (MISI). The first section of this chapter is dedicated to the mathematical illustration of how the MISI emerges from the reduced order model that was derived in the previous chapter. Moreover, this chapter presents some analytic results for the calculation of

steady state solutions. These are useful for comparing with numerical implementations. They can also be used as initial conditions in simulations.

We start by giving a general introduction to bifurcation mechanisms that can appear in complex climate systems in section 4.1. In section 4.2 the mechanism of the marine ice sheet instability is explained through some analytical arguments. It is first done for a power friction law. The same exercise is done for a Coulomb friction law in section 4.3. This chapter is mainly based on [24], [3] and [27]. .

4.1 Tipping points in climate systems

Marine Ice sheets are complex systems. Their behaviour is governed by non-linear partial differential equations. Under certain conditions they can exhibit a saddle point bifurcation. A mechanism that drives a system close to a stable equilibrium away from this equilibrium point. The current state becomes unstable and the system undertakes an irreversible shift towards another stable state. Such mechanisms occur when there exists a positive feedback between two processes that feed off of each other [29]. Other examples related to the climate system are vegetation-atmosphere interaction in Africa, Asian monsoons and marine heat waves.

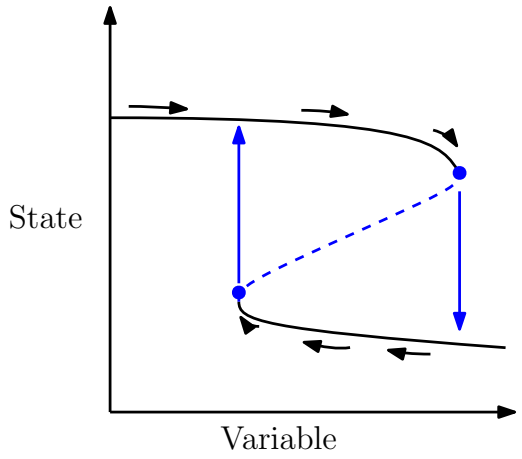

Figure 4.2: General bifurcation diagram of a system with saddle-point bifurcation. The equilibrium states of the system are sketched in function of a certain parameter. The dotted line corresponds to the unstable ones. The dots show the bifurcation or turning points.

These systems are traditionally characterized by bifurcation diagrams as shown in figure 4.2. The steady state profile is discontinuous. Moreover, a hysteresis loop can be observed, meaning that the system can have two possible states for certain particular values of the variable.

Uncertainties associated with the potential appearance of these sudden shifts are difficult to quantify, due to the complexity of the models [2] and [30]. These have to capture non-linear effects. Moreover, local processes often have a significant impact on the global response of such systems.

In glaciology they often have to be taken into account by numerical models through parametrizations, due to limited computational resources [5] and [4]. Their ability to reproduce reality correctly is still a matter of debate [32].

4.2 MISI and Steady State profiles

Longitudinal stresses can be neglected in the interior of the ice sheet [3]. They only play a significant role in the transition zone close to the grounding line, where velocity gradients are important. This hypothesis enables analytic study of the ice flow problem at steady state. Thus we have the following problem to solve for the grounded part 3.36:

$$\begin{cases} \dfrac{\partial q}{\partial x} = a \\ -\rho g h \dfrac{\partial (h+b)}{\partial x} - C|u|^{m-1}u = 0, \end{cases} \tag{4.1}$$

where $q = hu$ denotes the ice flux. From the second equation one gets

$$\frac{\partial u}{\partial x} = \frac{C}{\rho g}\frac{|u|^{m+3}}{q^2}. \tag{4.2}$$

The boundary conditions at the grounding line write

$$\begin{cases} h_g = -\rho/\rho_w b_g, \\ 2\bar{A}^{-1/n} h_g \left|\dfrac{\partial u}{\partial x}\right|^{1/n-1} \dfrac{\partial u}{\partial x} = \dfrac{1}{2}\rho\left(1 - \dfrac{\rho}{\rho_w}\right) g h_g^2, \end{cases} \tag{4.3}$$

where the subscript g means that the function is evaluated at $x = x_g$. Evaluating 4.2 at the grounding line and combining it with 4.3 gives the following expression for the flux at the grounding line

$$q_g(h_g) = \left(\frac{A(\rho g)^{n+1}\left(1-\rho/\rho_w\right)^n}{4^n C}\right)^{1/(m+1)} h_g^{(m+n+3)/(m+1)}, \tag{4.4}$$

The flux at the grounding line is a monotonically increasing function of the ice thickness at the grounding line [24] as shown in figure 4.4. This result is not only essential for explaining the mechanism of the marine ice sheet instability, it also serves as a parametrization of the grounding-line flux in certain numerical solvers [4].

The integration of the continuity equation at steady state in 4.3 yields for the flux at the grounding line

$$q_g = a x_g. \tag{4.5}$$

Equating 4.4 and 4.5 provides an implicit equation for the grounding line position at steady state through the knowledge of the bedrock profile. For future test cases it will be chosen as:

$$b(x) = -\left[729 - 2184.8\left(\frac{x}{750\text{km}}\right)^2 + 1031.72\left(\frac{x}{750\text{km}}\right)^4 - 151.72\left(\frac{x}{750\text{km}}\right)^6\right] \text{m}. \tag{4.6}$$

It has a portion above sea-level, an overdeepening and a shallow sill close to the continental shelf edge [3]. These geometrical properties were the reasons behind that choice.

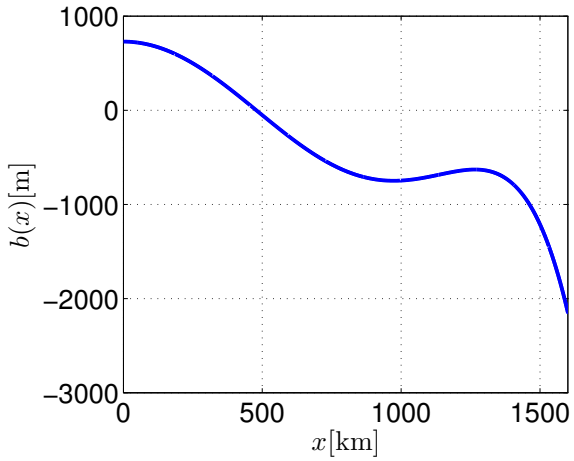

Figure 4.3: Bedrock profile we chose to work with. It has a portion above sea-level, an overdeepening and a shallow sill close to the continental shelf edge [3].

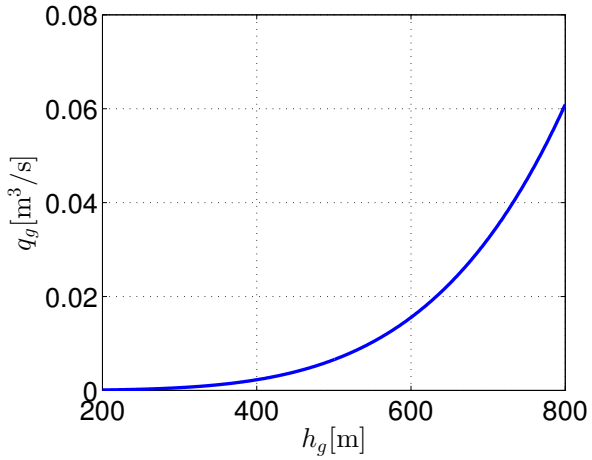

Parameter	Value	Unit
a	0.3	m year^{-1}
ρ_i	900	kg m^{-3}
ρ_w	1000	kg m^{-3}
g	9.81	m s^{-2}
n	3	/
m	1/3	/
C	7.624	MPa m$^{-1/3}$ s$^{1/3}$
A	1.37×10^{-25}	s^{-1} Pa^{-3}

Figure 4.4: Left: Ice flux in function of ice thickness at the grounding line at steady state: q_g is indeed a strictly monotonically increasing function of h_g. $A = 5 \times 10^{-25}$ s^{-1} Pa^{-3}. Right: Numerical parameters used.

Marine ice sheets resting on solid ground below sea-level with an upward slope are inherently unstable [3]. At equilibrium, there must be a balance between the accumulation of snow on top of the ice sheet and the flow of ice at the grounding line. The instability is triggered through a small perturbation of the grounding line position, which could be due, for example, to an increase or decrease in ocean temperature leading to the melting or accumulation of ice around the grounding line. Ice flux at the grounding line increases with ice thickness at the grounding line. Thus in case of a retreat, since the ice lays on a bed with an upward slope, the ice sheet is thicker at the new position of the grounding line and the flux at the grounding line increases, since the flux is an increasing function of the ice thickness. The equilibrium condition is not satisfied anymore and the ice sheet looses mass, causing the grounding line to retreat even further. This process stops when the grounding line reaches a stable position, where the imbalance is cancelled out, which is at a location where the bed has a downward slope. The mechanism is represented in figure 4.5.

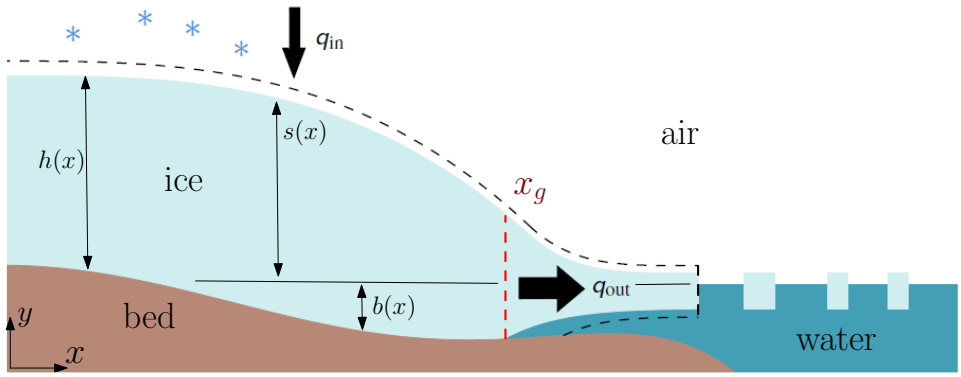

Figure 4.5: Scheme explaining the mechanism of MISI. The ice flux across the grounding line is denoted q_{out}, the precipitation rate q_{in}. Image adapted from [33].

4.3 Steady State profiles and Coulomb friction

In the previous section calculations were made using the traditional power friction law. This law is not satisfactory for two main reasons. The basal stress is not related to the normal stress. In the reduced model it depends only on the horizontal velocity. Thus, not only is it discontinuous at the grounding line, it also increases strongly in the transition zone as it can be observed in figure 4.6.

A more insightful choice could be to take a Coulomb-type friction law [27] of the follow form:

$$\tau_b = f_b(\rho g h - \pi_w)|u|^{m-1}u, \tag{4.7}$$

where the friction coefficient has to be specified. It was chosen equal to 0.32 by trial and error in order to recover a similar ice sheet profile as for the power law. The water pressure is denoted by π_w. Assuming a perfectly porous bedrock it can simply be taken as $\rho_w g b$.

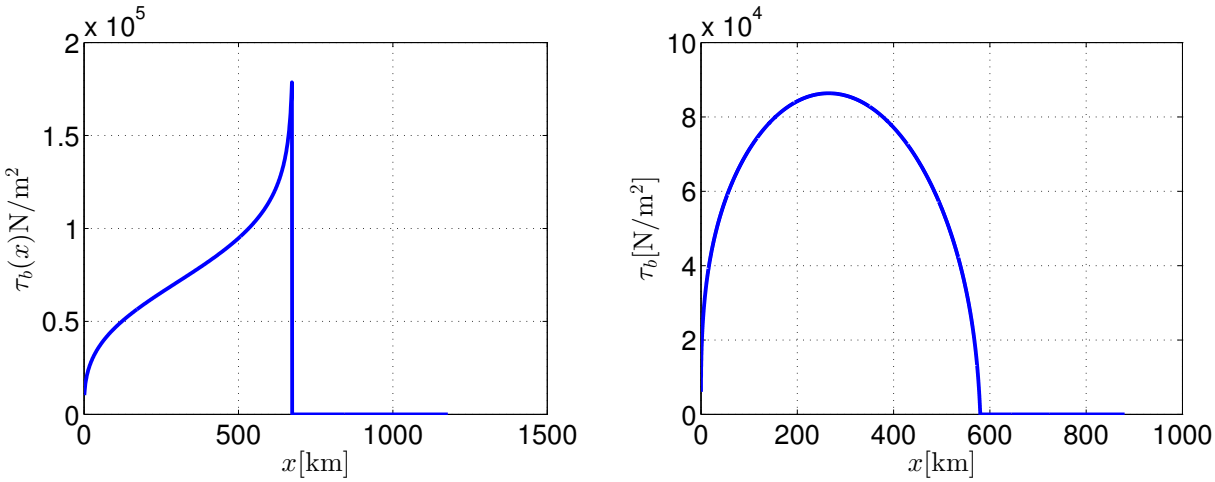

Figure 4.6: Friction term τ_b at steady state. The steady state velocities and grounding line position were calculated by means of their corresponding flux parametrizations. Left: Weertman's power law. Right: Coulomb law related to the overburden pressure.

Using the same arguments as in the previous section but introducing the modified friction law leads to a different parametrization at the grounding line [27]. It is given by:

$$q_g(h_g) = \left(\frac{1}{4}\rho \left(\left(1 - \frac{\rho}{\rho_w} \right) g \right)^n \frac{A}{\dfrac{\partial b(x_g)}{\partial x}} \right) h_g^{1/m+2}. \tag{4.8}$$

As a result steady state profiles and grounding line position are different than for the power friction law as can be seen in figure 4.7.

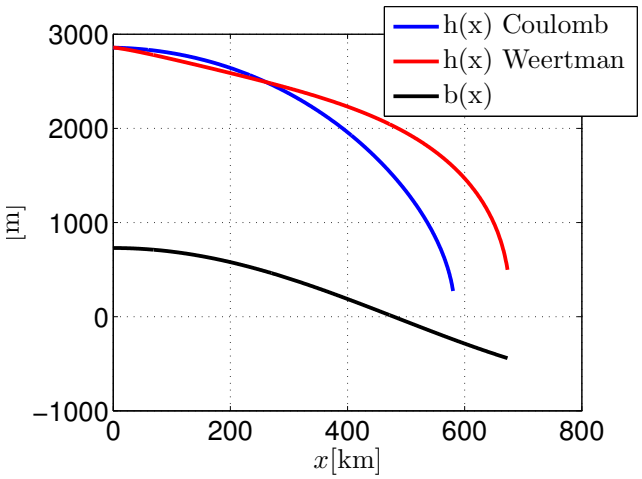

Figure 4.7: Comparison between steady state profiles computed with a power friction law and a Coulomb friction law using the parameters in 4.4.

Part II

Variational methods for the reduced model of a marine ice sheet

Chapter 5

One dimensional p-Laplace equation

In this chapter we consider the subproblem of finding the velocity field by solving the momentum balance equation for a given ice sheet geometry. Thus, the ice sheet is supposed to be at steady state. The use of Glen's law as constitutive equation for polycristalline ice leads to a non-linear so-called p-Laplace equation for horizontal momentum balance. Therefore adapted numerical methods have to be employed. Currently glaciologists employ a second order finite difference method on a coarse grid with an iterative Picard method to solve it [5]. The use of such a method requires the existence of the third derivative of the solution in order to have a control on the spatial discretization error. As was shown in the previous chapter, the friction term in the horizontal momentum balance is discontinuous. Thus the third derivative of the velocity field is not defined at the grounding line. Methods based on variational formulations have less strict continuity requirements for the solution. Therefore, in this chapter, we propose to solve the p-Laplace equation using a finite element method. We combine it with a Newton algorithm to deal with the non-linear p-Laplacian operator. It has faster convergence than the Picard method.

We show that the use of coarse meshes leads to a bad approximation of the steep gradients in the transition zone between grounded and floating regions of a marine ice sheet. We give a possible explanation on how the imposition of a flux condition a the grounding line [4] can improve numerical results without having to refine the mesh close to the grounding line.

Section 5.1 describes the problem at hand. Section 5.2 presents the variational formulation, its equivalent minimization problem and introduces a Newton method for dealing with the nonlinearity. Along the way some notions of functional analysis are given. They will help making sense of the variational formulations. It opens the door to the finite element method, which is described in section 5.3. Finally, section 5.4 is dedicated to several test cases. We show that coarse meshes lead to a bad approximation of steep gradients in the transition zone. This leads to a systematic overestimation of velocities near the grounding line. We also discuss some approaches used in the literature to remove this problem. This chapter is mainly based on [34], [35], [36] and [1]. More information on variational formulations for marine ice sheets can be found in [37] and [38]. A mathematical study of different friction laws for ice sheets can be found in [39].

5.1 Strong formulation

Let us rewrite model 3.37 and 3.36 in a unified way over the entire domain $\Omega = [0, x_c]$ at steady state. It is given by

$$\frac{\partial}{\partial x}\left(2A^{-1/n}h\left|\frac{\partial u}{\partial x}\right|^{1/n-1}\frac{\partial u}{\partial x}\right) - C|u|^{m-1}u\,\mathbb{1}_{x_g} = \rho g h\frac{\partial(h+l)}{\partial x} \qquad \text{in } \Omega \tag{5.1a}$$

The notations common in glaciology were kept. In the field of mathematics the exponent $1/n-1$ usually appears as $p-2$ [1]. Moreover, $\mathbb{1}_{x_g}$ denotes the indicator function. It is equal to one in the grounded part of the ice sheet, that is $x \in [0, x_g]$, and equal to zero in the floating part. The mass balance has to be satisfied as well. At steady state it provides a simple way of calculating the horizontal velocity knowing the ice thickness:

$$u = \frac{ax}{h}. \tag{5.2}$$

Formula 5.2 can be used to check numerical results. The horizontal velocity has to vanish at the ice divide. This serves as a homogeneous Dirichlet boundary condition. A Neuman boundary condition is imposed at the calving front by continuity of the stress tensor. They write:

$$u = 0 \qquad \text{at } x = 0 \tag{5.3a}$$

$$2A^{-1/n}h\left|\frac{\partial u}{\partial x}\right|^{1/n-1}\frac{\partial u}{\partial x} = 1/2\rho(1-\rho/\rho_w)gh^2 \qquad \text{at } x = x_c. \tag{5.3b}$$

In this chapter we will focus on the problem posed by equation 5.1a together with conditions 5.3a and 5.3b. We suppose that the ice thickness h, the inferior ice interface l and the grounding line position x_g are known.

5.2 Weak formulation

5.2.1 Notions of functional analysis

In this section the definition of a few important functional spaces that appear in weak formulations of partial differential equations are given. These are important because they define the correct framework for solutions of variational formulations. They are also essential for establishing existence and uniqueness results. For more information about functional analysis the reader is referred to [35].

Let us start with the definition of the Lebesgue space. Let Ω be a subset of $\mathbb{R}^n$. A Lebesgue space is noted $\mathbb{L}^p(\Omega)$ with $0 < p < +\infty$. It is a vector space defined by

$$\mathbb{L}^p(\Omega) = \left\{ f : \Omega \to \mathbb{R}; \int_\Omega |f|^p \,\mathrm{d}\Omega < \infty \right\}$$

If Ω is of finite measure $\mathbb{L}^p$ is included in $\mathbb{L}^q$ with $1 \leq p \leq q < \infty$ and a norm can be defined as

$$||f||_{\mathbb{L}^p} = \left(\int_\Omega |f|^p \,\mathrm{d}\Omega\right)^{1/p}$$

The scalar product of 2 elements f and g is noted (f, g). An example of a very common Lebesgue space is the space of square integrable functions $\mathbb{L}^2(\Omega)$. Functions that are in a Lebesgue space are guaranteed to have sufficient regularity to be integrable in some sense. To give sense to weak formulations the integrals that appear need to exist. This requires to work with Lebesgue spaces amongst others.

A second useful vector space is the Hilbert space. A Hilbert space $\mathbb{H}$ is defined by a vector space equipped with a scalar product such that $\mathbb{H}$ is complete for the norm $\langle \cdot, \cdot \rangle^{1/2}$.

We define the scalar product as:

$$\langle f, g \rangle = \int_\Omega f\, g \, \mathrm{d}\Omega.^{1}$$

Finally, we present the Sobolev space. A Sobolev space $\mathbb{W}^{1,p}(\Omega)$ is defined as

$$\mathbb{W}^{1,p}(\Omega) = \left\{ f \in \mathbb{L}^p(\Omega);\, \ni\, g_i \in \mathbb{L}^p(\Omega) : \int_\Omega f \frac{\partial \phi}{\partial x_i} \, \mathrm{d}\Omega = -\int_\Omega g_i \phi \, \mathrm{d}\Omega,\ \forall \phi \in \mathbb{C}^\infty(\Omega),\ \forall i \in [1, n] \right\}$$

and one has

$$\mathbb{H}^1(\Omega) = \mathbb{W}^{1,2}(\Omega)$$

For $f \in \mathbb{W}^{1,p}(\Omega)$ one denotes $\dfrac{\partial f}{\partial x_i} = g$. The ϕ are called test functions. They are indefinitely continuously differentiable and have compact support in Ω. Solutions of a variational formulation are sought in Sobolev spaces. They guarantee that the variational formulation makes sense.

It is also of interest to give the definition of the Gateaux derivative. It is the generalization of the concept of directional derivative. It formalizes how a change in a function affects a functional that depends on this function. The following definition comes from [6].

A functional $F : \mathcal{K} \to \mathbb{R}$[2] is G-differentiable at a point $u \in \mathcal{K}$ if there exists a linear functional $\mathrm{D}F(u)$ such that, for every $v \in \mathcal{K}$,

$$\lim_{\varepsilon \to 0} \frac{\partial}{\partial \varepsilon} F(u + \varepsilon v) = \langle \mathrm{D}F(u), v \rangle, \tag{5.4}$$

where ε is an arbitrary positive number. We call $\mathrm{D}F(u)$ the gradient of F at u and $\langle \mathrm{D}F(u), v \rangle$ the Gateaux derivative of F at u in the direction v. It will be denoted by $F'(u)(v)$ in the remainder of this work.

5.2.2 Variational equality and minimization problem

Let the functional space $\mathcal{V}$ be defined by:

$$\mathcal{V} = \left\{ v \in \mathbb{W}^{1,p}(\Omega) : v = 0 \text{ at } x = 0 \right\}, \tag{5.5}$$

where $p = 1/n + 1 = m + 1$. We also suppose that the functions involved in the right hand side of equation 5.1a is sufficiently regular. To obtain the variational formulation equation

[1] Actually $\langle \cdot, \cdot \rangle$ denotes duality pairing between a space and its dual space. By Riesz's representation theorem it is equivalent to the inner product for Hilbert spaces. We will not delve into the details of dual spaces.

[2] We suppose that $\mathcal{K}$ is a Hilbert space.

5.1a is multiplied by $v \in \mathcal{V}$ and integrated over the domain. Thus we have

$$\int_0^{x_c} \frac{\partial}{\partial x}\left(2A^{-1/n}h\left|\frac{\partial u}{\partial x}\right|^{1/n-1}\frac{\partial u}{\partial x}\right) v\,\mathrm{d}x = \int_0^{x_c}\left[\rho g h \frac{\partial(h+l)}{\partial x}\right] v\,\mathrm{d}x + \int_0^{x_c}\left[C|u|^{m-1}u\,\mathbb{1}_{x_g}\right] v\,\mathrm{d}x \tag{5.6}$$

The next step is to use the divergence theorem on the term in the left hand side. It gives:

$$\begin{aligned}&\int_0^{x_c} \frac{\partial}{\partial x}\left(2A^{-1/n}h\left|\frac{\partial u}{\partial x}\right|^{1/n-1}\frac{\partial u}{\partial x}\right) v\,\mathrm{d}x \\ &= \left[2A^{-1/n}h\left|\frac{\partial u}{\partial x}\right|^{1/n-1}\frac{\partial u}{\partial x}v\right]_0^{x_c} - \int_0^{x_c} 2A^{-1/n}h\left|\frac{\partial u}{\partial x}\right|^{1/n-1}\frac{\partial u}{\partial x}\frac{\partial v}{\partial x}\,\mathrm{d}x\end{aligned} \tag{5.7}$$

The term in $x = 0$ is zero because v vanishes at the left boundary. At x_c we have 5.3b. The definition of the following forms will come in handy:

$$a(u,v) = \int_0^{x_c} 2A^{-1/n}h\left|\frac{\partial u}{\partial x}\right|^{1/n-1}\frac{\partial u}{\partial x}\frac{\partial v}{\partial x}\,\mathrm{d}x \tag{5.8}$$

$$c(u,v) = \int_0^{x_c} C|u|^{m-1}u\,\mathbb{1}_{x_g}\,v\,\mathrm{d}x \tag{5.9}$$

$$f(v) = 1/2\rho(1-\rho/\rho_w)gh(x_c)^2 v(x_c) - \int_0^{x_c}\rho g h\frac{\partial(h+l)}{\partial x}\,v\,\mathrm{d}x \tag{5.10}$$

The variational formulation for the problem presented in section 5.1 then is:

Formulation 1 *Given h and l, find $u \in \mathcal{V}$ such that*

$$a(u,v) + c(u,v) = f(v)$$

for all $v \in \mathcal{V}$

It is possible to write the variational formulation 1 as an unconstrained minimization problem. For that purpose let us define the functional:

$$\mathcal{J}(v) = \frac{a(v,v)}{1/n+1} + \frac{c(v,v)}{m+1} - f(v). \tag{5.11}$$

$\mathcal{J}$ is not continuous. The minimization problem is given by:

Formulation 2 *Given h and l, find $u \in \mathcal{V}$ such that*

$$\mathcal{J}(u) = \min_{v\in\mathcal{V}} \mathcal{J}(v)$$

for all $v \in \mathcal{V}$

Physically $a(v,v)$ is linked to the viscous dissipation inside the ice, $c(v,v)$ corresponds to rate at which energy is lost by friction. The functional $f(v)$ has two contributions. The first corresponds work rate done by water pressure and second is linked to the variation of potential energy of the fluid. Thus the minimization principle corresponds to the minimization of a functional linked to a variation of energy. This is very similar to the principle of minimum of total potential energy in solid mechanics. Formulation 1 and 2 are equivalent. Indeed the minimizer of $\mathcal{J}$ is characterized by

$$\mathcal{J}'(u)(v) = 0, \tag{5.12}$$

which immediately leads to the variational formulation. Conversely, it is possible to show that if 1 holds

$$\mathcal{J}(u) \leq \mathcal{J}(v) \qquad \forall v \in \mathcal{V}. \tag{5.13}$$

Existence and uniqueness results for formulation 1 are difficult to establish. The main difficulty comes from the friction term, which is not continuous across the entire ice sheet in the case where a coupling between a grounded ice sheet and a floating shelf is considered. Thus well posedness does not simply follow from the minimization problem. These mathematical difficulties indicate that the transition zone will also be problematic during the numerical resolution of the problem.

Note that it can be shown that a solution exists and is unique if a Coulomb-type friction law is used[3] [38] and [39]. Intuitively it can be explained by the continuity of the friction term at the grounding line.

5.2.3 Newton algorithm

Solving 1 requires an adequate numerical method to deal with the non-linearity of the first two terms. The following iterative Newton-algorithm is proposed:

Algorithm 1 Newton algorithm for the calculation of u

1: **while** convergence not reached **do**
2: solve for Δu: ▷ Linear system to solve

$$\mathcal{J}'(u^k)(v) + \mathcal{J}''(u^k)(v)(\Delta u) = 0$$

3: set: $u^{k+1} = u^k + \Delta u$
4: increment k
5: **return** u

By direct calculation one has for the second derivative of $\mathcal{J}$ in some arbitrary direction w:

$$\mathcal{J}''(u)(v)(w) = \int_0^{x_c} \left(2A^{-1/n} h \frac{1}{n} \left|\frac{\partial u}{\partial x}\right|^{1/n-1}\right) \frac{\partial v}{\partial x} \frac{\partial \tilde{w}}{\partial x} \,\mathrm{d}x + \int_0^{x_c} \left[Cm|u|^{m-1}\,\mathbb{H}_{x_g}\right] v\, w \,\mathrm{d}x. \tag{5.14}$$

5.3 Finite Element Method

Up to now solely the continuous problem has been studied. In this section a finite element method for the Newton algorithm 1 is constructed with the goal to find an approximate solution to the problem presented in section 5.1.

[3] Some additional conditions are required, but we will not go into these details here.

Consider a finite dimensional space $\mathcal{V}_h$ included in $\mathcal{V}$. Let us introduce the following Galerkin approximation for u, v and Δu:

$$u_h(x) = \sum_{i=0}^{N} u_i \phi_i \tag{5.15}$$

$$v_h(x) = \sum_{i=0}^{N} v_i \phi_i \tag{5.16}$$

$$\Delta u_h(x) = \sum_{i=0}^{N} \Delta u_i \phi_i \tag{5.17}$$

The basis functions ϕ_i are in $\mathcal{V}_h$. Note that the same basis functions have been chosen for the solution of the problem and the test function. Thus we consider a Bubnov-Galerkin approximation. Introducing 5.15, 5.16 and 5.17 into the variational formulation 1 leads to a Newton algorithm that is suited for a numerical resolution with a computer. It is given by:

Algorithm 2 Newton algorithm for the calculation of u_h

1: **while** convergence not reached **do**
2: solve for Δu_h: ▷ Linear System to solve

$$\mathcal{J}'(u_h^k)(v_h) + \mathcal{J}''(u_h^k)(v_h)(\Delta u_h) = 0$$

3: set: $u_h^{k+1} = u_h^k + \Delta u_h$
4: increment k
5: **return** u

At each iteration of the Newton algorithm a linear system of the form:

$$\mathbf{A} \times \Delta \mathbf{u} = \mathbf{F} \tag{5.18}$$

has to be solved. The components of the matrices are given by:

$$\mathrm{A}_{ij} = \mathcal{J}''(u_h^k)(\phi_i)(\phi_j) \tag{5.19}$$

$$\mathrm{F}_i = -\mathcal{J}'(u_h^k)(\phi_i) \tag{5.20}$$

and $\Delta \mathbf{u}$ is a vector that collects the Δu_i. We restrict our study to piecewise linear basis functions. They are defined as:

$$\phi_i(x) = \begin{cases} \dfrac{x - x_{i-1}}{x_i - x_{i-1}} & x_{i-1} \leq x \leq x_i \\ \dfrac{x_{i+1} - x}{x_{i+1} - x_i} & x_i \leq x \leq x_{i+1} \\ 0 & \text{otherwise} \end{cases} \tag{5.21}$$

In that case $\mathbf{A}$ is symmetric and tridiagonal.

5.4 Numerical illustrations

In this section the method based on the variational formulation of the problem that was derived in the previous section is applied to four different cases.

5.4.1 Ice shelf ramp

The first test case is used to verify the correct functioning of the finite element method. An analytic solution for the horizontal velocity inside an ice shelf with an ice thickness of the form:

$$h(x) = h(x_g) - \frac{h(x_c) - h(x_g)}{L} x \tag{5.22}$$

exists. It can be found in [13]. The length of the ice sheet is denoted $L = x_c - x_g$. The ice ramp geometry is depicted in figure 5.1.

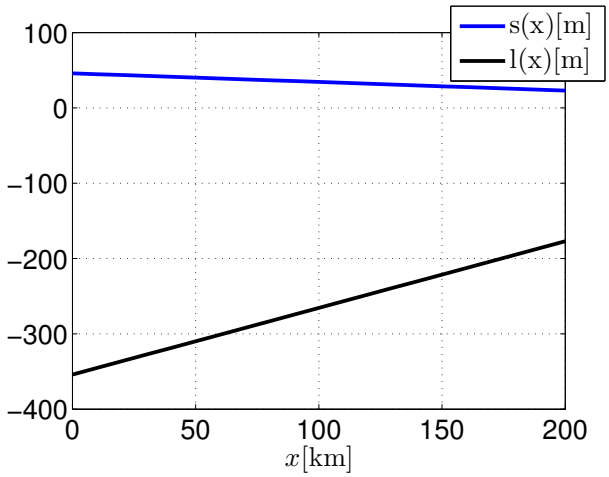

Parameter	Value	Unit
ρ	910	kg m^{-3}
ρ_w	1028	kg m^{-3}
g	9.81	m s^{-2}
n	3	/
m	1/3	/
A	4.9×10^{-25}	s^{-1} Pa^{-3}

Figure 5.1: Left: Ice ramp geometry. The upper ice surface is denoted $s(x)$, the lower ice surface is denoted $l(x)$. Parameters: $h(x_g) = 400$[m], $h(x_c)$[m], $L = 200$[km], $u_g = 0.1$[km/a]. Right: Physical parameters.

At the grounding line non-zero velocity $u(x_g) = u_g$ is specified and the calving front the usual Neuman boundary condition 5.3b is imposed. A special treatment of the non-homogeneous boundary condition is required [35]. It consists in defining a function $\hat{u}$, which is equal to u_0 at $x = 0$ and to solve the problem for $\tilde{u} = u - \hat{u}$. The function $\tilde{u}(x)$ verifies a homogeneous Dirichlet boundary condition and $u(x)$ can easily be inferred from it since $\hat{u}$ is known.

As in a shelf there is no friction, the second term in variational formulation 1 drops. Without the difficulty of having to deal with the discontinuous friction term, well posedness of the problem can be shown without difficulty. Indeed the $\mathcal{J}$ becomes strictly convex and continuous on $\mathcal{V}$ and a unique solution exists [1]. In this case the variational formulation for the ice shelf ramp writes:

Formulation 3 *Given $\hat{u}$ and h, find $\tilde{u}$, with $\tilde{u}(0) = 0$ such that:*

$$\int_{x_g}^{x_c} \left[2A^{-1/n} h \left| \frac{\partial \tilde{u}}{\partial x} + \frac{\partial \hat{u}}{\partial x} \right|^{m-1} \left(\frac{\partial \tilde{u}}{\partial x} + \frac{\partial \hat{u}}{\partial x} \right) \right] \frac{\partial \tilde{v}}{\partial x} \, \mathrm{d}x$$
$$= 1/2\rho(1 - \rho/\rho_w) g h_{x_c}^2 - \int_{x_g}^{x_c} \left[\rho(1 - \rho/\rho_w) g h \frac{\partial h}{\partial x} \right] \tilde{v} \, \mathrm{d}x$$

for all $\tilde{v}$, with $\tilde{v}(0) = 0$.

Starting from there the methodology is the same as presented in the previous sections.

Results are presented in figure 5.2. The approximate solution has no difficulties of matching the analytic solution even with a relatively coarse spatial discretization. Indeed, the ice shelf geometry does not present any steep gradients and is approximated perfectly by linear basis functions. This will not be the case for a more realistic ice sheet geometry.

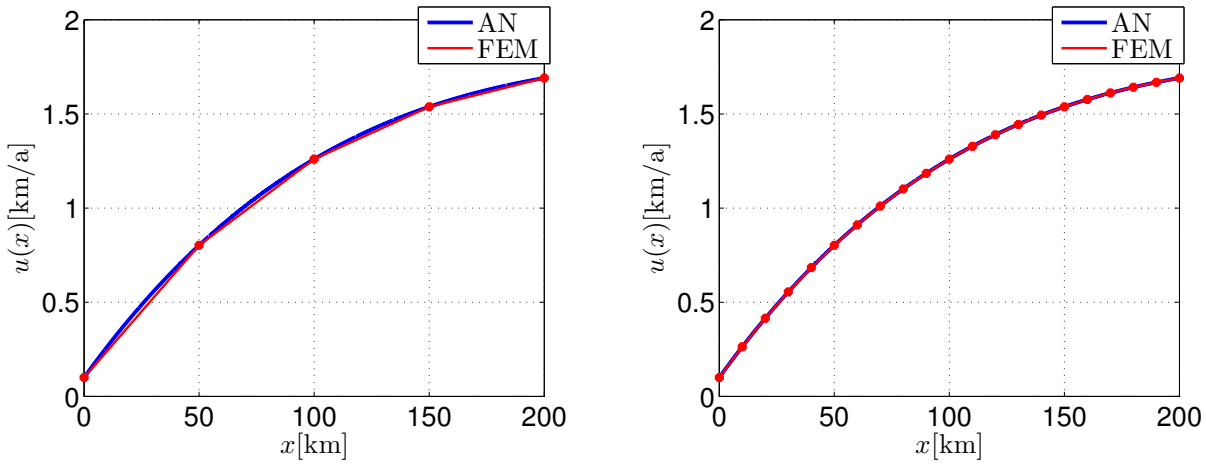

Figure 5.2: Velocity field inside the ice ramp. Comparison between analytic solution and finite element approximation. Left: $N = 4$, right: $N = 20$.

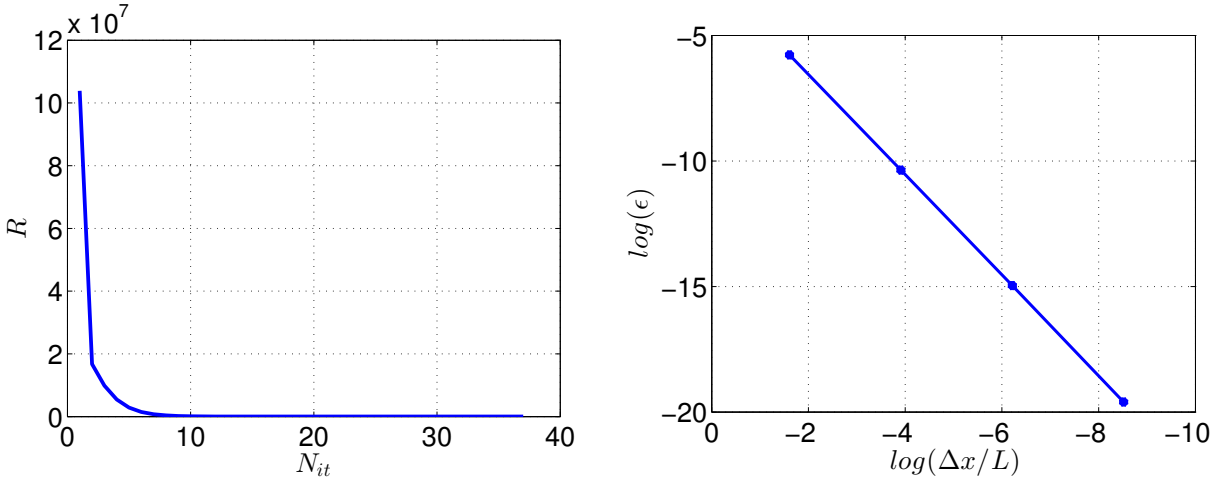

Figure 5.3: Left: Convergence check for the Newton method: $N = 20$. R stands for the total residual and N_{it} for the number of iterations. Right: Loglog plot of the error in function of grid spacing. Convergence is of order 2.

Convergence was checked for the Newton iteration. Moreover it can be seen in figure 5.3 on the right that linear finite elements are spatially convergent of order 2 for the $1D$ p-Laplace problem [40]. The error was calculated in the $\mathbb{L}^p$ norm:

$$\epsilon = ||u - u_h||_{\mathbb{L}^p} = \left[\int_0^{x_c} |u - u_h|^p \, \mathrm{d}x\right]^{1/p}. \tag{5.23}$$

5.4.2 Floating ice shelf

At steady state an analytic solution for the reduced model of the ice shelf profile exists [41]. The associated velocity profile can be deduced from the continuity equation as explained in section 4.2.

Let us place ourselves in the case where h and l are known only at the grid points, as it would be the case for a complete numerical solver. It can be seen in figure 5.4 that a coarse mesh poorly captures the steep geometry gradients close to the grounding line and the method converges to a wrong solution.

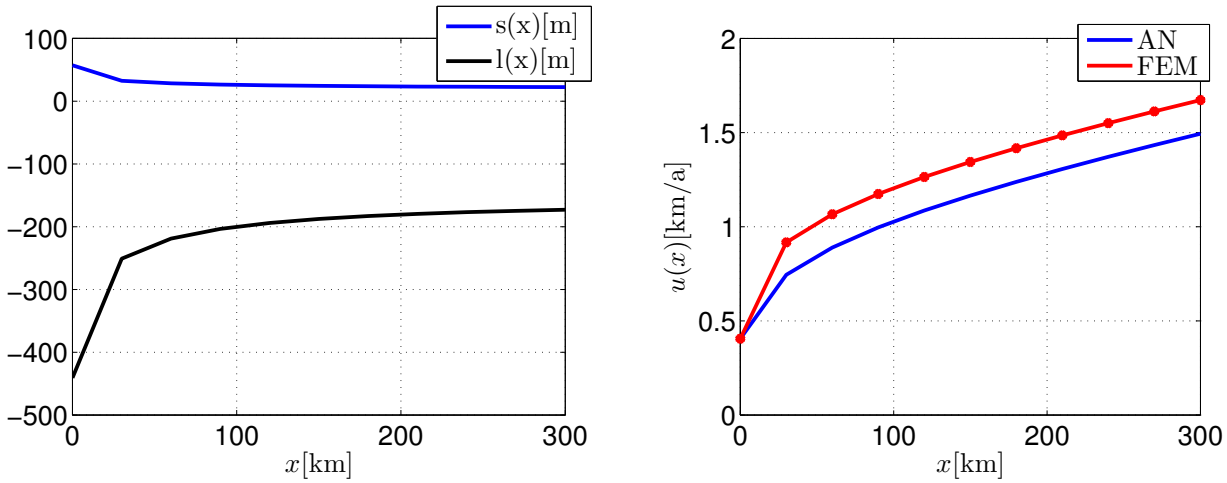

Figure 5.4: Left: Ice shelf geometry for $N = 10$. Right: Comparison between associated analytic solution and finite element approximation. Length of the domain $L = 300$km

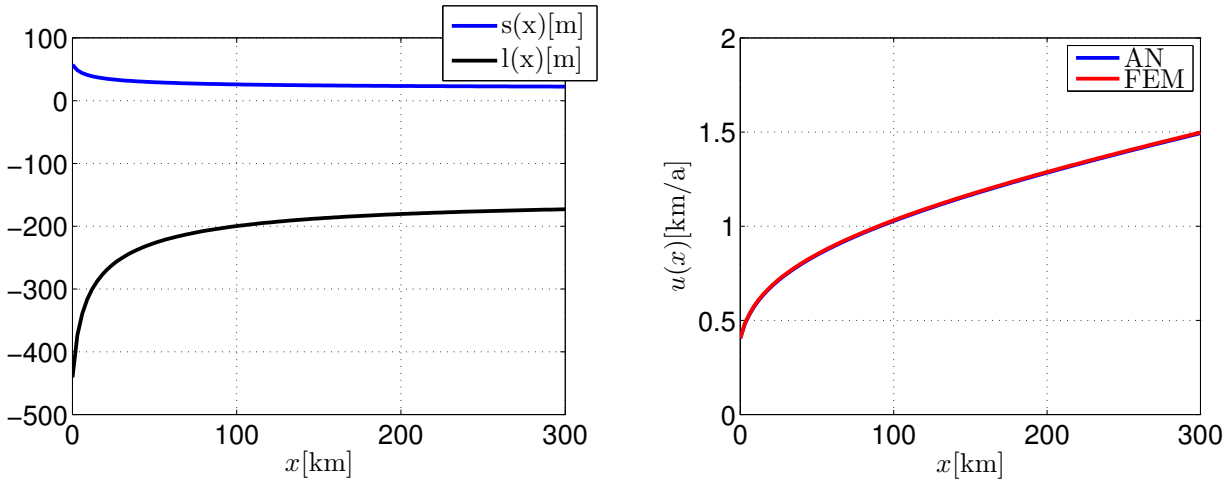

Figure 5.5: Left: Ice shelf geometry for $N = 100$. Right: Comparison between associated analytic solution and finite element approximation. Length of the domain $L = 300$km

The Dirichlet boundary condition on the left is correctly imposed. So is the Neuman boundary condition on the right as suggests the observation that the approximate solution has the same slope as the analytic solution at the right end of the domain. The first element has a steeper slope than predicted by the analytic solution. It is a consequence of the coarse mesh close to the grounding line that overestimates the variations in h and l locally. The approximate velocity overshoots at the second node and then becomes parallel to the analytic solution

carrying the error through the whole domain.

A sufficiently refined mesh (at the grounding line) can remove this problem. We find that for a simple steady state case for a frictionless shelf a horizontal resolution of around 3km to 5km is needed, similar to what can be found in the literature [42].

5.4.3 Grounded Ice sheet

A realistic ice profile for the grounded part of the ice sheet is slightly more difficult to obtain than in the previous case. It can be computed by solving an ODE that appears by combining the two equation in 4.1 and using the flotation condition as a boundary condition [3].

Without coupling with the ice shelf the friction term 5.9 is continuous over the considered domain. It can then be shown that a solution to the minimization problem 2 exists and is unique [6].

Results are shown in figure 5.6 and 5.7. The same problem as for the ice shelf appears. The velocity is overestimated in the transition zone. For the same reasons as before a sufficiently refined mesh is needed at the grounding line. The even steeper gradients close to the grounding line on the grounded part of the ice sheet impose an even more restrictive horizontal resolution of around 0.5km to 1km.

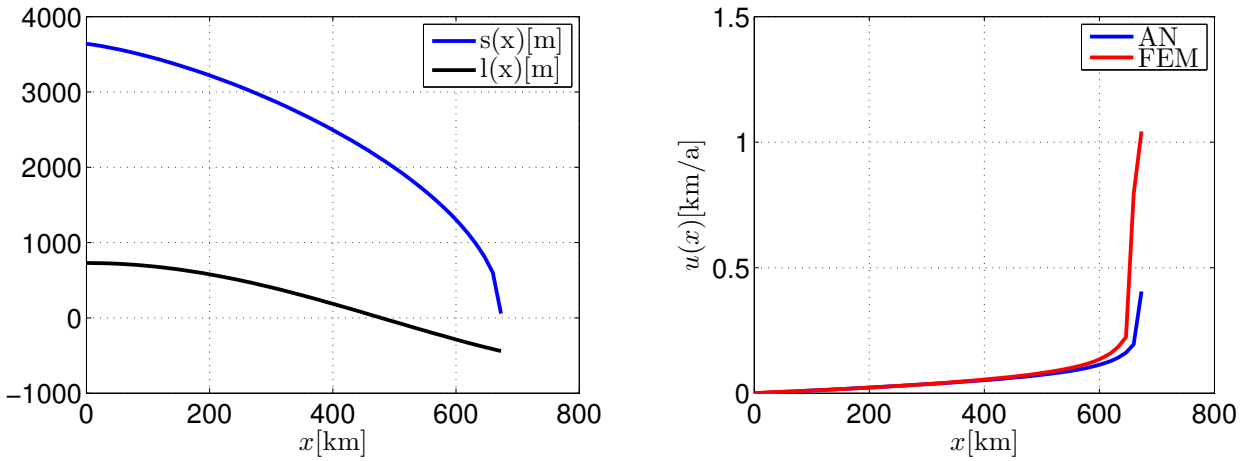

Figure 5.6: Left: Ice sheet geometry for $N = 50$. Right: Comparison between associated analytic solution and finite element approximation. Length of the domain $L = 673$km.

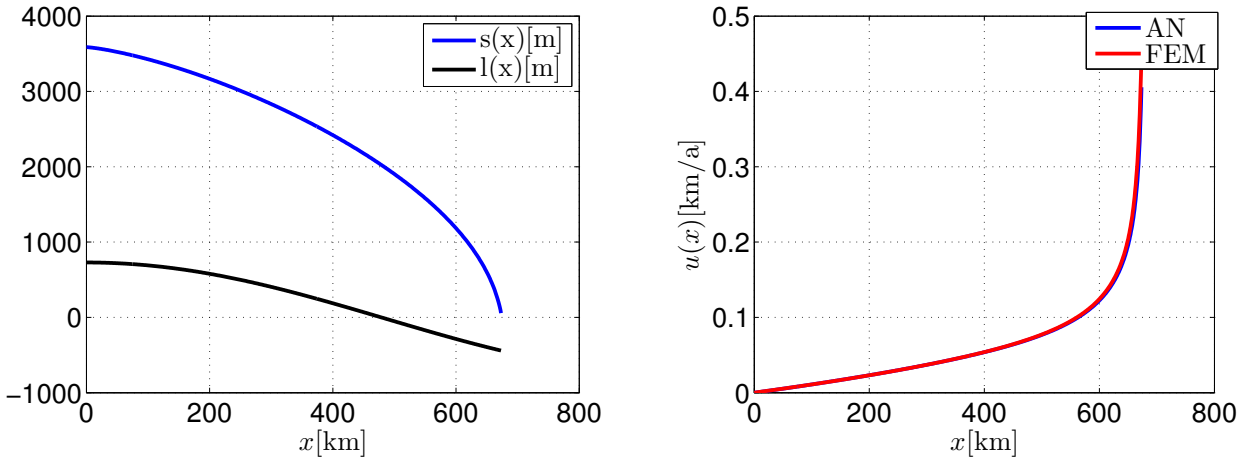

Figure 5.7: Left: Ice sheet geometry for $N = 673$. Right: Comparison between associated analytic solution and finite element approximation. Length of the domain $L = 673$km.

5.4.4 Marine Ice sheet

A steady state ice sheet profile for coupled ice sheet-ice shelf model can simply be constructed by attaching the steady state profiles of the grounded and the floating part together. Results are presented in figures 5.9 and 5.8. The same restrictions on the grid spacing as for the grounded part are found.

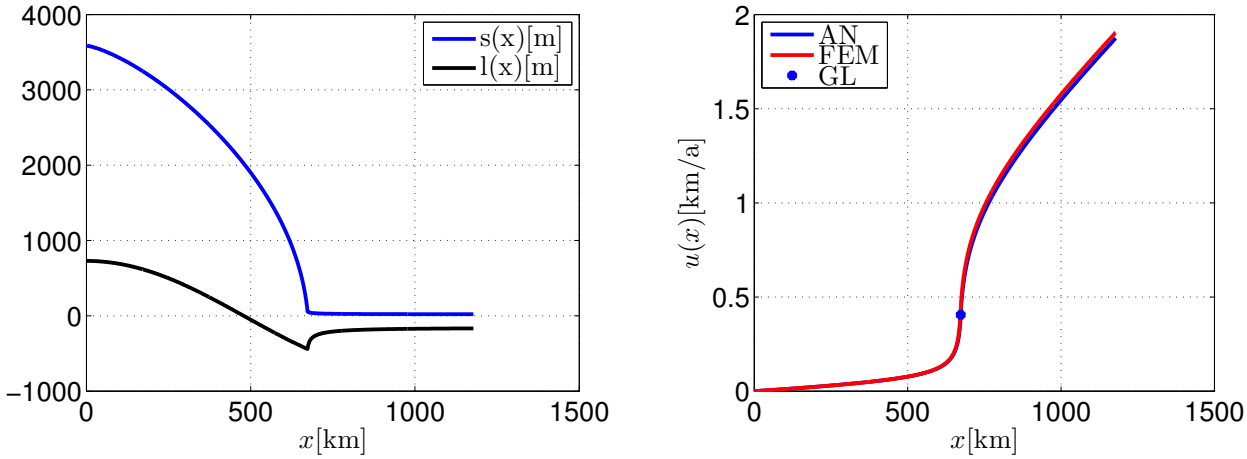

Figure 5.8: Left: Ice sheet geometry for $N = 1750$. Right: Comparison between associated analytic solution and finite element approximation. Length of the domain $L = 1177$km.

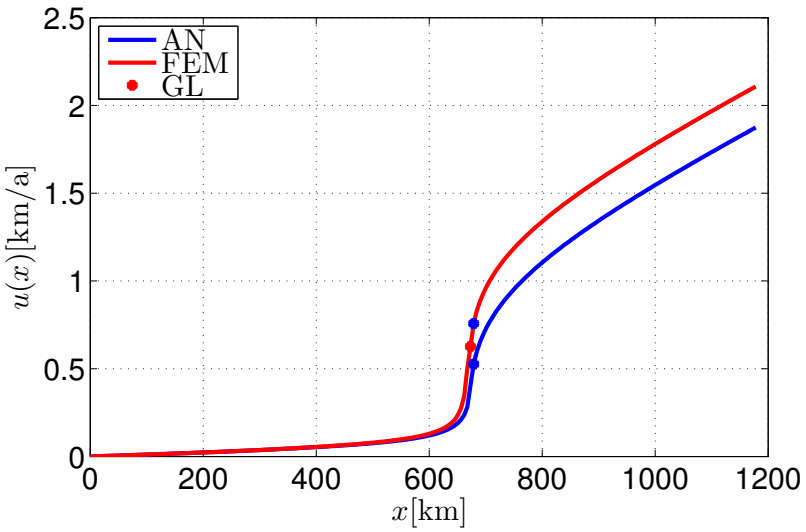

Figure 5.9: Comparison between associated analytic solution and finite element approximation. Length of the domain $L = 1177$km. Number of elements: $N = 150$. The blue dots show the downstream neighbour node of the grounding line.

In large scale models for the Antarctic Ice Sheet such a fine mesh cannot be attained. A different method widely used in glaciology to ensure correct velocities in the transition zone consists in calculating the flux at the grounding analytically by equation 4.4 and deducing the velocity by $q_g = h_g u_g$. This analytic velocity is then imposed as a boundary condition at the node downstream of the grounding line [4]. No clear explanations behind that reasoning is given in the literature.

As seem to indicate results in figure 5.9 this procedure amounts to shifting the velocity profile downwards such that the two blue dots coincide. In that case this procedure would corresponds to solving the grounded and the floating part separately and matching the solution at the grounding line by imposing a Dirichlet boundary condition, where the value of the velocity at the interface is supposed to be known a priory from an analytical calculation.

However, this is not really what is done in current finite difference codes [4] and [5]. Instead, the p-Laplace equation is first solved on the entire domain and then the velocity is corrected through the parametrization only at the grounding line. With the corrected flux the ice thickness adapts through the coupling with the continuity equation and so does in turn the velocity profile by an iterative process. The question that remains to be answered is if is equivalent to what was discussed in the previous paragraph.

Chapter 6

Contact formulation for marine ice sheets

Distinguishing between the grounded and the floating parts is one of the major challenges in modeling the dynamics of marine ice sheets. We have seen in previous chapters that for the reduced order model it boils down to the simple flotation condition that is verified point per point on the grid. The simulation domain being extremely large the mesh has to be coarse in order to have reasonable computation times. As was concluded in chapter 4 subgrid processes close to the grounding line have to be captured correctly [30]. Using a node to node approach on a coarse grid leads to a bad approximation of the bedrock profile.

In this chapter we place the problem into the mathematical framework of variational formulations for contact problems. Such a framework can give information on how to model the friction between the ice sheet and the bedrock and how to distinguish grounded and floating regions in a more general way. With this idea in mind we apply a Mortar Finite Element method to the unilateral contact problem that was proposed in [21]. The ice sheet is treated as solid body in contact with a rigid foundation, very similar to the classical Signorini problem. Note that classical contact mechanics deals with interactions between solids. The methodology has to be slightly adapted for marine ice sheets, which are modeled as fluids.

Starting from the non-linear complementarity problem, that arises when writing the contact conditions, an equivalent variational inequality is derived in section 6.1. Variational inequalities can written under the form of a constrained minimization problem over a closed convex set 6.2. It is common knowledge that constrained minimization problems can be reformulated as saddle point problems through the method of Lagrangian multipliers. A functional is minimized over a linear space instead of a closed set. This approach is presented in section 6.3. When discretized using the Mortar Finite Element Method saddle point formulations give access to some very efficient numerical methods. Among them is the semi-smooth Newton algorithm, which is the generalization of the well known active set strategy for solving minimization problems under inequality constraints. It can be found in section 6.4. Finally, section 6.6 is dedicated to some numerical illustrations.

The references for contact mechanics are [6], [43] and [44]. More information on variational inequalities can be found in [45] and [46]. Concerning the numerical aspects this chapter is based on [7], [47] and [48].

6.1 Variational Inequality

We consider a marine ice sheet as depicted in figure 3.1. Suppose that the interior ice surface l, the ice thickness h and the bedrock profile b are functions defined over $\Omega = \{x \in \mathbb{R} : x \in [0, x_c]\}$. We assume that l is in $\mathcal{V} := [\mathbb{L}^2(\Omega)]$. In this chapter h and b are supposed to be known and l has be determined by solving the following contact problem:

NCP 1 *Given h and b, find l such that:*

$$\begin{aligned} l - b &\geq 0 \\ \rho g h - \pi_w &\geq 0 \\ (l - b)\left[\rho g h - \pi_w\right] &= 0 \end{aligned}$$

The first inequality constraint simply expresses that there is no penetration possible between the ice sheet and the bedrock. When it is active the ice is in contact with the bedrock and thus grounded. Otherwise it is floating and l is determined by the equilibrium between ice mass and buoyancy.

The second condition corresponds to the positivity of the overburden pressure. The overburden pressure is the pressure or stress applied on the bedrock by the weight of the ice. In the present case it is simply the difference between the mass of the ice column and the water pressure. We calculate water pressure underneath the lower ice surface l as:

$$\pi_w = \pi_b - \rho_w g(l - b), \tag{6.1}$$

where π_b is the water pressure at the bedrock.

The equality is the complementarity condition. It expresses the fact that everywhere in the domain either the gap is closed or the overburden pressure vanishes. It can be verified that:

- When the ice floats: $\pi_b = \rho_w g(z_{wl} - b)$. Thus the overburden pressure becomes:

$$\rho g h - \rho_w g(z_{wl} - l) = 0 \tag{6.2}$$

- When the ice is grounded: $l - b = 0$. Thus the overburden pressure becomes:

$$\rho g h - \pi_b \tag{6.3}$$

The water pressure at the bedrock for the grounded part of the ice sheet depends on the hydrology inside the lithosphere. In the present case a perfectly porous bedrock is assumed. The water pressure at the bedrock is then given by:

$$\pi_b = -\rho_w g \min(0, b). \tag{6.4}$$

Problem NCP1 is called a non-linear complementarity problem (NCP). It can be written as a variational inequality [45]. For that purpose we define the set $\mathcal{K}$, a closed convex subset of $\mathcal{V}$, as $\mathcal{K} := \{k \in \mathcal{V} : k \geq b, \forall x \in \Omega\}$[1]. The variational inequality (VI) then writes:

[1]The partial ordering $\geq$ has to be rigorously defined for functional spaces. We omit this kind of detail. For more information see [6].

VI 1 *Given $h \in \mathbb{L}^2$, find $l \in \mathcal{K}$ such that*

$$\int_0^{x_c} (k-l)\left[\rho g h - \pi_w\right] \mathrm{d}x \geq 0$$

for all $k \in \mathcal{K}$

Proof: Multiply $\rho g h - \pi_w$ by $(k-l)$ with $k, l \in \mathcal{K}$ and integrate over the domain. One has

$$\begin{aligned}\int_0^{x_c} (k-l)\left[\rho g h - \pi_w\right] \mathrm{d}x = &\int_0^{x_c} (k-b)\left[\rho g h - \pi_w\right] \mathrm{d}x \\ &+ \int_0^{x_c} (b-l)\left[\rho g h - \pi_w\right] \mathrm{d}x \\ &\geq 0 \quad \forall k \in \mathcal{K}\end{aligned}$$

The second term in the right hand side vanishes because of the complementarity condition in NCP1. The first term in the right hand side is always greater than 0 since $k \in \mathcal{K}$ and the overburden pressure is always positive. Therefore if the NCP leads to the VI. Conversely, it can be checked that if the VI is true one can recover the unilateral contact conditions in NCP 1.

The following functionals are defined:

$$a(k, \tilde{k}) = \int_0^{x_c} \rho_w g k \tilde{k} \, \mathrm{d}x \tag{6.5}$$

$$f(k) = \int_0^{x_c} \left(\pi_b + \rho_w g b - \rho g h\right) k \, \mathrm{d}x, \tag{6.6}$$

The form $a(\cdot, \cdot)$ is a bilinear positive symmetric and continuous mapping from $\mathcal{V}$ to $\mathbb{R}$ and f is linear and continuous. The variational inequality VI 1 can be cast into a standard form [6].

VI 1 *Given $h \in \mathbb{L}^2$, find $l \in \mathcal{K}$ such that*

$$a(l, k-l) \geq f(k-l)$$

for all $k \in \mathcal{K}$

Writing the contact conditions defined in NCP 1 under the form of a variational inequality involving a bilinear and a linear form, such as in VI 1 gives access to a whole range of mathematical tools. It allows to draw from methods developed in computational mechanics for contact problems. Existence and uniqueness of a solution to this type of inequalities are well established [6].

6.2 Minimization Problem

Let $\mathcal{F} : \mathcal{K} \to \mathbb{R}$ be a functional such as

$$\mathcal{F}(k) = \frac{1}{2} a(k, k) - f(k). \tag{6.7}$$

Before showing that the solution of the variational inequality 1 is equivalent to a constrained minimization problem let us first recall some important properties of functional $\mathcal{F}$.

$\mathcal{F}$ is convex. Indeed, using the properties of a and f one has

$$\begin{aligned}\mathcal{F}(\theta l + (1-\theta)k) =& \frac{1}{2}\theta^2 a(l,l) + \theta(1-\theta)a(l,k) + \frac{1}{2}(1-\theta)^2 a(k,k) - \theta f(l) - (1-\theta)f(k) \\ \leq& \frac{1}{2}\theta a(l,l) + \frac{1}{2}(1-\theta)a(k,k) - \theta f(l) - (1-\theta)f(k) = \theta\mathcal{F}(l) + (1-\theta)\mathcal{F}(k),\end{aligned}$$

which is true iff

$$\begin{aligned}&\frac{1}{2}\theta(\theta-1)a(l,l) + \theta(1-\theta)a(l,k) + \frac{1}{2}\theta(1-\theta)a(k,k) \leq 0 \\ \Leftrightarrow\ & -\frac{1}{2}\theta(1-\theta)(a(l,l) + 2a(l,k) + a(k,k)) \leq 0 \\ \Leftrightarrow\ & -\frac{1}{2}\theta(1-\theta)a(l+k, l+k) \leq 0.\end{aligned}$$

This is indeed the case for all θ between 0 and 1, since a is positive.

$\mathcal{F}$ is G-differentiable on $\mathcal{K}$. Indeed one has for all $k \in \mathcal{K}$:

$$\lim_{\varepsilon\to 0}\frac{\mathrm{d}}{\mathrm{d}\varepsilon}\mathcal{F}(l+\varepsilon k) = \lim_{\varepsilon\to 0}\left[a(l+\varepsilon k, k) - \langle f, k\rangle\right] = a(l,k) - \langle f, k\rangle = \langle D\mathcal{F}(l), k\rangle. \tag{6.8}$$

Moreover, $\mathcal{F}$ is continuous and coercive. Since $\mathcal{F}$ enjoys all these properties existence of a minimizer of $\mathcal{F}$ on $\mathcal{K}$ is guaranteed by the generalized Weierstrass minimization theorem [6].

The variational inequality 1 follows from the minimization of $\mathcal{F}$. It is an immediate consequence of the following theorem [6].

Theorem 1 *Let $\mathcal{K}$ be a nonempty closed convex subset of a normed linear space $\mathcal{V}$ and let $\mathcal{F}$ be a G-differentiable functional mapping $\mathcal{K}$ into $\mathbb{R}$. If l is a minimizer of $\mathcal{F}$ in $\mathcal{K}$, then l may be characterized in the following way:*

$$\langle D\mathcal{F}(l), k-l\rangle \geq 0 \quad \forall k \in \mathcal{K}.$$

Let us now show that the functional $\mathcal{F}$ is bounded at all $k \in \mathcal{K}$ by the functional evaluated at the solution of the variational inequality 1:

$$\begin{aligned}\mathcal{F}(k) =& \frac{1}{2}a(l+k-l, l+k-l) - f(l+k-l) \\ =& \mathcal{F}(l) + a(l, k-l) + \frac{1}{2}a(k-l, k-l) - f(k-l) \\ \geq& \mathcal{F}(l) + a(l, k-l) - f(k-l) \\ \geq& \mathcal{F}(l).\end{aligned}$$

First the bilinearity of a and the linearity of f were used, followed by the positivity of a. The last step follows from the assumption that l is the solution of the variational inequality. Thus one has:

$$\mathcal{F}(l) \leq \mathcal{F}(k) \qquad \forall k \in \mathcal{K}$$

and the NCP 1 is equivalent to the following minimization problem:

Formulation 4 *Given $h \in \mathbb{L}^2$, find $l \in \mathcal{K}$ such that*

$$l = \arg\inf_{k\in\mathcal{K}} \frac{1}{2}\int_0^{x_c} \rho_w g l^2 \,\mathrm{d}x - \int_0^{x_c} (\pi_b + \rho_w g - \rho g h)\, k \,\mathrm{d}x$$

6.3 Saddle Point Problem

Constrained minimization problems can be written be written as saddle point problems. The minimization is no longer done on the close convex set $\mathcal{K}$, but in the linear space $\mathcal{V}$. We start by introducing a Langrange multiplier $\mu \geq 0$[2] in Ω. If $k \in \mathcal{K}$, one has for any μ:

$$\langle b - k, \mu\rangle = \int_0^{x_c} (b-k)\mu \,\mathrm{d}x \leq 0. \tag{6.9}$$

There is at least one $\mu \geq 0$ such that:

$$\langle b - k, \mu\rangle = 0. \tag{6.10}$$

For example when $\mu = 0$ it is always the case. Therefore, one can write

$$\sup_{\mu\geq 0}\langle b - k, \mu\rangle = 0 \quad \forall k \in \mathcal{K}. \tag{6.11}$$

If $k \in \mathcal{V}\backslash\mathcal{K}$ it is possible that $b \geq k$ for some points in the domain and thus one has

$$\sup_{\mu\geq 0}\langle b - k, \mu\rangle = +\infty \quad \forall k \in \mathcal{V}\backslash\mathcal{K}. \tag{6.12}$$

Following these consideration it is now possible to write the constrained minimization problem as the following saddle point problem

Formulation 5 *Given $h \in \mathbb{L}^2(\Omega)$, find $l \in \mathcal{V}$ such that*

$$l = \arg\inf_{k\in\mathcal{V}} \sup_{\mu\geq 0} \mathcal{L}(k, \mu)$$

The Lagrangian functional is defined as:

$$\mathcal{L}(k, \mu) = \frac{1}{2}a(k, k) - f(k) + \langle b - k, \mu\rangle. \tag{6.13}$$

[2]The correct definition of the space μ lies in has to be defined rigorously using the notion trace spaces and dual spaces.

The Lagrangian functional is Gateaux differentiable for all $k \in \mathcal{K}$ and all $\mu \geq 0$. Moreover, it is strictly convex with respect to k and concave with respect to μ. Therefore, the saddle point (l, λ) can be characterized by the system [6]:

$$\begin{aligned} &l \in \mathcal{V} \text{ and } \lambda \geq 0 : \\ &\quad a(l,k) - f(k) + B(k,\lambda) = 0 && \forall k \in \mathcal{V} \\ &\quad B(l, \mu - \lambda) \leq G(\mu - \lambda) && \forall \mu \geq 0, \end{aligned}$$

where B and G were defined as

$$B(k,\mu) = \langle -k, \mu \rangle \tag{6.14a}$$
$$G(\mu) = \langle -b, \mu \rangle. \tag{6.14b}$$

Formulation 6 *Given $h \in \mathbb{L}^2(\Omega)$, find $l \in \mathcal{V}$ and $\lambda \geq 0$ such that*

$$\int_0^{x_c} \rho_w g l k \,\mathrm{d}x - \int_0^{x_c} (\pi_b + \rho_w g b - \rho g h) k \,\mathrm{d}x - \int_0^{x_c} \lambda k \,\mathrm{d}x = 0 \quad \forall k \in \mathcal{V}$$
$$\int_0^{x_c} (b - l)(\mu - \lambda) \,\mathrm{d}x \leq 0 \quad \forall \mu \geq 0$$

A nice physical interpretation can be given to the Lagrangian multiplier. Indeed working out λ in the variational equality above gives:

$$\lambda = \rho g h - [\pi_b - \rho_w g (l - b)] = \rho g h - \pi_w. \tag{6.15}$$

Thus the Lagrangian multiplier appears as the overburden pressure. It was to be expected, since the conditions in NCP 1 translate the vertical equilibrium of the ice sheet and in traditional contact mechanics the normal component of the Lagrangian multiplier is the contact pressure.

6.4 Discretization

Consider a simple uniform spatial discretization of space. Mortar Finite Elements is a hybrid method, where both the primal variable (velocity u) and the dual variable (overburden pressure λ) are discretized with shape functions. Standard linear first order basis functions as in 5.21 are used for the discretization of u. Let $\mathcal{V}_h \subset \mathcal{V}$ be the finite dimensional space of approximated primal variables such that:

$$l_h(x) = \sum_{i=0}^{N} l_i \phi_i \qquad k_h(x) = \sum_{i=0}^{N} k_i \phi_i. \tag{6.16}$$

We will use the same standard linear shape functions for the discretization of the dual variables. Let $\mathcal{M}_h^+$ be the space of approximated dual variables such that:

$$\mathcal{M}_h^+ := \left\{ \mu_h = \sum_{i=0}^{N} \mu_i \phi_i,\ \mu_i \in \mathbb{R},\ \mu_i \geq 0 \right\}.$$

Next to their simplicity, the main advantage of using linear first order basis functions is that they are positive and that implies that:

$$\langle \mu, \phi_i \rangle \geq 0, \qquad \forall \mu \geq 0, \forall i, \tag{6.17}$$

which guarantees that the contact conditions can be correctly described. It can be shown that by the choice of such shape functions the discrete inf-sup condition from Brezzi's theorem [49] is verified and the saddle point problem admits a unique solution.

The discretized problem is:

Discrete Formulation 1 *Given* $h \in \mathbb{L}^2(\Omega)$, $(l_h, \lambda_h) \in \mathcal{V}_h \times \mathcal{M}_h^+$

$$\begin{aligned} a(l_h, k_h) - f(k_h) + B(k_h, \lambda_h) = 0 \quad & \forall k_h \in \mathcal{V}_h \\ B(l_h, \mu_h - \lambda_h) \leq G(\mu_h - \lambda_h) \quad & \forall \mu_h \in \mathcal{M}_h^+ \end{aligned}$$

It can be shown that we have the following equivalence [48]:

$$\begin{cases} \lambda_h \in \mathcal{M}_h^+ \\ B(l_h, \mu_h - \lambda_h) \leq G(\mu_h - \lambda_h) \quad \forall \mu_h \in \mathcal{M}_h^+ \end{cases} \iff \begin{cases} \lambda_i \geq 0, \forall i \\ \langle b - l_h, \phi_i \rangle \leq 0, \ \lambda_i \langle b - l_h, \phi_i \rangle = 0, \forall i \end{cases}$$

Finally, the system can also be written under a matrix form. The concatenation of the l_i and λ_i are vectors noted $\boldsymbol{l}$ and $\boldsymbol{\lambda}$ respectively. Similarly, the concatenation of the k_i and μ_i are vectors noted $\boldsymbol{k}$ and $\boldsymbol{\mu}$ respectively. The discrete problem is rewritten as follows:

Discrete Formulation 2 *Given* $h \in \mathbb{L}^2(\Omega)$, *find* $\boldsymbol{l}$ *and* $\boldsymbol{\lambda}$ *such that*

$$\begin{aligned} & \mathrm{A}\boldsymbol{l} + \mathrm{B}\boldsymbol{\lambda} = \mathbf{f} \\ & \lambda_i \geq 0, \forall i, \ \langle b - l_h, \phi_i \rangle \leq 0, \ \lambda_i \langle b - l_h, \phi_i \rangle = 0, \forall i \end{aligned}$$

where A *and* B *are defined such that*

$$\begin{aligned} \boldsymbol{k}^T \mathrm{A}\boldsymbol{l} &= a(l_h, k_h) \\ \boldsymbol{k}^T \mathrm{B}\boldsymbol{\lambda} &= B(k_h, \lambda_h) \end{aligned}$$

6.5 Semi-smooth Newton Method

The discrete problem derived in the previous section has inequality constrains. Therefore, the system is non-linear and cannot be solved by means of a direct method. In this section an active set method used to solve the problem that was derived in the previous section. It follows

from the application of a semi-smooth Newton algorithm to 2. It is based on the introduction of a semi-smooth complementarity function, which is defined as:

$$C(\lambda_i, l_h) = \lambda_i - \max(0, \lambda_i + c\langle b - l_h, \phi_i \rangle), \tag{6.18}$$

where c is a positive constant. We have that the contact conditions in 6.4 are equivalent to

$$C(\lambda_i, l_h) = 0. \tag{6.19}$$

Indeed the two following cases can be distinguished:

- if $\lambda_i + c\langle b - l_h, \phi_i \rangle > 0$:
$$C(\lambda_i, l_h) = -c\langle b - l_h, \phi_i \rangle. \tag{6.20}$$
The constraint is active and node i is part of the active set $\mathscr{A}$.

- if $\lambda_i + c\langle b - l_h, \phi_i \rangle \leq 0$:
$$C(\lambda_i, l_h) = \lambda_i \tag{6.21}$$
The constraint is inactive and node i is part of the inactive set $\mathscr{I}$.

Therefore the discrete system can be written as

$$\begin{cases} \mathrm{A}\boldsymbol{l} + \mathrm{B}\boldsymbol{\lambda} = \mathbf{f} \\ C(\lambda_i, l_h) = 0 \qquad \forall i \end{cases} \tag{6.22}$$

C is continuous, but not differentiable at the origin. However, the derivative is defined piecewise. Thus when constructing the Newton algorithm as in 2 depending if node i is part of the active or inactive set the corrections have to be computed differently.

The derivative of the max function is given by:

$$\frac{\mathrm{d}}{\mathrm{d}x} \max(0, x) = \begin{cases} 0 & \text{if } x \leq 0 \\ 1 & \text{if } x > 0 \end{cases} \tag{6.23}$$

Starting from an initial guess $[\boldsymbol{l}^0 \boldsymbol{\lambda}^0_{\mathscr{A}} \boldsymbol{\lambda}^0_{\mathscr{I}}]^T$, the current solution is corrected at each step of the method:

$$\begin{bmatrix} \boldsymbol{l}^{k+1} \\ \boldsymbol{\lambda}^{k+1}_{\mathscr{A}} \\ \boldsymbol{\lambda}^{k+1}_{\mathscr{I}} \end{bmatrix} = \begin{bmatrix} \boldsymbol{l}^{k} \\ \boldsymbol{\lambda}^{k}_{\mathscr{A}} \\ \boldsymbol{\lambda}^{k}_{\mathscr{I}} \end{bmatrix} + \begin{bmatrix} \Delta\boldsymbol{l} \\ \Delta\boldsymbol{\lambda}_{\mathscr{A}} \\ \Delta\boldsymbol{\lambda}_{\mathscr{I}} \end{bmatrix} \tag{6.24}$$

where the increments are computed such that:

$$C(\lambda^k_i, l^k_h) + \Delta C(\lambda^k_i, l^k_h) = 0 \tag{6.25}$$

Depending if the node is active or inactive the gap is either closed or open and the overburden pressure is either positive or vanishes. Using 6.23 corrections are can be computed. They are:

- If $i \in \mathscr{A}$ 6.25 yields:
$$\begin{aligned} &\langle b - l^{k+1}_h, \phi_i \rangle = 0 \\ \rightarrow\ &\mathrm{B}_{\mathscr{A}}\, \boldsymbol{l}^{k+1} = \boldsymbol{G}_{\mathscr{A}} \end{aligned} \tag{6.26}$$
and the gap is closed.

- If $i \in \mathscr{I}$ 6.25 yields:

$$\begin{aligned} \lambda_i^{k+1} &= 0 \\ \rightarrow \mathbb{I}\, \boldsymbol{\lambda}_{\mathscr{I}}^{k+1} &= \mathbf{0} \end{aligned} \tag{6.27}$$

  and the overburden pressure is set to zero.

Hence we have the following algorithm:

Algorithm 3 Newton algorithm for the calculation of l and λ

1: set $k = 0$
2: Choose an initial guess for the active set $\mathscr{A}^0$
3: **while** $\mathscr{A}^k \neq \mathscr{A}^{k-1}$ **do**
4: Given $\mathscr{A}^k$ solve for $\boldsymbol{l}^{k+1}$, $\boldsymbol{\lambda}_{\mathscr{A}}^{k+1}$ and $\boldsymbol{\lambda}_{\mathscr{I}}^{k+1}$: ▷ Linear System to solve

$$\begin{bmatrix} \mathrm{A} & \mathrm{B}_{\mathscr{A}}^T & 0 \\ \mathrm{B}_{\mathscr{A}} & 0 & 0 \\ 0 & 0 & \mathbb{I} \end{bmatrix} \begin{bmatrix} \boldsymbol{l}^{k+1} \\ \boldsymbol{\lambda}_{\mathscr{A}}^{k+1} \\ \boldsymbol{\lambda}_{\mathscr{I}}^{k+1} \end{bmatrix} = \begin{bmatrix} \mathbf{f} \\ \mathbf{G}_{\mathscr{A}} \\ \mathbf{0} \end{bmatrix}$$

5: set $\mathscr{A}^{k+1}$ to $\left\{ i : \lambda_i^{k+1} + c\langle b - l_h, \phi_i \rangle > 0 \right\}$
6: increment k
7: **return** l and λ

In algorithm 3 we recognize the matrix to be solved at each iteration as a matrix of the saddle-point type. Existence of a solution to these kind of systems has been studied in [49]. It can be solved using a direct method.

6.6 Numerical Illustration

In this section we present results from the application of the previously derived method. The ice thickness h is assumed to be known at the grid points, whereas the bedrock profile is known for a more refined data grid. First it is applied to a steady state profile as described in section 4.2. Results are provided in figure 6.1. The approximate solution is always represented in red.

For a smooth bedrock there is no noticeable difference between simply using the flotation condition to determine the grounding line position and then setting $l = b$ for all $x \leq x_g$ and $l = -\rho/\rho_w h$ for all $x > x_g$ and solving the contact problem by a variational method. This was to be expected since in the absence of subgrid rugosity the bed is almost perfectly approximated by the mesh and a node to node approach would be difficult to improve.

Figure 6.1 on the right shows that the Lagrangian multiplier λ is indeed the overburden pressure. The shape depends on the water pressure at the bedrock. Since we chose it as 6.4 a dump appears at the location where the bedrock is at sea-level. The Lagrangian multiplier can be used to determine the grounding line position by locating where the overburden pressure vanishes.

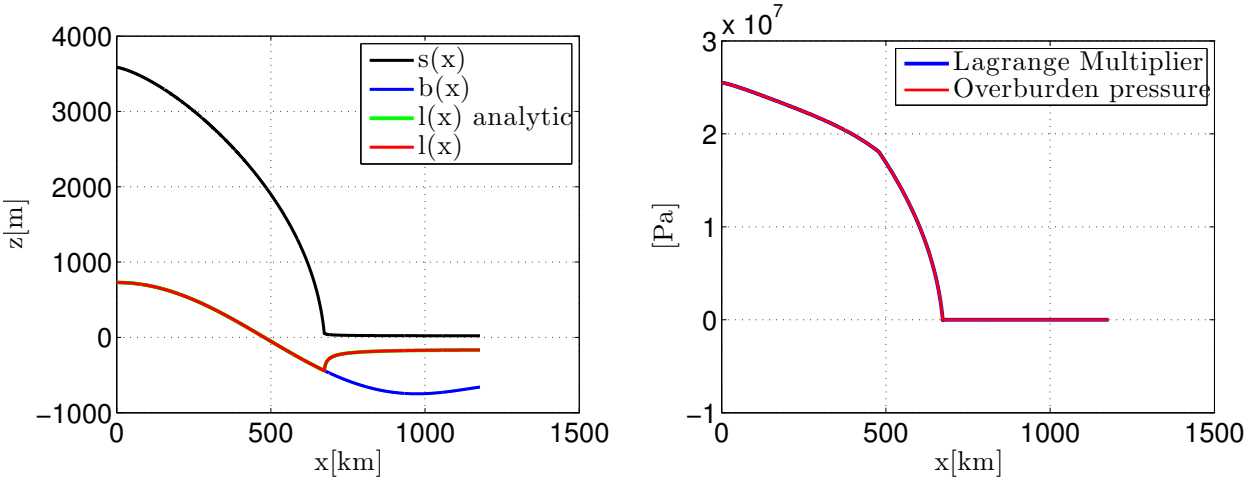

Figure 6.1: Left: ice sheet geometry. Upper ice surface: s. Bedrock: b and the unknown inferior ice sheet surface: l. Right: Comparison between analytically calculated overburden pressure and the Lagrangian multipliers. $N = 1000$, $L = 1177$km.

As a second test case a realistic data set for the bedrock profile and the ice thickness of the Antarctica was taken [26]. The data set has a resolution of 500 m. Grid resolution in current FD codes for the Antarctic ice sheet is limited to 20 km for the majority of the domain and is sometimes refined to a few kilometers close to the grounding line [5]. Still, a large part of the bedrock rugosity is not taken into account. The bedrock plays an essential role in the mechanism of the marine ice sheet instability [3]. It is therefore particularly important to model the bedrock correctly. Especially close to the grounding line.

Figures 6.2 and 6.3 show the results for a grid resolution of 20 km and 10 km respectively.

The main difference between a finite difference and the finite elements approach chosen in this chapter is location where known data about the bedrock is taken into account. For the traditional FD method the bedrock profile is only evaluated at the grid points of the FD grid. On the other hand, for the FEM, the bedrock is integrated over each element by Gaußian quadrature. Thus the bedrock is also evaluated at the Gauß points inside the element. The consequences of this can be observed in figures 6.2 and 6.3. The rugosity of the bedrock averaged out by the method and the resulting inferior ice sheet surface appears as a weighted mean bedrock profile for the grounded part.

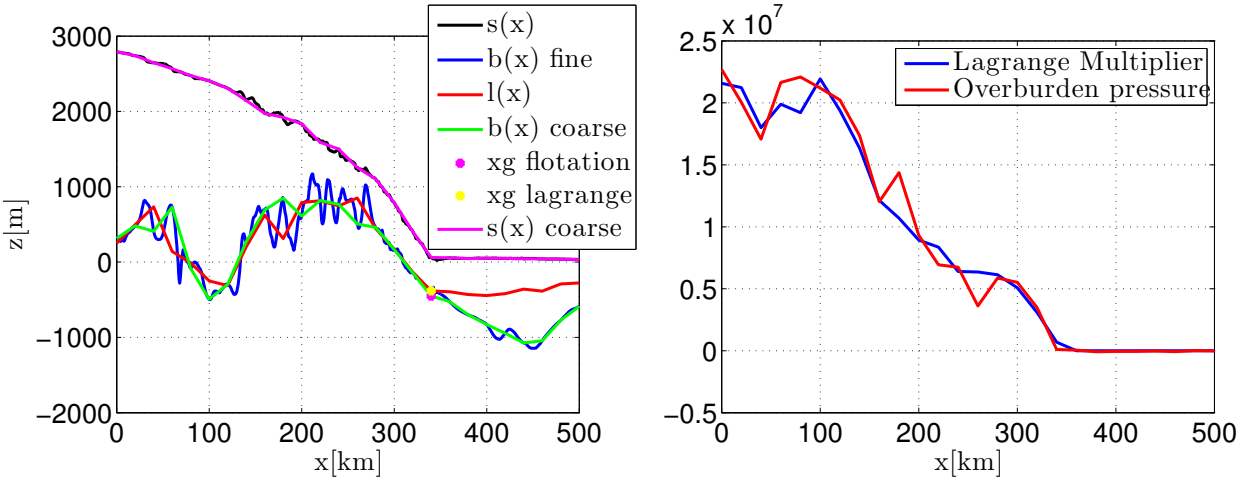

Figure 6.2: Left: Realistic ice sheet geometry. Data taken from [26]. Upper ice surface: s. Bedrock: b and the unknown inferior ice sheet surface: l. Grounding line: x_g. Right: Comparison between calculated overburden pressure calculated node per node and the Lagrangian multipliers. $N = 25$, $L = 500$km.

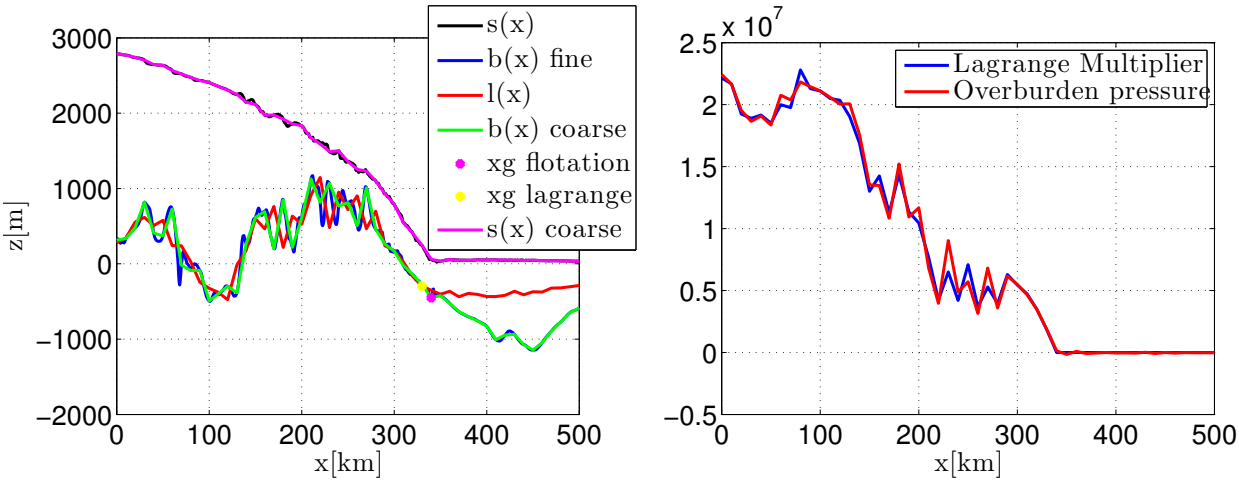

Figure 6.3: Left: Realistic ice sheet geometry. Data taken from [26]. Upper ice surface: s. Bedrock: b and the unknown inferior ice sheet surface: l. Grounding line: x_g. Right: Comparison between calculated overburden pressure calculated node per node and the Lagrangian multipliers. $N = 50$, $L = 500$km.

Chapter 7

Linear transport equation

In this chapter the linear transport equation describing the evolution of the ice thickness is studied in more detail. This type of convective transport problem is governed by a hyperbolic partial differential equation linking space and time. Therefore, it is not surprising that the discretization of one has a strong influence on the discretization of the other. For the space discretization we have the choice between the Finite Difference Method, the Finite Element Method and the Finite Volume Method. In this chapter we take a step towards stabilized Finite Element Methods or discontinuous Galerkin methods by considering a simple Finite Element formulation. It is combined with an implicit time stepping procedure to construct a hybrid FD-FEM method.

Section 7.1 recalls the initial boundary value problem that is considered. It is followed by a brief presentation of the time stepping problematic for convective transport problems in section 7.2. The variational formulation of the semi-discretized equation is presented in 7.3. It naturally leads to the fully discretized system in section 7.4. Finally, some numerical experiments are presented in section 7.5. This chapter is based on [50],[51] and [52].

7.1 Strong formulation

Let us introduce the strong form of the one dimensional linear unsteady convection problem it is conservative form. If Ω denotes the domain $[0, x_c]$ and τ a simulation period the governing equations are

$$\frac{\partial h}{\partial t} + \frac{\partial}{\partial x} Q(h) = a \qquad \text{in } \Omega \times]0, \tau[\tag{7.1a}$$

$$h(x, 0) = h_0(x) \qquad \text{in } \Omega \text{ at } t = 0 \tag{7.1b}$$

$$Q = 0 \qquad \text{on } x = 0 \text{ in }]0, \tau[\tag{7.1c}$$

The source term a is considered constant. In the presence of a hyperbolic equation only one boundary condition is imposed on the inflow boundary $x = 0$. No additional information is required on $x = x_c$. Note that no Dirichlet boundary condition is imposed. In this case a zero normal flux across the ice divide is imposed as a consequence of zero velocity. The ice flux $Q(h)$ is defined in terms of the horizontal velocity field u as

$$Q(h) = uh \tag{7.2}$$

If the velocity field u is supposed to be a known function of x and t only, the problem is indeed linear. In the context of modeling a marine ice sheet the transport equation has to

be coupled with the p-Laplace equation expressing horizontal equilibrium. The horizontal velocity is then part of the solution of the system and the transport equation becomes non-linear.

It shall be noted that even if $h(x,t)$ can be assumed differentiable throughout this work, due to the simplicity of the model, it does not have to be. Indeed an important property of hyperbolic equations is the transport of non-smooth quantities along its characteristic lines. This kind of non-smooth solution to the transport problem opens a path towards the concept of weak solutions, fundamental to the development of the finite element method.

Due to the presence of both time at space derivatives, the numerical approximation obviously involves two distinct discretization procedures. One in time, that will be discussed in the next section, and one in space, that will be performed by finite elements in sections 7.3 and 7.4.

7.2 Time stepping

The traditional approach for applying finite elements to time evolution problems is the method of lines, in which space is discretized first. It leads to a system of first-order ordinary differential equations that have to be integrated in time [50]. These are called semi-discretized equations. This allows the use of a range of numerical ODE solvers. A second approach consists in first discretizing the time variable before performing the spatial discretization. In conjunction with finite elements the second option is preferable.

For stability reasons laid out in chapter 4 an implicit Euler method was chosen. If time is discretized using a time step Δt and $h(x)^j = h(x, j\Delta t)$, then the transport equation discretized in time is:

$$\frac{h^{j+1} - h^j}{\Delta t} = a - \left(\frac{\partial}{\partial x} Q\right)^{j+1}, \tag{7.3}$$

where the second term in the right hand side is the spatial derivative of the flux evaluated at time step $j+1$.

The backward Euler method is of order Δt. More elaborate higher order schemes for time integration could be employed [50].

7.3 Variational formulation

The time discretized equation 7.3 can be interpreted as a spatial strong form to solved at each time step. With this idea in mind the usual approach for deriving the variation formulation of the problem can be applied.

Multiplying 7.3 by a test function ϕ and integrating over the domain yields

$$\frac{1}{\Delta t}\int_0^{x_c} h^{j+1}\varphi \,\mathrm{d}x + \int_0^{x_c} \left(\frac{\partial}{\partial x} hu\right)^{j+1} \varphi \,\mathrm{d}x = \int_0^{x_c} a\varphi \,\mathrm{d}x + \frac{1}{\Delta t}\int_0^{x_c} h^j \varphi \,\mathrm{d}x \tag{7.4}$$

Applying Gauß' theorem to the second term in the left hand side allows for a simpler treatment

of the boundary condition:

$$\begin{aligned}\int_0^{x_c} \left(\frac{\partial}{\partial x} hu\right)^{j+1} \varphi \,\mathrm{d}x &= \left[h^{j+1}u^{j+1}\varphi\right]_0^{x_c} - \int_0^{x_c} h^{j+1}u^{j+1}\frac{\partial \varphi}{\partial x}\,\mathrm{d}x \\ &= h^{j+1}(x_c)u^{j+1}(x_c)\varphi(x_c) - \int_0^{x_c} h^{j+1}u^{j+1}\frac{\partial \varphi}{\partial x}\,\mathrm{d}x\end{aligned} \tag{7.5}$$

The term in $x = 0$ vanishes because of the zero flux condition imposed at the ice divide.

The variational formulation of problem 7.1 is then:

Formulation 7 *At time t_{j+1}, given $h^j \in \mathcal{H}^1$ and $u \in \mathbb{L}^2(\Omega)$, find $h^{n+1} \in \mathcal{H}^1$ such that*

$$\frac{1}{\Delta t}\int_0^{x_c} h^{j+1}\varphi \,\mathrm{d}x - \int_0^{x_c} h^{j+1}u^{j+1}\frac{\partial \varphi}{\partial x}\,\mathrm{d}x + h_{x_c}^{j+1}u_{x_c}^{j+1}\varphi_{x_c} = \int_0^{x_c} a\varphi \,\mathrm{d}x + \frac{1}{\Delta t}\int_0^{x_c} h^j\varphi \,\mathrm{d}x$$

for all $\varphi \in \mathcal{H}^1$.

7.4 Discretized system

Space is discretized using a Galerkin approximation with the usual linear shape function as in 5.21:

$$h_h^j(x) = \sum_{i=0}^{N} h_i^j \phi_i \qquad \varphi_h(x) = \sum_{i=0}^{N} \varphi_i \phi_i \tag{7.6}$$

This naturally leads to a finite element formulation of the problem. In matrix form the problem that has to solved for $\mathbf{h}^{j+1}$ at each time step is the following:

$$\left[\frac{1}{\Delta t}\mathrm{H} - \mathrm{U}\right] \times \mathbf{h}^{j+1} + \mathrm{u}_N^{j+1}\mathrm{h}_N^{j+1} = \mathbf{f} + \frac{1}{\Delta t}\mathrm{H} \times \mathbf{h}^j, \tag{7.7}$$

where the matrices involved are defined as:

$$\begin{aligned}\mathrm{H}_{ij} &= \int_0^{x_c} \phi_i\phi_j \,\mathrm{d}x \qquad f_i = \int_0^{x_c} a\phi_i \,\mathrm{d}x \\ \mathrm{U}_{ij} &= \int_0^{x_c} u^{n+1}\phi_i \frac{\partial \phi_j}{\partial x}\,\mathrm{d}x\end{aligned} \tag{7.8}$$

and the vector $\mathbf{h}^j$ collects all the h_i^j.

7.5 Numerical illustration

In this section we motivate the choice of an implicit integration scheme through a simple numerical experiment. Moreover, the mechanism behind the evolution of the ice thickness is illustrated. The initial condition is a steady state computed in the same manner as in section 5.4.4. The physical parameters are the same as in table 5.1. The initial state is perturbed my

modifying the velocity. This will forces the ice thickness to adapt to reach a new steady state.

A short calculation of the CFL condition [53] shows that for a grid spacing of around 1 km an upper bound for a stable time step is around 0.4 years. This depends of course on the ice velocity, but a it gives an idea of the order of magnitude. An example is shown in figure 7.1. It can be seen that oscillations start near the calving front, where velocities are the largest. Long term calculations would require a substantial amount of time steps to be computed. Here the movement of the grounding line is not yet taken into account. The ladder adds some numerical instability to the problem. For these reasons an implicit time integration procedure is chosen.

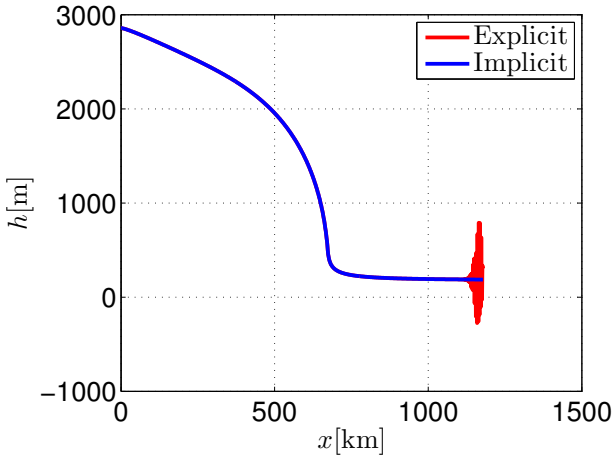

Figure 7.1: Ice thickness h after 30 simulated years. The initial condition is a steady state computed as in section 5.4.4. The initial steady state is perturbed by setting $u = 5/4u_0$, where u_0 is the initial velocity field. Comparison between an implicit and an explicit integration scheme. Numerical parameters: $N = 875$, $L = 1177$[km] and $\Delta t = 0.4$[a]. Physical parameters: see table 5.1.

Figure 7.2 shows a numerical experiment. Starting from an initial steady state the velocity profile is slightly modified and then maintained at this new velocity.

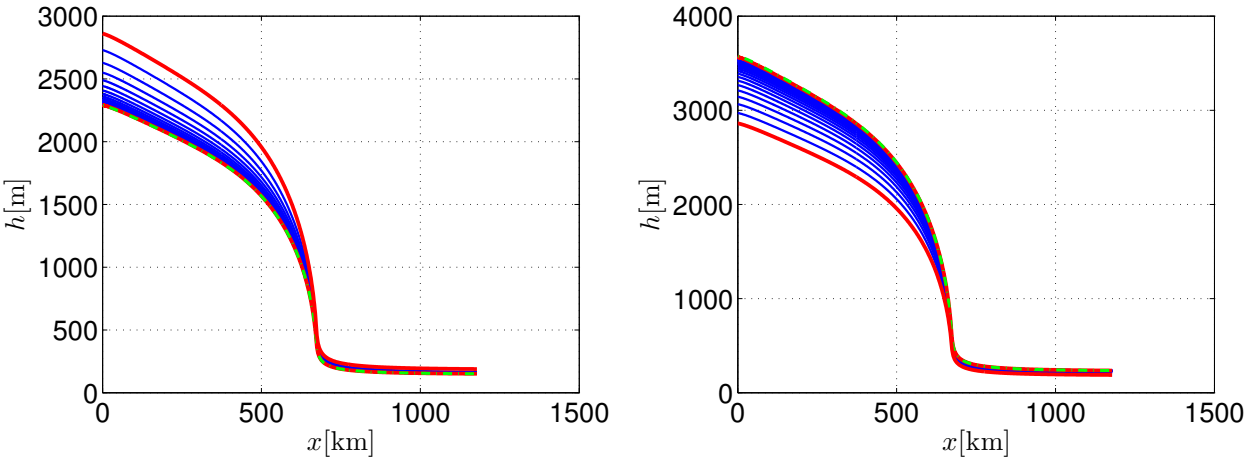

Figure 7.2: Evolution of the ice thickness h with time. The initial and final steady state are represented in red. The intermediate states are shown in blue. They are given every 2000 years. The green dashed line represents the final steady state calculated analytically. The simulation time is 40000 years. Numerical parameters: $N = 875$, $L = 1177$[km] and $\Delta t = 10$[a]. Physical parameters: see table 5.1. Left: Perturbation is a velocity increase. The velocity is set to $u = 5/4u_0$, where u_0 is the initial velocity field. Right: Perturbation is a velocity decrease. The velocity is set to $u = 4/5u_0$

A step-wise perturbation is of course unphysical, but it serves an illustrative purpose. It can be imagined as the resulting effect of a modification of the ice temperature. The rheological behaviour of the ice changes and through the horizontal momentum balance the velocity is adjusted. This has for effect to change the ice fluxes. In the case where the horizontal velocity is suddenly increased the ice flux across the grounding line increases and becomes larger than the total precipitation rate. Thus there is a mass imbalance and the ice sheet looses mass until the fluxes are again equal. The ice sheet has reached its new steady state. A similar reasoning can be applied for the case of sudden decrease in velocity.

Chapter 8

Coupled problem

In the previous chapters we have looked at each subproblem individually. The transport equation was seen as an equation for the ice thickness and the velocity field was considered to be known. It was concluded that an implicit time integration scheme was better suited for the the type of applications we are considering. Similarly, the horizontal momentum equation was solved for a given ice sheet geometry at steady state. Finally, the vertical equilibrium was formulated as a saddle point problem and resolved using a semi-smooth Newton algorithm. As for the previous subproblems, the ice sheet was considered at steady state and the ice thickness was therefore a known quantity. In this chapter the individual pieces are assembled together. Full coupling of the four variables, as well as the coupling of both the ice shelf and the ice sheet, with an implicit integration procedure is considered. These variables are ice thickness, horizontal velocity, the lower ice surface and the overburden pressure. In section 8.1 the system of equations to solve is presented in detail. In section 8.2 the equations are discretized in space and a finite element approximation is applied. The numerical algorithm based on an active set strategy is constructed. This leads to linear system of algebraic equations to be solved at each Newton iteration. Finally, some numerical results are presented in section 8.3.

8.1 Variational formulation of the coupled system

In this section the coupled system of equations to be solved is presented. We start by recalling the strong form of the complete problem. The domain is $\Omega = [0, x_c]$ a subset of $\mathbb{R}$ and τ denotes the total simulation time.

Given an initial state $h_0 = h(x, 0)$, $u_0 = u(x, 0)$ and $l_0 = l(x, 0)$ the variables h, u and l have to verify on $\Omega \times [0, \tau]$ the following equations:

$$\frac{\partial h}{\partial t} + \frac{\partial}{\partial x}(hu) = a, \tag{8.1a}$$

$$\frac{\partial}{\partial x}\left(2A^{-1/n} h \left|\frac{\partial u}{\partial x}\right|^{1/n-1} \frac{\partial u}{\partial x}\right) = \rho g h \frac{\partial (h+l)}{\partial x} + C|u|^{m-1} u \mathbb{1}_G, \tag{8.1b}$$

with the boundary conditions:

$$u = 0 \qquad \text{at } x = 0, \tag{8.2a}$$

$$2A^{-1/n} h \left|\frac{\partial u}{\partial x}\right|^{m-1} \frac{\partial u}{\partial x} = \frac{1}{2}\rho(1 - \rho/\rho_w) g h^2 \qquad \text{at } x = x_c, \tag{8.2b}$$

and the contact conditions:

$$l - b \geq 0, \tag{8.3a}$$
$$\rho g h - \pi_w \geq 0, \tag{8.3b}$$
$$(l - b)\left[\rho g h - \pi_w\right] = 0 \qquad \forall x \in \Omega. \tag{8.3c}$$

The function $\mathbb{1}_G$ is defined as the indicator function which is 1 on the grounding part of the domain and 0 on the floating part. This domain has to be computed as part of the solution by solving the contact conditions.

It can be noted that the ice thickness h appears in every equation. A modification of h will have an impact on the velocity field u and on the position of the grounding line through the contact conditions. Conversely, when the velocity field changes the ice surface adapts to reach a new dynamic equilibrium. Finally, the shape of the lower ice surface also plays a part in dictating the velocity field. It appears explicitly in the second term in equation 8.1b and implicitly in the third term.

Using the similar procedures as in sections 5.2.2, 6.3 and 7.3 we obtain a system of integral equations that have to be solved[1].

Formulation 8 *Find h, u with $u = 0$ at $x = 0$, l and $\lambda \geq 0$ such that:*

$$\int_0^{x_c} \frac{\partial h}{\partial t}\varphi \,\mathrm{d}x - \int_0^{x_c} hu\frac{\partial \varphi}{\partial x}\,\mathrm{d}x + h_{x_c}u_{x_c}\varphi_{x_c} - \int_0^{x_c} a\varphi \,\mathrm{d}x = 0$$

Non linear hyperbolic equation

$$\int_0^{x_c} 2A^{-1/n}h\left|\frac{\partial u}{\partial x}\right|^{1/n-1}\frac{\partial u}{\partial x}\frac{\partial v}{\partial x}\,\mathrm{d}x + \int_0^{x_c} C|u|^{m-1}u\,\mathbb{1}_G\, v\,\mathrm{d}x$$
$$+\int_0^{x_c} \rho g h\frac{\partial(h+l)}{\partial x}\, v\,\mathrm{d}x - 1/2\rho(1-\rho/\rho_w)gh_{x_c}^2 = 0$$

p-Laplace equation

$$\int_0^{x_c} \rho_w g l k\,\mathrm{d}x - \int_0^{x_c} (\pi_b + \rho_w g b - \rho g h)k\,\mathrm{d}x - \int_0^{x_c} \lambda k\,\mathrm{d}x = 0$$
$$\int_0^{x_c} (b-l)(\mu-\lambda)\,\mathrm{d}x \leq 0$$

Saddle point problem

---

for all φ, v with $v = 0$ at $x = 0$, k and $\mu \geq 0$.

The subscript x_c denotes a function that is evaluated at $x = x_c$. The system is comprised of three variational equalities and one variational inequality. It has to be solved for four variables. In addition to the usual ice thickness and velocity field the method requires to solve

[1] The λ and μ have to be larger than ae.

two additional equations for the two additional variables l and λ.

In usual formulations the gravity term and the friction term in the p-Laplace equation take a different form whether the floating part or the grounded part of the ice sheet is considered. Thus the knowledge of the grounding line position is required. It is not simply determined by the simple flotation condition. In the case of a power law friction, independent of the overburden pressure, the position of the grounding line has to be deduced somewhat artificially from the overburden pressure λ. A more elegant formulation follows from the use of a Coulomb friction law as discussed in section 4.3. Indeed the friction term in the horizontal momentum balance then simply takes the form of:

$$\int_0^{x_c} f_b \lambda |u|^{m-1} uv \, \mathrm{d}x. \tag{8.4}$$

Moreover, explicitly using the lower ice sheet surface l as a variable to be determined allows to write the gravity term in a unified way over the entire domain. In that case no explicit distinction between the grounded and the floating part is required anymore.

There are several sources of non-linearity in the equations. The first one is the product of h and u in the transport problem. In the horizontal momentum equation the non-linearities stem from the p-Laplace operator, the friction term and the terms quadratic in h. Finally, the inequality induces an additional non-linearity. Additionally, these equations have to be solved in space and in time.

8.2 Discretization and semi-smooth Newton algorithm

In this section the numerical resolution techniques developed in sections 5.3, 6.5 and 7.4 the solve the problem in formulation 8. We apply an implicit time integration procedure with a Mortar Finite Element approximation in space using the standard hat basis functions $\phi_i(x)$. The nodes are denoted by the indice i such that we write $x_i = i\Delta x$. A function evaluated at a time instant $t = j\Delta t$ is denoted f^j:

$$h_h^j(x) = \sum_{i=0}^{N} h_i^j \phi_i, \quad u_h^j(x) = \sum_{i=0}^{N} u_i^j \phi_i, \quad l_h^j(x) = \sum_{i=0}^{N} l_i^j \phi_i, \quad \lambda_h^j(x) = \sum_{i=0}^{N} \lambda_i^j \phi_i. \tag{8.5}$$

The associated test functions φ, v, k and μ are discretized with the same basis functions. The basis function for the dual variable λ is chosen to be the same as for the primal variables.

The method consists in marching in time and solving the semi-discretized version of the variational equations for h_h^{j+1}, u_h^{j+1}, l_h^{j+1} and λ_h^{j+1} knowing h_h^j. Thus at each time step we have the following variational system to be solved:

Formulation 9 *Given h_h^j, find h_h^{j+1}, u_h^{j+1} with $u_h^{j+1} = 0$ at $x = 0$, l_h^{j+1} and $\lambda_h^{j+1} \geq 0$ such that:*

$$\frac{1}{\Delta t}\int_0^{x_c} h_h^{j+1}\varphi_h \,\mathrm{d}x - \int_0^{x_c} h_h^{j+1}u_h^{j+1}\frac{\partial \varphi_h}{\partial x}\,\mathrm{d}x + h_h^{j+1}(x_c)u_h^{j+1}(x_c) = \int_0^{x_c} a\varphi_h \,\mathrm{d}x + \frac{1}{\Delta t}\int_0^{x_c} h_h^{j}\varphi_h \,\mathrm{d}x,$$

$$\int_0^{x_c} 2A^{-1/n}h_h^{j+1}\left|\frac{\partial u_h^{j+1}}{\partial x}\right|^{1/n-1}\frac{\partial u_h^{j+1}}{\partial x}\frac{\partial v_h}{\partial x}\,\mathrm{d}x + \int_0^{x_g(\lambda_h^{j+1})} C\left|u_h^{j+1}\right|^{m-1}u_h^{j+1}v_h\,\mathrm{d}x$$
$$= 1/2\rho(1-\rho/\rho_w)g\left(h_h^{j+1}(x_c)\right)^2 - \int_0^{x_c}\rho g h_h^{j+1}\frac{\partial\left(h_h^{j+1}+l_h^{j+1}\right)}{\partial x}v_h\,\mathrm{d}x,$$

$$\int_0^{x_c}\rho_w g l_h^{j+1}k_h\,\mathrm{d}x - \int_0^{x_c}(\pi_b + \rho_w g b - \rho g h_h^{j+1})k_h\,\mathrm{d}x - \int_0^{x_c}\lambda_h^{j+1}k_h\,\mathrm{d}x = 0,$$
$$\int_0^{x_c}(b - l_h^{j+1})(\mu_h - \lambda_h^{j+1})\,\mathrm{d}x \leq 0,$$

for all φ_h, v_h with $v_h = 0$ at $x = 0$, k_h and $\mu_h \geq 0$.

It leads to a non-linear system of equations of the form:

$$[f_{tr}\ f_{pL}\ f_c\ f_{\mathscr{A}}\ f_{\mathscr{I}}]^T = \mathbf{0}^2 \tag{8.6}$$

As in chapter 6 we choose to work with a semi-smooth Newton algorithm. The discretized increments for the Newton method are noted $[\Delta h_h\ \Delta u_h\ \Delta l_h\ \Delta\lambda_{\mathscr{A},h}\ \Delta\lambda_{\mathscr{I},h}]^T$. The system to be solved at each Newton iteration r can be cast into a matrix form. We define the following matrices:

$$\begin{aligned}
\mathrm{M}\Delta\boldsymbol{h} &= \langle Df_{tr}(h_h^{j+1}), \Delta h_h\rangle, & \mathrm{C}\Delta\boldsymbol{u} &= \langle Df_{tr}(u_h^{j+1}), \Delta u_h\rangle,\\
\mathrm{S}\Delta\boldsymbol{h} &= \langle Df_{pL}(h_h^{j+1}), \Delta h_h\rangle, & \mathrm{K}\Delta\boldsymbol{u} &= \langle Df_{pL}(u_h^{j+1}), \Delta u_h\rangle,\\
\mathrm{Q}\Delta\boldsymbol{l} &= \langle Df_{pL}(l_h^{j+1}), \Delta l_h\rangle, & \mathrm{R}\Delta\boldsymbol{h} &= \langle Df_{c}(h_h^{j+1}), \Delta h_h\rangle,\\
\mathrm{A}\Delta\boldsymbol{l} &= \langle Df_{c}(l_h^{j+1}), \Delta l_h\rangle, & \mathrm{B}\Delta\boldsymbol{l} &= \langle Df_{\mathscr{A}}(l_h^{j+1}), \Delta l_h\rangle.
\end{aligned} \tag{8.7}$$

The directional derivatives are evaluated for the known functions at iteration r. The vectors $\Delta\boldsymbol{h}$, $\Delta\boldsymbol{u}$, $\Delta\boldsymbol{l}$, $\Delta\boldsymbol{\lambda}_{\mathscr{A}}$ and $\Delta\boldsymbol{\lambda}_{\mathscr{I}}$ collect the values at the nodes for the approximated increments. The vectors $\mathbf{f}_{tr}$, $\mathbf{f}_{pL}$, $\mathbf{f}_c$, $\mathbf{f}_{\mathscr{A}}$ and $\mathbf{f}_{\mathscr{I}}$ collect the values at the nodes of equations 8.6 at iteration step r. We then have the following resolution strategy for formulation 8:

[2]The same approach as in section 6.5 was applied for dealing with the inequality.

Algorithm 4 Time marching algorithm with inner Newton iterations

Set $j = 0$
Compute an initial steady state: $\boldsymbol{h}^0$, $\boldsymbol{u}^0$, $\boldsymbol{l}^0$ and $\boldsymbol{\lambda}^0$
while $j < N_\tau$ **do**
    Set $r = 0$
    Choose an initial guess for the active set $\mathscr{A}^0$
    while *Convergence not reached* **do**
        Given $\mathscr{A}^r$ solve for $\Delta\boldsymbol{h}$, $\Delta\boldsymbol{u}$, $\Delta\boldsymbol{l}$, $\Delta\boldsymbol{\lambda}_{\mathscr{A}}$ and $\Delta\boldsymbol{\lambda}_{\mathscr{I}}$: ▷ Linear System to solve

$$\begin{bmatrix} \mathrm{M} & \mathrm{C} & 0 & 0 & 0 \\ \mathrm{S} & \mathrm{K} & \mathrm{Q} & 0 & 0 \\ \mathrm{R} & 0 & \mathrm{A} & \mathrm{B}^T & 0 \\ 0 & 0 & \mathrm{B} & 0 & 0 \\ 0 & 0 & 0 & 0 & \mathbb{I} \end{bmatrix} \begin{bmatrix} \Delta\boldsymbol{h} \\ \Delta\boldsymbol{u} \\ \Delta\boldsymbol{l} \\ \Delta\boldsymbol{\lambda}_{\mathscr{A}} \\ \Delta\boldsymbol{\lambda}_{\mathscr{I}} \end{bmatrix} = - \begin{bmatrix} \mathbf{f}_{tr} \\ \mathbf{f}_{pL} \\ \mathbf{f}_c \\ \mathbf{f}_{\mathscr{A}} \\ \mathbf{f}_{\mathscr{I}} \end{bmatrix}$$

        Update the solution with a relaxation step: ▷ $\xi \in]0, 1[$

$$\begin{bmatrix} \boldsymbol{h}^j_{r+1} \\ \boldsymbol{u}^j_{r+1} \\ \boldsymbol{l}^j_{r+1} \\ \boldsymbol{\lambda}^j_{\mathscr{A},r+1} \\ \boldsymbol{\lambda}^j_{\mathscr{I},r+1} \end{bmatrix} = \begin{bmatrix} \boldsymbol{h}^j_r \\ \boldsymbol{u}^j_r \\ \boldsymbol{l}^j_r \\ \boldsymbol{\lambda}^j_{\mathscr{A},r} \\ \boldsymbol{\lambda}^j_{\mathscr{I},r} \end{bmatrix} + \xi \begin{bmatrix} \Delta\boldsymbol{h} \\ \Delta\boldsymbol{u} \\ \Delta\boldsymbol{l} \\ \Delta\boldsymbol{\lambda}_{\mathscr{A}} \\ \Delta\boldsymbol{\lambda}_{\mathscr{I}} \end{bmatrix}$$

        Set $\mathscr{A}^{r+1}$ to $\left\{i : \lambda_i^{r+1} + c\langle b - l_h, \phi_i\rangle > 0\right\}$
        Increment r
    Increment j
return $\boldsymbol{h}$, $\boldsymbol{u}$, $\boldsymbol{l}$ and $\boldsymbol{\lambda}$

8.3 Numerical results

In this section we consider a marine ice sheet initially at steady state. The profile is calculated by the usual procedure 4.2. We simulate a decrease in ice temperature by decreasing the rheological coefficient A. Results are given in figures 8.1 and 8.2. It can be seen that the movement of the grounding line accelerates in the zone were the bedrock has an upward slope. In a stable portion the movement of the grounding line simply decelerates. Indeed, when the grounding line reaches a position where the bedrock is downward the movement decelerates until the ice sheet reaches its new steady state. The final ice geometry is very close to the analytical predictions based on section 4.2.

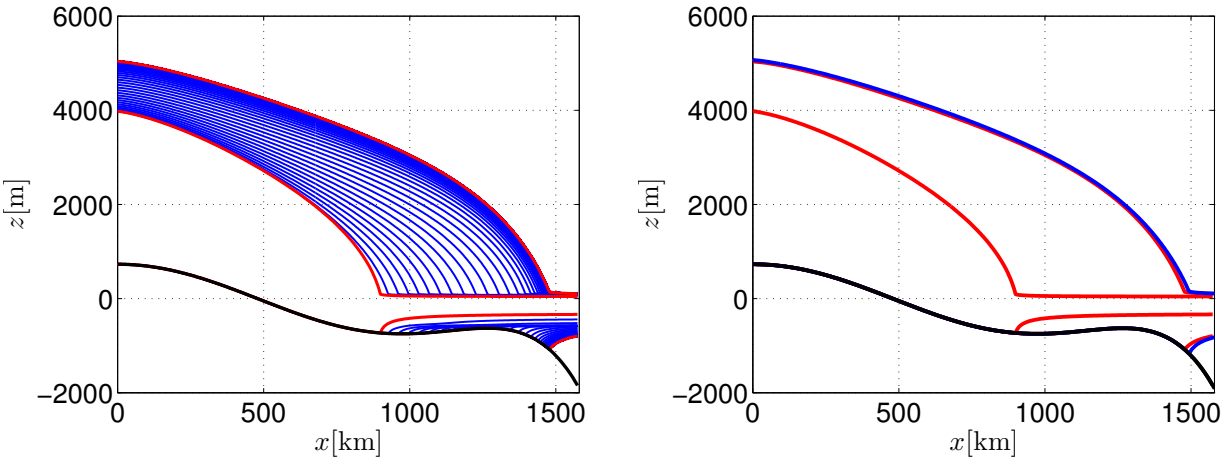

Figure 8.1: Left: Evolution of the ice sheet geometry composed of the upper surface $s(x)$ and the lower surface $l(x)$ with time. The initial and final steady state are represented in red. The intermediate states are shown in blue. They are given every 500 years. The bedrock $b(x)$ is represented in black. The simulation time is 100000 years. Numerical parameters: $N = 525$, $L = 1574$[km] and $\Delta t = 10$[a]. Physical parameters: see table 5.1. Initially the rheology coefficient is set to $A_0 = 3 \cdot 10^{(-26)}$[s^{-1} Pa^{-3}]. Perturbation is a decrease in this coefficient, which simulates temperature drop. It is set to $A = A_0/10$, where A_0 is the initial rheology coefficient. Right: Initial and final steady state profile in red. The final steady state profile is compared to the analytic approximation 4.2 represented in blue.

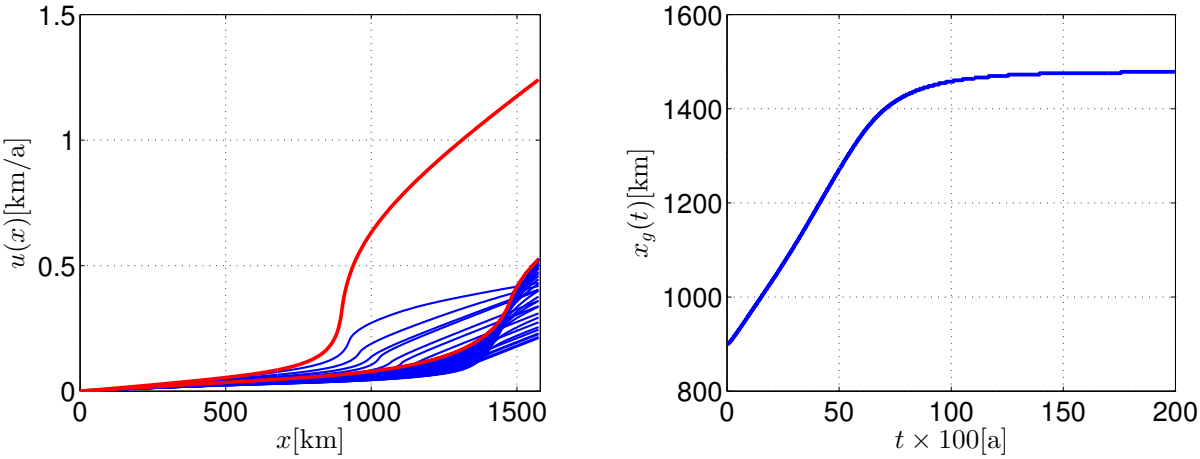

Figure 8.2: Left: Evolution of the velocity profile $u(x)$ with time. The initial and final steady state are represented in red. The intermediate states are shown in blue. They are given every 500 years. The simulation time is 100000 years. Numerical parameters: $N = 525$, $L = 1574$[km] and $\Delta t = 10$[a]. Physical parameters: see table 5.1. Initially the rheology coefficient is set to $A_0 = 3 \cdot 10^{(-26)}$[s^{-1} Pa^{-3}]. Perturbation is a decrease in this coefficient, which simulates temperature drop. It is set to $A = A_0/10$, where A_0 is the initial rheology coefficient. Right: Evolution of the grounding line position x_g in function of time. The figure stops after 20000 years.

Perspectives

In this master's thesis we took some steps towards improving currently employed numerical methods for the modeling of marine ice sheets. For that purpose we placed the problem into the framework of computational mechanics. A field of applied mathematics that has been extensively studied both theoretically and from a numerical point of view. It provides the adequate tools for facing the difficulties currently encountered by glaciologists. Even though the main focus was the modeling of ice sheets the mathematical methods that were made used of are very general and can be applied to numerous domains in computational physics. It is clear that we barely scratched the surface of the numerous thematics addressed in this work. Therefore, we provide a list of possible subjects that could be further investigated based on the work that was done in this thesis.

- In chapter 5 we solved the p-Laplace equation for a power friction law. It might be interesting to apply the same procedure for a Coulomb-type friction law proportional to the overburden pressure and compare it the results we obtained. A step in this direction has already been made in section 4.3, where a method for calculating steady state profiles is derived.
- Also in chapter 5, a first attempt for explaining the implications of the flux condition employed by glaciologists was made. However, they are still not perfectly well understood. Similar numerical experiments, but away from steady state might give more insight.
- In chapter 6 the vertical equilibrium of the ice sheet was identified as a contact problem and reformulated as a saddle point problem, where the overburden pressure plays the role of Langriangian multiplier. In traditional contact mechanics this corresponds to the normal part of the Langrangian multiplier. The tangential part is usually identified as the the friction force. It could be possible to formulate the coupled horizontal and vertical equilibrium in a similar fashion.
- In chapter 6 simple standard hat functions were employed for the discretization. Actually, choosing the correct basis function for Mortar Finite Element Methods is a discipline of its own. Indeed, taking dual shape functions could increase the efficiency of the method.
- Finite Element Methods do not work very well for non-linear hyperbolic equations as they were employed in chapter 7. It would probably be advantageous to move towards the Discontinuous Galerkin Method or the Finite Volume Method. Moreover, very simple time integration schemes were studied. The use of higher order schemes or stabilization methods could lead to great improvement in the efficient resolution of the transport equation.

- The reduced-order model for the marine ice sheet can also be rewritten as a double obstacle problem [34].
- In chapter 8 only simulations for the power sliding law in the simplified case of a smooth bedrock were performed. An interesting next step would be to apply a Coulomb-type sliding law and to take a realistic bedrock profile, as was done in section 6.6.

Conclusion

In this work the goal was to reformulate a reduced-order model for marine ice sheets as a unilateral contact problem. Such a reformulation gives access to an array of mathematical and numerical tools from computational contact mechanics that form an adapted framework for facing some of the issues encountered currently by glaciologists.

This work started by the presentation of a mechanical model for marine ice sheets. The particularities of the model were identified as the complex rheology of ice leading to the p-Laplace equation for the horizontal momentum balance, the presence of friction on some parts of the ice sheet boundary and the modeling of the transition zone between grounded and floating ice parts. It was followed by the derivation of reduced-order model that was obtained by studying the behaviour of the solution when the aspect ratio of the sheet tends to zero in a fast sliding ice regime. It was shown that it leads to a closed system of two equations with a simple criterion for distinguishing the grounded and floating parts of the ice sheet. Based on this simplified model an explanation for the mechanism of the Marine Ice Sheet Instability was provided. It was shown that some regions of the West Antarctic Ice Sheet risk experiencing such an irreversible bifurcation in the future. Moreover, an analytic expression for the flux at the grounding line was found. Next, we combined a finite element method with a Newton algorithm for solving the p-Laplace equation. An explanation for the implications of using a flux condition at the grounding line, such as it is currently done in some finite difference implementations, was given. Thereafter, the vertical equilibrium of the marine ice sheet was identified as a contact problem and formulated as saddle point problem. A Mortar Finite Element discretization was employed and a semi-smooth Newton algorithm was constructed. It was shown that the segment per segment integration approach, as opposed to the node per node approach, was capable of taking subgrid sized rugosity of the bedrock into account up to some extend. Subsequently, simple time integration schemes combined with a finite element space discretization for the transport equation were compared. Finally, a strong coupling of all the equations was considered. The previously studied methods for the subproblems where assembled together to solve the complete problem.

The methods presented in this work are not restricted to marine ice sheets. They are rather general and could be employed in other domains of computational physics as well. Indeed contact problems, or more abstractly, variational equalities and inequalities arise in numerous applications in continuum mechanics. This work could then serve as a starting point for anyone who encounters a problem of this nature during their research.

Appendix A: Finite Difference Method

The traditional approach by glaciologists for solving the governing equations for ice sheets is the finite difference method [3] and [5]. It is the conceptually most simple method for solving PDEs. This section presents in detail a numerical algorithm, based on finite differences, for solving the model of a grounded ice sheet governed by equations 3.36 and completed by the boundary conditions 3.38, 3.39 and 3.44, in an attempt to illustrate the major difficulties associated to the numerical modeling of marine ice sheets.

The first obvious challenge is the moving boundary $x = x_g(t)$. One way to deal with is to introduce the change of variables:

$$\sigma = \frac{x}{x_g}, \qquad \tau = t. \tag{8.8}$$

Using the chain rule one gets for the derivatives in terms of the new variables:

$$\frac{\partial}{\partial x} = \frac{1}{x_g}\frac{\partial}{\partial \sigma} \tag{8.9}$$

$$\frac{\partial}{\partial t} = \frac{\partial}{\partial \tau} - \frac{\sigma}{x_g}\frac{\mathrm{d}x_g}{\mathrm{d}\tau}\frac{\partial}{\partial \sigma} \tag{8.10}$$

Inserting them into the model gives for the governing equations:

$$\left.\begin{aligned} &\frac{\partial h}{\partial \tau} + \frac{1}{x_g}\frac{\partial (hu)}{\partial \sigma} - \frac{\sigma}{x_g}\frac{\mathrm{d}x_g}{\mathrm{d}\tau}\frac{\partial h}{\partial \sigma} = a \\ &\frac{1}{x_g^{1+1/n}}\frac{\partial}{\partial \sigma}\left[2A^{-1/n}h\left|\frac{\partial u}{\partial \sigma}\right|^{1/n-1}\frac{\partial u}{\partial \sigma}\right] - C|u|^{1/n-1}u - \frac{1}{x_g}\rho_i g h\frac{\partial (h+b)}{\partial \sigma} = 0 \end{aligned}\right\} \text{ for } \sigma \in]0,1[\tag{8.11}$$

An additional term appears in the transport equation. It is related to the movement of the grounding line. The boundary conditions simply become under the coordinate stretching:

$$\frac{\partial (h+l)}{\partial \sigma} = 0 \qquad \text{at } \sigma = 0 \tag{8.12}$$

$$\frac{1}{x_g^{1/n}}2A^{-1/n}\left|\frac{\partial u}{\partial \sigma}\right|^{1/n-1}\frac{\partial u}{\partial \sigma} = -\frac{1}{2}\rho_w\left(1-\rho_i/\rho_w\right)g b(x_g) \qquad \text{at } \sigma = 1, \tag{8.13}$$

with the flotation condition

$$h = -\rho_w/\rho\, l \qquad \text{at } \sigma = 1. \tag{8.14}$$

Discretization

The equations are discretized using finite differences on a uniform staggered grid for u and h. There are N grid points for both h and u. The ice divide at $\sigma = 0$ is taken as a h grid point and the grounding line $\sigma = 1$ is taken as u grid point. The u grid points are labeled $\alpha = 3/2, 5/2, ..., N + 1/2$ and the h grid points are labeled $\alpha = 1, 2, .., N$. Note that a ghost u grid point is added at $\alpha = 1/2$, that will help take care of the boundary condition at the ice divide. The discretized time instants are denoted by the integer j and the integer i is reserved for the grid points. A constant time step $\Delta\tau$ is chosen and we have the discrete variables

$h_i^j = h(\sigma_i, j\Delta\tau)$, $u_{i+1/2}^j = u(\sigma_{i+1/2}, j\Delta\tau)$ and $x_g^j = x_g(j\Delta\tau)$. The bed does not change under coordinate stretching thus one has $b_i^j = b(x_g^j\sigma_i)$.

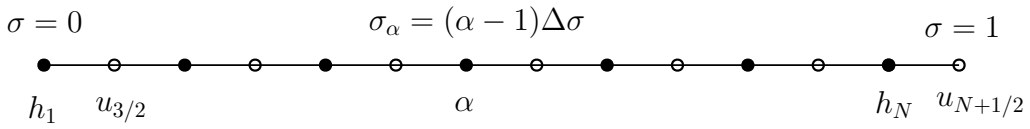

Figure 8.3: Discretized Domain: full circles are h-grid points, empty circles are u-grid points.

The transport equation in 8.11 is discretized using an upwind scheme with a forward Euler step for u and x_g and a backward step for h to get a first guess for h at the next time step. The discretized equation writes

$$\frac{h_i^j - h_i^{j-1}}{\Delta\tau} - \frac{\sigma_i(x_g^{j-1} - x_g^{j-2})(h_{i+1}^j - h_{i-1}^j)}{2\Delta\tau\Delta\sigma x_g^{j-1}} + \frac{h_i^j(u_{i+1/2}^{j-1} + u_{i-1/2}^{j-1}) - h_{i-1}^j(u_{i-1/2}^{j-1} + u_{i-3/2}^{j-1})}{2x_g^{j-1}\Delta\sigma} = a, \tag{8.15}$$

for $i \in]1, N[$. When $i = 2$ the equation involves the ghost grid point $u_{1/2}$. By symmetry one has $u_{1/2} = -u_{3/2}$. Thus when $i = 2$ one has the following equation

$$\frac{h_2^j - h_2^{j-1}}{\Delta\tau} - \frac{\sigma_2(x_g^{j-1} - x_g^{j-2})(h_3^j - h_1^j)}{2\Delta\tau\Delta\sigma x_g^{j-1}} + \frac{h_2^j(u_{5/2}^{j-1} + u_{3/2}^{j-1})}{2x_g^{j-1}\Delta\sigma} = a, \tag{8.16}$$

At $i = 1$ the symmetry yields

$$\frac{h_1^j - h_1^{j-1}}{\Delta\tau} + \frac{2h_1^j u_{3/2}^{j-1}}{\Delta\sigma x_g^{j-1}} + a = 0 \tag{8.17}$$

and finally at $i = N$ the centered finite difference involves the non existing point h_{N+1}, therefore a one sided finite difference formula is used instead. It is given by

$$\frac{h_N^j - h_N^{j-1}}{\Delta\tau} - \frac{\sigma_i(x_g^{j-1} - x_g^{j-2})(h_N^j - h_{N-1}^j)}{\Delta\tau\Delta\sigma x_g^{j-1}} + \frac{h_N^j(u_{i+1/2}^{j-1} + u_{N-1/2}^{j-1}) - h_{N-1}^j(u_{N-1/2}^{j-1} + u_{N-3/2}^{j-1})}{2x_g^{j-1}\Delta\sigma} = a. \tag{8.18}$$

The system of equations formed by 8.15, 8.17 and 8.18 written for each grid point can be cast into a matrix form as

$$\mathbf{H} \times \mathbf{h} = \mathbf{b}, \tag{8.19}$$

where $\mathbf{h} = [h_1^j, ..., u_N^j]^T$. The matrix $\mathbf{H}$ does not depend on h. The system is solved using a direct method to obtain a first guess for $\mathbf{h}$.

The guessed values for $\mathbf{h}$ are used to obtain a guess for the grounding line position by solving the discretized flotation condition valid at $i = N + 1/2$. It is obtained by matching the linear extrapolation of h at $h_{N+1/2}$. Thus one has for the boundary condition at $\sigma = 1$

$$3h_N^j - h_{N-1}^j + 2(\rho_w/\rho)b_{N+1/2}^j = 0. \tag{8.20}$$

The Bedrock elevation being a function of the grounding line position, this involves solving a non linear equation.

Finally, the momentum equation is discretized using an implicit scheme, where the h^j and x_g^j are supposed to be known from the previous calculations.

For $i \in [1, N-1]$ one has:

$$\frac{2\bar{A}^{-1/n}}{(\Delta\sigma x_g)^{1+1/n}}\left[h^j_{i+1}\left|u^j_{i+3/2}-u^j_{i+1/2}\right|^{1/n-1}\left(u^j_{i+3/2}-u^j_{i+1/2}\right)-h^j_i\left|u^j_{i+1/2}-u^j_{i-1/2}\right|^{1/n-1}\left(u^j_{i+1/2}-u^j_{i-1/2}\right)\right]$$
$$-C|u^j_{i+1/2}|^{1/n-1}u^j_{i+1/2}-\frac{1}{x_g^{j-1}}\rho_i g(h^j_i+h^j_{i+1})\frac{h^j_{i+1}+b^j_{i+1}-h^j_i-b^j_i}{\Delta\sigma}=0. \tag{8.21}$$

As before, for $i=1$ the scheme involves the ghost grid point $u_{1/2}$. It is treated in the same way using the symmetry at the ice divide. Thus when $i=1$ the equation writes:

$$\frac{2\bar{A}^{-1/n}}{(\Delta\sigma x_g)^{1+1/n}}\left[h^j_2\left|u^j_{5/2}-u^j_{3/2}\right|^{1/n-1}\left(u^j_{5/2}-u^j_{3/2}\right)-2h^j_1\left|2u^j_{3/2}\right|^{1/n-1}\left(u^j_{3/2}\right)\right]$$
$$-C|u^j_{3/2}|^{1/n-1}u^j_{3/2}-\frac{1}{x_g^{j-1}}\rho_i g(h^j_1+h^j_2)\frac{h^j_2+b^j_2-h^j_1-b^j_1}{\Delta\sigma}=0. \tag{8.22}$$

The second boundary condition valid at $i=N+1/2$ is discretized in the following way

$$\frac{2\bar{A}^{-1/n}}{x_g^{1/n}}h^j_{i+1}\left|u^j_{N+1/2}-u^j_{N-1/2}\right|^{1/n-1}\left(u^j_{N+1/2}-u^j_{N-1/2}\right)+\frac{1}{2}(1-\frac{\rho_i}{\rho_w})\rho_w g b^j_{N+1/2}. \tag{8.23}$$

The system formed by 8.21, 8.22 and 8.23 can be written in matrix form as

$$\mathbf{U}(\mathbf{u})\times\mathbf{u}=\mathbf{c}, \tag{8.24}$$

where $\mathrm{u}=[u^j_{3/2},...,u^j_{N+1/2}]^T$. The detailed procedure for constructing the matrices can be found in the appendix.

Resolution algorithm

A weak coupling of the transport equation and the horizontal momentum was chosen, due to its simpler implementation. The transport equation is interpreted as an equation for the ice thickness with u and x_g being parameters. Similarly, the momentum equation is seen as an equation for velocity with h and x_g being parameters. Finally, the flotation condition is used to determine the grounding line position with u and h being interpreted as mere parameters. System 8.24 is non-linear. Therefore an iterative method is required for solving it. There exists a multitude of non-linear solvers such as the Gauß-Seidel method or the Newton-Method. Here we decided to work with the Picard method. It is simple to implement and relatively robust. The general resolution algorithm is synthesised in algorithm 5

Results

Starting from a steady state calculated as in section 4.2 a perturbation is introduced by increasing the rheological coefficient A. It translates the effect of a temperature increase. As can be observed in figures 8.4 and 8.5 the flux across the grounding line increases and ice sheet looses mass. As a consequence the grounding line retreats, first rapidly and then slowing down until a new steady state is reached.

Algorithm 5 Algorithm for obtaining h, x_g and u at each time j step

1: Initialize $h^{(0)}$, $u^{(0)}$ and $x_g^{(0)}$
2: **For** $k = 1, 2, ...$ until convergence **do**:
3: Find a guess $\tilde{h}$ for the ice thickness by solving:

$$\mathbf{H} \times \tilde{\mathbf{h}}^{(k)} = \mathbf{b}$$

4: Compute $x_g^{(k)}$ through the flotation condition with $h = \tilde{h}$
5: Solve the system:

$$\mathbf{U}\left(\mathbf{u}^{(k-1)}\right) \times \tilde{\mathbf{u}}^{(k)} = \mathbf{c}$$

6: Do a relaxation step:

$$\begin{aligned} \mathbf{h}^{(k)} &= r\mathbf{h}^{(k-1)} + (1-r)\tilde{\mathbf{h}}^{(k)} \\ x_g^{(k)} &= r x_g^{j-1} + (1-r) x_g^j \\ \mathbf{u}^{(k)} &= r\mathbf{u}^{(k-1)} + (1-r)\tilde{\mathbf{u}}^{(k)} \end{aligned}$$

▷ $r \in [0, 1]$

7: **return** h^j, x_g^j, u^j

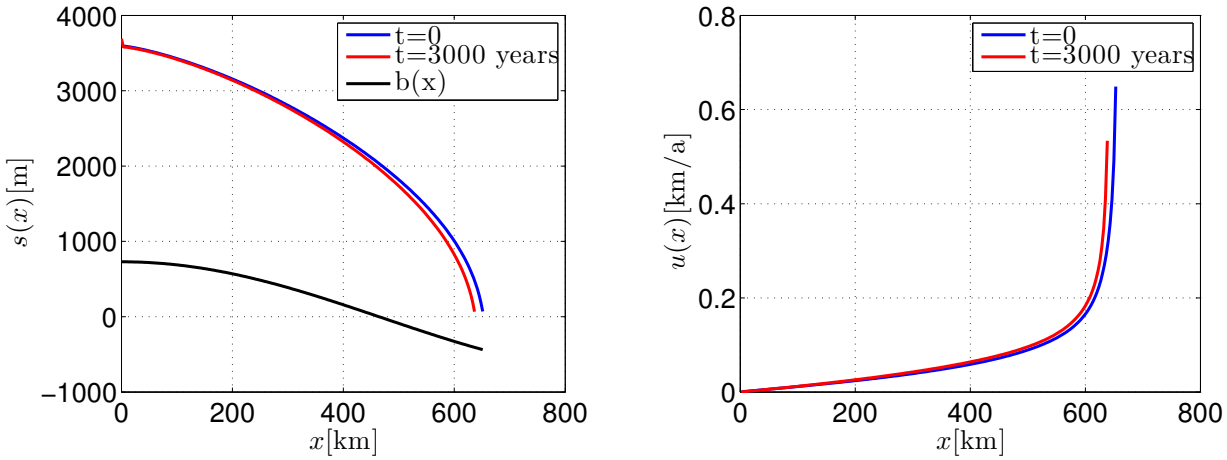

Figure 8.4: Left: Initial and final ice surface. Right: Initial and final velocity field. Number of elements: $N = 200$. Size of the domain: $L = 673$ km. Parameters from table 4.4 were used. The initial steady state is perturbed by setting $A = 4A$, which simulates a temperature increase of the ice sheet.

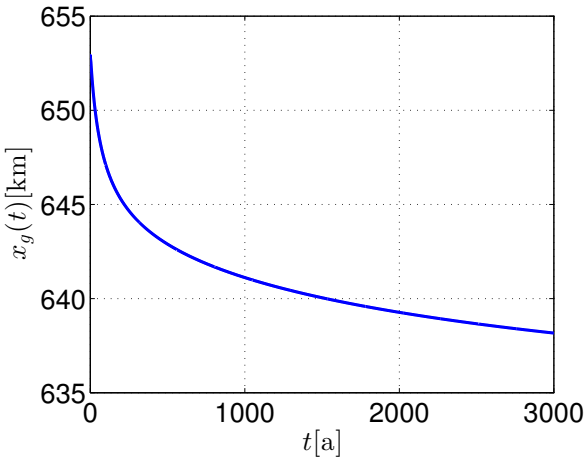

Figure 8.5: Grounding line position in function of time.Number of elements: $N = 200$. Size of the domain: $L = 673$ km. Parameters from table 4.4 were used. The initial steady state is perturbed by setting $A = 4A$, which simulates a temperature increase of the ice sheet.

The numerical method employed in this section is rather slow. The movement of the boundary as a consequence of grounding line migration induced some additional instability in the numerical scheme. In order to have a stable uncoupled method a large relaxation r coefficient had to be used. This slowed down the convergence of the fixed point iteration substantially. Therefore, spatial resolution was limited and geometry gradients near the grounding were not well approximated. Moreover, it made very long term simulations difficult.

In the finite difference method the matrices are filled in the following way:

$$
\text{For } i = 1,2 \begin{cases}
\mathrm{H}_{11} = \dfrac{1}{\Delta\tau} + \dfrac{2u_{3/2}^{j-1}}{\Delta\sigma x_g^{j-1}} \\
\mathrm{b}_1 = \dfrac{h_1^{j-1}}{\Delta\tau} - a \\
\mathrm{H}_{22} = \dfrac{1}{\Delta\tau} + \dfrac{(u_{5/2}^{j-1} + u_{3/2}^{j-1})}{2x_g^{j-1}\Delta\sigma} \\
\mathrm{H}_{21} = \dfrac{\sigma_2(x_g^{j-1} - x_g^{j-2})}{2\Delta\tau\Delta\sigma x_g^{j-1}} \\
\mathrm{H}_{23} = -\dfrac{\sigma_2(x_g^{j-1} - x_g^{j-2})}{2\Delta\tau\Delta\sigma x_g^{j-1}} \\
\mathrm{b}_2 = \dfrac{h_2^{j-1}}{\Delta\tau} + a
\end{cases}
$$

$$
\text{For } i = 3,..,N-1 \begin{cases}
\mathrm{H}_{ii} = \dfrac{1}{\Delta\tau} + \dfrac{(u_{i+1/2}^{j-1} + u_{i-1/2}^{j-1})}{2x_g^{j-1}\Delta\sigma} \\
\mathrm{H}_{ii-1} = \dfrac{\sigma_i(x_g^{j-1} - x_g^{j-2})}{2\Delta\tau\Delta\sigma x_g^{j-1}} - \dfrac{(u_{i-1/2}^{j-1} + u_{i-3/2}^{j-1})}{2x_g^{j-1}\Delta\sigma} \\
\mathrm{H}_{ii+1} = -\dfrac{\sigma_i(x_g^{j-1} - x_g^{j-2})}{2\Delta\tau\Delta\sigma x_g^{j-1}} \\
\mathrm{b}_i = \dfrac{h_i^{j-1}}{\Delta\tau} + a
\end{cases}
$$

$$
\text{For } i = N \begin{cases}
\mathrm{H}_{NN} = \dfrac{1}{\Delta\tau} - \dfrac{\sigma_i(x_g^{j-1} - x_g^{j-2})}{\Delta\tau x_g^{j-1}\Delta\sigma} + \dfrac{(u_{N+1/2}^{j-1} + u_{N-1/2}^{j-1})}{2x_g^{j-1}\Delta\sigma} \\
\mathrm{H}_{NN-1} = \dfrac{\sigma_i(x_g^{j-1} - x_g^{j-2})}{\Delta\tau\Delta\sigma x_g^{j-1}} - \dfrac{(u_{N-1/2}^{j-1} + u_{N-3/2}^{j-1})}{2x_g^{j-1}\Delta\sigma} \\
\mathrm{b}_N = \dfrac{h_N^{j-1}}{\Delta\tau} + a
\end{cases}
$$

$$
\text{for } i=1 \begin{cases} \mathrm{U}_{11} = \dfrac{2\bar{A}^{-1/n}}{(\Delta\sigma x_g^j)^{1+1/n}} \left[-h_2^j \left| u_{5/2}^j - u_{3/2}^j \right|^{1/n-1} - 2 * h_1^j \left| 2u_{3/2}^j \right|^{1/n-1} \right] - C|u_{3/2}^j|^{1/n-1} \\ \mathrm{U}_{12} = \dfrac{2\bar{A}^{-1/n}}{(\Delta\sigma x_g^j)^{1+1/n}} h_2^j \left| u_{5/2}^j - u_{3/2}^j \right|^{1/n-1} \\ \mathrm{c}_1 = \dfrac{1}{2}\rho_i g(h_1^j + h_2^j) \dfrac{h_2^j + b_2^j - h_1^j - b_1^j}{x_g^j \Delta\sigma} \end{cases}
$$

$$
\text{for } i=1,..N-1/2 \begin{cases} \mathrm{U}_{ii} = \dfrac{2\bar{A}^{-1/n}}{(\Delta\sigma x_g^j)^{1+1/n}} \left[-h_{i+1}^j \left| u_{i+3/2}^j - u_{i+1/2}^j \right|^{1/n-1} - h_i^j \left| u_{i+1/2}^j - u_{i-1/2}^j \right|^{1/n-1} \right] \\ \qquad -C|u_{i+1/2}^j|^{1/n-1} \\ \mathrm{U}_{ii+1} = \dfrac{2\bar{A}^{-1/n}}{(\Delta\sigma x_g^j)^{1+1/n}} h_{i+1}^j \left| u_{i+3/2}^j - u_{i-1/2}^j \right|^{1/n-1} \\ \mathrm{U}_{ii-1} = \dfrac{2\bar{A}^{-1/n}}{(\Delta\sigma x_g^j)^{1+1/n}} h_i^j \left| u_{i+1/2}^j - u_{i-1/2}^j \right|^{1/n-1} \\ \mathrm{c}_i = \dfrac{1}{2}\rho_i g(h_i^j + h_{i+1}^j) \dfrac{h_{i+1}^j + b_{i+1}^j - h_i^j - b_i^j}{x_g^j \Delta\sigma} \end{cases}
$$

$$
\text{for } i=N \begin{cases} \mathrm{U}_{NN} = \dfrac{2\bar{A}^{-1/n}}{(\Delta\sigma x_g^j)^{1/n}} \left| u_N^j - u_{N-1}^j \right|^{1/n-1} \\ \mathrm{U}_{NN-1} = -\dfrac{2\bar{A}^{-1/n}}{(\Delta\sigma x_g^j)^{1/n}} \left| u_N^j - u_{N-1}^j \right|^{1/n-1} \\ \mathrm{c}_N = -\dfrac{1}{2}(1 - \rho_i/\rho_w)\rho_w g b_g^j \end{cases}
$$

Appendix B

The space $\mathcal{N}$ is defined the trace of $\mathcal{V}$ on the potential contact surface Γ_c. Since the present problem is set in $\Omega = \mathbb{R}$ and the potential contact area is the entire space Ω, $\mathcal{N}$ can be identified with $\mathcal{V}$. The space $\mathcal{M}$ is defined as the dual space of $\mathcal{N}$. Therefore, we have $\mathcal{M} = \mathbb{L}^2(\Omega)$. Duality pairing between $\mathcal{N}$ and $\mathcal{M}$ is noted $\langle k, \mu \rangle$. Furthermore, $\mathcal{N}_+$ is defined as $\mathcal{N}_+ \coloneqq \{k \in N : k \geq b \text{ a.e}\}$. We are now in a position to rigorously define the set of Lagrange multipliers as

$$
\mathcal{M}_+ = \{\mu \in \mathcal{M} : \langle k - b, \mu \rangle \geq 0, \forall k \in \mathcal{N}_+\}.
$$

The set $\mathcal{M}_+$ is a closed convex cone [6]. Moreover, $\mathcal{K}$ can alternatively be defined as

$$
\mathcal{K}_+ = \{k \in \mathcal{V} : \langle k - b, \mu \rangle \geq 0, \forall \mu \in \mathcal{M}_+\}.
$$

Bibliography

[1] J.W. Barrett and W.B. Liu. *Finite Element Approximation for the p-Laplacian.* Mathematics of Computations, 1993.

[2] K. Bulthuis M. Arnst, S. Sun and F. Pattyn. *Uncertainty quantification of the multi-centennial response of the Antarctic ice sheet to climate change.* The Cryosphere, 2019.

[3] Christian Schoof. *Ice sheet grounding line dynamics: Steady states, stability, and hysteresis.* Journal of Geophysical Research,, 2007.

[4] D. Pollard and M. DeConto. *Description of a hybrid ice sheet-shelf model and application to Antarctica.* Geoscientific Model Development, 2012.

[5] F. Pattyn. *Sea-level response to melting of Antarctic ice shelves on multi-centennial timescales with the fast Elementary Thermomechanical Ice Sheet model.* The Cryosphere, 2017.

[6] N. Kikuchi and J.T. Oden. *Contact Problems in Elasticity:A Study of Variational Inequalities and Finite Element Methods*. Studies in Applied Mathematics, 1988.

[7] Barbara Wohlmuth. *Variationally consistent discretization schemes and numerical algorithms for contact problems.* Cambridge University Press, 2011.

[8] Sylvain Coutterand. *Calottes glaciaires et inlandsis.* https://www.glaciers-climat.com/gp/calottes-glaciaires/. (Accessed: 2019-04-20).

[9] Jürg Alean. *SwissEduc - Glaciers online.* https://swisseduc.ch/glaciers/earth_icy_planet/glaciers02-en.html?id=6. (Accessed: 2019-04-20).

[10] Pedro Fernandez. *La línea de tierra antártica se está retirando.* https://cazatormentas.com/linea-tierra-banquisa-antartica-retirando/. (Accessed: 2019-04-21).

[11] Bruce F. Molnia. *Glacier and Landscape Change in Response to Changing Climate.* https://www2.usgs.gov/climate_landuse/glaciers/repeat_photography.asp. (Accessed: 2019-04-23).

[12] C. Schoof A. Robel, E. DeGiuli and E. Tziperman. *Dynamics of ice stream temporal variability: Modes, scales and hysteresis.* Journal of Geophysical Research Letters, 2013.

[13] Ralf Greve and Heinz Blatter. *Dynamics of Ice Sheets and Glaciers*. Springer, 2009.

[14] G. Maze T. Maze, R. Smelzer. *Continuum Mechanics for Engineers*. CRC Press, 2010.

[15] Pierre C. Dauby. *Irreversibility, Instability and Chaos*. University of Liège, 2017.

[16] Kevin Bulthuis. *Modélisation multiphysique de l'écoulement des glaciers: analyse et résolution numérique d'un problème couplé non linéaire*. University of Liège, 2015.

[17] Kenneth G. Libbrecht. *Science-Contents*. http://snowcrystals.com/. (Accessed: 2019-05-20).

[18] Thorsten et al. Bartels-Rausch. *Ice structures, patterns, and processes: A view across the ice-fields*. http://inspirehep.net/record/1122769/plots. (Accessed: 2019-05-20).

[19] Guillaume Jouvet. *Modélisation, analyse mathématique et simulation numérique de la dynamique des glaciers*. Ecole Polytechnique Fédérale de Lausanne, 2010.

[20] Jean-Marie Beckers. *Geophysical Fluid Dynamics*. Université de Liège, 2011.

[21] G. Durand R. Hindmarsh F. Pattyn O. Gagliardini A. S. Drouet, D. Docquier and T. Zwinger. *Grounding line transient response in marine ice sheet models.* The Cryosphere, 2009.

[22] P. Noble E. Nieto and J. Vila. *Shallow Water equations for Non-Newtonian fluids*. Journal of Non-Newtonian Fluid Mechanics, 2010.

[23] E.J. Hinch. *Perturbation Methods*. Cambridge University Press, 1995.

[24] Christian Schoof. *Marine ice-sheet dynamics. Part 1. The case of rapid sliding*. J. Fluid Mech., 2007.

[25] ASOC. *The Future of the West Antarctic Ice Sheet: Observed and Predicted Changes, Tipping Points, and Policy Considerations*. Information Paper Submitted by ASOC, 2010.

[26] P. Fretwell et al. *Bedmap2: improved ice bed, surface and thickness datasets for Antarctica*. The Cryosphere, 2013.

[27] A. Thompson V. Tsai, A. Stewart. *Marine ice-sheet profiles and stability under Coulomb basal conditions*. Journal of Glaciology, 2015.

[28] Maarten Arnst. *Towards uncertainty-quantified prediction of marine ice-sheet instabilities of the Antarctic ice sheet*. Project report. 2019.

[29] M. Crucifixd V. Dakose V. Brovkinb M. Williamsonf T. Lentonf S. Bathianya, H. Dijkstrac and M. Scheffera. *Beyond bifurcation: using complex models to understand and predict abrupt climate change*. DSCS, 2016.

[30] L. Favier T. Zwinger G. Durand, O. Gagliardini and E. Le Meur. *Impact of bedrock description on modeling ice sheet dynamics*. Geophysical Research Letters, 2011.

[31] Armin Bosten. *Uncertainty quantification of the dynamics of the Antarctic ice sheet*. Reliability and stochastic modeling of engineering systems. 2018.

[32] E. Larour E. Rignot H. Seroussi, M. Morlighem and A. Khazendar. *Hydrostatic grounding line parameterization in ice sheet models*. The Cryosphere, 2014.

[33] Kevin Bulthuis Kim Liegeois and Maarten Arnst. *Towards uncertainty-quantified prediction of marine ice-sheet instabilities of the Antarctic ice sheet.* Sandia, Albuquerque. 2019.

[34] G. Jouvet and C. Gräser. *An adaptive Newton multigrid method for a model of marine ice sheets.* Journal of Computational Physics, 2013.

[35] Haïm Brezis. *Analyse Fonctionelle: Théorie et Applications*. Dundod, 1999.

[36] M.E. Hubbard K.J Brabazon and P.K. Jimack. *Nonlinear Multigrid Methods for Second Order Differential Operators with Nonlinear Diffusion Coefficient.* Computers and Mathematics with Applications, 2014.

[37] Christian Schoof. *Variational methods for glacier flow over plastic till.* Journal of Fluid Mechanics, 2005.

[38] Christian Schoof. *A variational approach to ice stream flow.* Journal of Fluid Mechanics, 2005.

[39] Christian Schoof. *Coulomb friction and other sliding laws in a higher order glacier flow.* Mathematical Models and Methods in Applied Sciences, 2008.

[40] Alfio Quarteroni. *Numerical Models for Differential Problems*. Springer, 2017.

[41] Ed Bueler. *An exact solution for a steady, flowline marine ice sheet.* Journal of Glaciology, 2014.

[42] S. Conford R. Gladstone, A. Payne. *Resolution requirements for grounding-line modelling: sensitivity to basal drag and ice-shelf buttressing.* Journal of Glaciology, 2012.

[43] Tod A. Laursen. *Computational Contact and Impact Mechanics*. Springer, 2002.

[44] Peter Wriggers. *Computational Contact Mechanics*. Springer, 2006.

[45] F. Facchinei and J. S. Pang. *Finite-Dimensional Variational Inequalities and Complementarity Problems*. Springer, 2003.

[46] Anca Capatina. *Variational Inequalities and Frictional Contact Problems.* Springer, 2014.

[47] Faker Ben Belgacem. *The mortar finite element method with lagrange multipliers.* Numerische Mathematik,, 1999.

[48] Kim Liegeois. *Two bodies in thermomechanical contact modeled with the Mortar Finite Element Method.* University of Liège. 2017.

[49] D. Boffi F. Brezzi and M. Fortin. *Mixed Finite Elements and Applications.* Springer, 2013.

[50] Jean Donea and Antonio Huerta. *Finite Element Methods for Flow Problems*. Wiley, 2003.

[51] Per Loetstedt Gong Cheng and Lina von Sydow. *Accurate and stable time stepping in ice sheet modeling.* arXiv, 2016.

[52] Eric Sonnendrücker. *Finite Element methods for hyperbolic systems*. Max-Planck-Institut für Plasmaphysik, 2015.

[53] H. Lewy R. Courant, K. Friedrichs. *On the Partial Difference Equations of Mathematical Physics*. Mathematische Annalen, 1928.